THE STELLAR CONTENT OF THE NUCLEAR REGIONS OF Sc GALAXIES

Thesis by

Barry Edmund Turnrose

In Partial Fulfillment of the Requirements
for the Degree of
Doctor of Philosophy

California Institute of Technology
Pasadena, California

1976

(Submitted July 30, 1975)

When I heard the learn'd astronomer,
When the proofs, the figures, were ranged in columns
before me,
When I was shown the charts and diagrams, to add, divide,
and measure them,
When I sitting heard the astronomer where he lectured
with much applause in the lecture-room,
How soon unaccountable I became tired and sick,
Till rising and gliding out I wander'd off by myself,
In the mystical moist night-air, and from time to time,
Look'd up in perfect silence at the stars.

Walt Whitman

ACKNOWLEDGEMENTS

I wish to thank many people for helping to make this thesis a reality. I am most grateful to my advisor, Dr. J. B. Oke, for suggesting the topic and for his constant encouragement and sound advice throughout the entire course of the work. He generously obtained the necessary MCSP observations of the program galaxies, for which I am most appreciative. I also owe a special debt to Dr. J. E. Gunn for allowing me to use his MCSP data in advance of publication, for providing numerous computer programs to manipulate those data, and for many helpful discussions on varied aspects of stellar-population-synthesis work.

I am indebted to Dr. H. Spinrad for his unflagging interest and useful advice and for sharing much of his unpublished data with me. Dr. S. Faber generously provided detailed information regarding the use of quadratic programming in synthesis work, for which I am very grateful. This information was most useful in setting up the present synthesis program.

I am very grateful to Dr. J. N. Franklin for teaching me what linear programming I know and for helpful suggestions regarding the use of linear programming.

I am grateful to Drs. A. Toomre, L. Searle, J. L. Greenstein, M. Schmidt, W. L. W. Sargent, A. Sandage, and C. Christensen for useful discussions and ideas, and to

J. Kormendy and E. Turner for most helpful discussions regarding the interpretation of several of the present results, particularly those of Section VI b.

I wish to thank Dr. R. W. O'Connell for several helpful discussions regarding stellar spectrophotometry and for generously providing data in advance of publication.

Larry Blakee, Martin Olsiewski, Bob Cadman, and Bud Smith provided much-needed assistance with the electronics at both Palomar and Mount Wilson, and the efficient work of Gene Hancock, Jim Dittmar, John Kondratowicz, Dennis Palm, Chip Williams, and Gary Tuton made my observing runs enjoyable.

I am very grateful to the Hale Observatories for generous allotments of telescope time and for allowing me to reproduce the photographs in Figure 1 of the text.

I am also very grateful to the National Science Foundation, the ARCS Foundation, the State of California, and Mrs. Virginia Steele Scott for financial assistance in the form of fellowships during my years at Caltech.

For the friendship and ideas of many people, including Bob Kirshner, Ed Turner, John Kormendy, Steve Shectman, Gus Oemler, Ted Williams, John Huchra, Richard Green, Paul Hickson, and Richard Gott, I am most appreciative.

Special thanks are due to Helen Holloway for her expert assistance in typing nearly every table in this thesis.

Finally, I wish to express a very special personal thank-

you to my wife Kathy for bearing with me over the course of my graduate education, especially the last few hectic months, and for indispensable assistance in the preparation of the manuscript.

ABSTRACT

The stellar content of the nuclear regions of seven nearby Sc galaxies has been determined by means of population syntheses utilizing narrow-band spectrophotometric observations covering the wavelength range 3300Å-10400Å. A linear-programming fitting technique is used in conjunction with simple models of star formation to provide physically consistent population models incorporating multiple generations of stars. Evidence is found for substantial intrinsic reddening in the nuclear regions studied. Upper main-sequence stars are significant contributors in most cases, and the lower main sequence contributes insignificantly in all cases. All available indicators are consistent with M-giant-star dominance at the longest wavelengths.

Absolute measurements of the emission-line spectra of the nuclear regions are presented and discussed. The O-B stars arising naturally in the population models are found to be just sufficient to provide the observed nuclear ionization in all cases but NGC 5194, which may be collisionally ionized. The observed stellar populations are largely consistent with simple evolutionary models of star formation using a "local" initial mass function and a variety of time dependences ranging from exponential decays with time constants $\sim$3-6 billion years to constant rates. A possibly significant correlation between stellar content and dynamical properties among four of the program galaxies is pointed out.

TABLE OF CONTENTS

TABLE OF CONTENTS (continued)

I. INTRODUCTION

In recent years, techniques of empirical stellar-population synthesis have been applied by a number of authors to the problem of recovering information about the stellar content of galaxies from their integrated light (see, e.g., Tifft (1963), Wood (1966), McClure and van den Bergh (1968), Lasker (1970), Spinrad and Taylor (1971), Faber (1972), Alloin, Andrillat, and Souffrin (1971), Andrillat, Souffrin, and Alloin (1972), Alloin (1973), Joly and Andrillat (1973), Joly (1973, 1974) and O'Connell (1974).

The majority of the galaxies so studied have been ellipticals or early-type spiral systems ("k-nuclei" galaxies--see Morgan and Mayall (1957) and Morgan (1958, 1959)). The k-nuclei galaxies, although shown by Morgan and Mayall (1957) and others to be obviously composite systems, are dominated by late-type stars (main-sequence turnoff near 1 $m_{\odot}$; Spinrad and Taylor 1971, and Faber 1972) and are marked by a large degree of homogeneity. Evolutionary models of elliptical galaxies by Tinsley (1968, 1972a) and Larson and Tinsley (1974) imply that the bulk of star formation in such galaxies must have occurred within a relatively short period of time ($\sim$1-2 10^9 years) some 10^{10} years ago. It is consequently not surprising that successful stellar-population syntheses of such systems can be based on the simplifying assumptions that only a single generation of stars is present and that the distribution of the stars over type can be patterned roughly after that of old galactic clusters.

"Intermediate" type stellar systems (Morgan and Osterbrock 1969), comprising the nuclear regions and main bodies of middle and late-type spiral galaxies, present a considerably more complicated situation and their stellar content has heretofore not been studied in great detail. The integrated light of these galaxies, which belong principally to Yerkes classes f or fg , has been shown from photographic spectra to include substantial contributions from stars earlier than those found in k systems (Morgan 1958, 1959, 1962). Indeed, intermediate systems appear to be the most spectrally composite stellar systems of all (Morgan 1962). This highly-composite nature thus makes systems such as the nuclei of late-type spirals rather intriguing but at the same time somewhat difficult to study by spectral synthesis techniques, since the usual assumption of a single epoch of star formation is in this case clearly untenable. Further compounding the difficulties are the frequent occurrence of gaseous emission in the nuclei of late-type spiral galaxies and the possible presence of absorption and reddening intrinsic to the nuclei.

Despite the problems inherent in attempts to gain an understanding of the stellar content of the nuclei of late-type spiral galaxies, it seems clear that such knowledge is desirable and worth obtaining. For instance, such information could conceivably shed light on the conditions and processes governing the formation and evolution of spiral

galaxies (Saslaw 1971) and on the similarities or differences between past and present conditions in spiral and elliptical galaxies. Consequently, we have undertaken a program to recover the intrinsic stellar properties of the nuclear regions ($\sim$ inner several hundred parsecs) of several nearby Sc galaxies by means of stellar-population syntheses utilizing absolute spectral energy distributions covering the wavelength interval 3300Å-10400Å. In the following sections we describe the overall program, including our approach to the special difficulties mentioned above. Section II describes the basic stellar energy-distribution data used; Section III contains the galaxy observations, including a compilation of emission-line strengths from which the gaseous continuum radiation is inferred. Section IV describes the linear-programming synthesis procedure employed and includes discussions of the treatment of intrinsic nuclear absorption and the problem of multiple stellar generations. Sections V and VI discuss and interpret the synthesis results for all galaxies in the program, and Section VII contains a summary.

II. STELLAR DATA

a) Data Sources and Wavelengths

The spectrophotometric system employed in the present stellar-population synthesis program consists of photoelectric scanner measurements of the absolute flux density f_ν (ergs cm^{-2} sec^{-1} Hz^{-1}) calibrated on the Oke and Schild (1970) system at 66 wavelengths between 3300Å and 10680Å, with 20Å resolution for $\lambda < 5740$Å and 40Å resolution for $\lambda \geq 5740$Å. In the case of the local stellar data, for spectral types later than A3 these measurements represent data sampled from the complete spectral energy distributions of approximately 100 local stars observed by Gunn (1974) with the multichannel spectrometer (MCSP, Oke 1969) on the Palomar 5-meter Hale telescope. (The author is greatly indebted to Dr. J. E. Gunn for permission to use his MCSP data prior to publication.) Data for earlier spectral types and supergiants were unavailable from the Gunn survey and have thus been adapted from the 20Å and 30Å bandpass spectrophotometry of O'Connell (1973) as supplemented by scanner data obtained by the author (Appendix A).

The wavelengths chosen for use in the synthesis program follow closely the selections of O'Connell (1973) and Spinrad and Taylor (1971) and measure both continuum points and a number of absorption features sensitive to stellar temperature and luminosity.

Some general considerations influencing the selection of specific synthesis wavelengths have been discussed by O'Connell (1973). The close correspondence between the present system and that of O'Connell was dictated primarily by the obvious requirement of overall compatibility with his system. The total number of points included, 66, was chosen for computational convenience, although it seems unlikely that a larger number of wavelengths over the observed range would be significantly more useful inasmuch as most important absorption features are already included, and the addition of more relatively line-free points would be largely redundant.

Table 1 lists the synthesis wavelengths used, with identification of the principal absorption features. Because of the bandpass spacing of the MCSP data, exact matches with the O'Connell (1973) central wavelengths are not always possible. The wavelengths employed, however, include either all of the O'Connell wavelengths or their nearest equivalents. In the blue and ultraviolet spectral regions several adjacent wavelengths are sometimes used to measure a common feature; these extra bandpasses were included to increase the number points that could be compared with the galaxy energy distributions. (Due to galaxy redshifts, it is not in general possible to center all synthesis wavelengths with the standard observing procedure--see Section III). Other additions to the basic O'Connell system include several Fe I absorption

TABLE 1

SYNTHESIS WAVELENGTHS AND SPECTRAL FEATURES

20 Å bandpasses		40 Å bandpasses	
λ(Å)	Feature	λ(Å)	Feature
3300		5820	
3350		5900	NaI 5890,5896
3400		6100	
3450		6180	TiO
3570		6380	
3620		6560	Hα
3780		6620	
3800	H10	6800	CaH
3820	HeI 3820	7040	
3830	H9,(FeI)	7100	TiO
3840	H9,(FeI)	7400	
3860	CN	8060	
3870	CN	8180	NaI 8183,8195 (⊕ H_2O)
3890	H8	8400	
3910		8540	CaII 8542, TiO
3930	CaII K	8800	
3970	CaII H, Hε	8880	TiO
4020		9200	CN (⊕ H_2O)
4100	Hδ	9880	
4170	CN	9920	Wing-Ford band
4200	CN	9960	
4230	CaI 4227	10400	
4270		10680	
4300	CH (G-band)		
4340	Hγ		
4360			
4380	FeI 4383		
4400			
4430			
4500			
4530	FeI 4529		
4620			
4780	MgH		
4860	Hβ		
4900			
5050			
5180	MgI "b"		
5250			
5270	FeI 5269		
5300			
5330	FeI 5328		
5400	FeI 5400		
5450			

features, a point at λ6800 measuring a portion of a luminosity-sensitive CaH band in late-type stars (Fäy, Stein, and Warren 1974) and a point at λ9920 measuring the M-star luminosity-sensitive Wing-Ford band (Wing and Ford 1969). The behavior of the strengths of the absorption features included in O'Connell (1973) survey are discussed in that reference; the behavior of all feature strengths in the present survey is summarized by the series of diagrams in Appendix C.

b) Averaged Synthesis Groups

The MCSP stellar data of Gunn (1974) were gathered into 25 distinct groupings of stars of similar temperature and luminosity, and reduced to a single average energy distribution for each group. In the grouping process, some consideration of the existing spectral types of individual stars was made, but the primary criterion was overall similarity of energy distributions. (The de-reddening of individual energy distributions was effected by means of the Whitford law and a model for the distribution of dust in the Galaxy (Gunn 1974), a procedure expected to be at least statistically valid.)

No metal-poor groups are included. A number of strong-lined K giant stars have been put in groups apart from the normal giant stars. The strong-lined stars in these groups (many of them M67 giants) are not the same bright "SMR"

stars observed by Spinrad and Taylor (1971); a number of them, however, were included in an earlier study by Spinrad and Taylor (1969) and thus their important feature strengths may be directly compared with those of the SMR stars. The blocking fractions tabulated by Spinrad and Taylor (1969) indicate that the strong-lined stars in the present sample are rather similar to the Spinrad-Taylor SMR stars. In view of Griffin's (1975) recent analysis indicating low metal abundances in the M67 giant IV-202 (a member of our reddest strong-lined group) and the previous history of controversy over the interpretation of the "SMR" phenomenon, we conservatively denote the strong-lined groups by "SL".

In addition to the 25 synthesis groups formed from the Gunn MCSP data, a total of 9 additional groups representing the upper main sequence and blue and red supergiants were taken in slightly modified form from the O'Connell (1973) survey. A discussion of the procedures used to adapt the O'Connell data, along with complete lists of the member stars in each synthesis group and the adopted average group energy distributions, is given in Appendix B.

Table 2 lists the adopted masses and absolute V-magnitudes for each of the 34 synthesis groups. These intrinsic properties were drawn from a number of sources, including Schmidt-Kaler (1965), Blaauw (1963), Keenan (1963), Harris, Strand, and Worley (1963), Stothers (1972a), Veeder (1974), Spinrad and Taylor (1971), Faber (1972), Morton and

TABLE 2

MEAN SYNTHESIS-GROUP PROPERTIES

GROUP NO.	NAME	M_V	$m/m_\odot$
1	O5-9 V	-5.2	20.
2	B1-3 V	-2.8	8.2
3	B5 V	-1.0	4.8
4	B8-9 V	0.2	3.2
5	A0-3 V	1.3	2.3
6	A4-5 V	2.1	1.9
7	A7-F0 V	2.6	1.7
8	F1-5 V	3.4	1.4
9	F6-8 V	4.2	1.1
10	G0-5 V	4.8	1.0
11	G8 V	5.5	0.85
12	K0-2 V	6.2	0.80
13	K3-5 V	7.1	0.70
14	K7 V	8.0	0.60
15	M0 V	8.9	0.55
16	M1-4 V	10.7	0.35
17	M5-6 V	13.0	0.20
18	M7-8 V	15.4	0.10
19	F5-8 IV	2.7	1.3
20	G0-4 IV	3.1	1.1
21	G5-8 IV	3.2	1.1
22	K0-2 IV	3.2	1.1
23	G5-K1 III	1.4	1.5
24	K2-5 III	0.5	1.5
25	K0-1 III SL	1.7	1.2
26	K2-3 III SL	1.1	1.2
27	K4-5 III SL	0.7	1.2
28	M0-1 III	-0.4	1.5
29	M2-5 III	-0.7	1.5
30	M6-8 III	-0.7	1.5
31	B0-1 I	-6.3	15.
32	B5-7 I	-6.3	15.
33	A2 I	-6.3	15.
34	M1-4 I	-5.6	15.

Adams (1968), O'Connell (1970) and Greenstein (1975). The mean group energy distributions in the present study have all been normalized numerically to a common flux integral over the V-band rather than to a common monochromatic flux, so that to the extent to which they are themselves known, the broad-band absolute V magnitudes can in fact provide a rather accurate overall luminosity ranking for the groups.

III. GALAXY DATA

a) Galaxy Selection and Observations

The nuclear regions of seven nearby Sc galaxies have been observed with the MCSP for the present synthesis program. (The author is deeply indebted to Dr. J. B. Oke for his substantial investment of time and effort in obtaining these observations.) The galaxies were selected for the program by a number of criteria, including galactic latitude, inclination, previous investigations (e.g., photometry, rotation curves), and nuclear surface brightness. Table 3 lists the following pertinent properties of the observed galaxies:

Col. (1). van den Bergh type and luminosity class (van den Bergh 1960a,b).

Col. (2). Yerkes form classification (Morgan 1958, 1959).

Col. (3). Byurakan nuclear classification (Iskudaryan 1968).

Col. (4). Galactic latitude in degrees.

Col. (5). Adopted B-V color excess (Galactic) calculated from the Sandage (1973) reddening-free polar cap model.

Col. (6). Observed velocity w.r.t. ⊙ in km/sec. Mean of values given by Sandage and Tammann (1975) or Humason, Mayall and Sandage (1956) and velocities measured from image tube spectra obtained by the author.

Col. (7). Velocities in km/sec corrected for galactic rotation in the sense $V_o = V + 300\ (\sin \ell)(\cos b)$.

Col. (8). Assumed distance in Mpc, calculated from the systemic velocities using $H_o = 55$ km/sec/Mpc (Sandage and Tammann 1975). In the case of NGC 1073, NGC 1084, NGC 4321, and NGC 5194, the mean velocities appropriate to the groups in which these galaxies are found are used (Sandage and Tammann 1975). In the case of NGC 2903, the mean optical and radio systemic velocity adopted by Simkin (1975) is used.

Col. (9). Integrated absolute photographic magnitudes on the Holmberg (1958) system, corrected for galactic absorption and inclination as in Sandage and Tammann (1974) and using the distance r from Col. 8. For NGC 1084, an equivalent magnitude is calculated from the de Vaucouleurs B(0) magnitude (de Vaucouleurs and de Vaucouleurs 1964) by the relation quoted in Sandage and Tammann (1974).

Col. (10). Assumed inclination (angle between plane of galaxy and the line of sight). Wherever possible, the values given are means of the inclination computed from the Sandage and Tammann (1974) geometrical formula and the inclination given by the rotation-curve references. In degrees.

Col. (11). Total mass, estimated from rotation curves or HI profiles, and referred to the distances of Col. 8 and the inclinations of Col. 10. References are given in the footnotes. In solar units.

Col. (12). Total photographic mass-to-light ratio in solar units, from columns 11 and 9, assuming $M_{pg}(\odot) = +5.37$ (Stebbins and Kron 1957).

Col. (13). Scanner aperture diameter in arc sec.

Col. (14). Axes, in pc, of the ellipse defining the nuclear region observed (scanner aperture projected onto the plane of the galaxy) calculated from the inclinations of Col. 10, the distances of Col. 8, and the apertures of Col. 13.

Figure 1 contains prints of short-exposure direct photographs of the program galaxies, taken from the plate files of the Hale Observatories. All of the galaxies have been discussed by Sandage (1961) and are reproduced here at a uniform plate scale in order to illustrate the nature of their central regions. In the case of NGC 2903, the brightest knot, indicated on the print, was centered in the 7 arc sec scanner aperture. (See also Figure 1b in Simkin 1975). For all other galaxies, the nuclear region observed is unambiguous.

The rest-frame spectral energy distributions of the program galaxies are shown in Figure 2, corrected for galactic reddening according to the Whitford law (Miller and Mathews 1972) and the color excesses assumed in Table 3. With a few exceptions, the galaxies have been observed at 20/40Å resolution with complete spectral coverage over the range 3300-10400Å. The exceptions are NGC 628 for which only selected bandpasses were observed, NGC 5194 for which coverage is incomplete due to a temporary data-system failure at the time of observation, and NGC 2903 for which extra bandpasses in excess of complete coverage were observed. For all galaxies but NGC 1073, which with an observed equivalent

TABLE 3

PROPERTIES OF PROGRAM GALAXIES

NGC	L_c (1)	Y (2)	B (3)	b^{II} (4)	E(B-V) (5)	V_{obs} (6)	V_o (7)	r (8)	M_{pg}^{oi} (9)
628	Sc I	fgS1	2	-45.70	0.01	658	797	14.5	-21.12
1073	S(B)c II	afB1,fB1	...	-50.71	0.00	1198	1228	24.2	-20.50
1084	Sc I-II	aS4	2	-56.56	0.00	1422	1415	24.2	-20.96
1637	Scn	fS2,fS3	4	-30.02	0.03	693	606	11.0	-19.14
2903	Sb^+ I-II	fS4	2s	44.54	0.01	580	477	7.8	-20.31
4321	Sc I	fgS1	...	76.90	0.00	1555	1487	20.2	-21.48
5194	Sc(t) I	fS1,fgS1	4	68.56	0.00	464	570	11.0	-21.48

TABLE 3 (continued)

NGC	i (10)	M_{tot} (11)	M_{tot}/L_{pg} (12)	Ap (13)	Region (14)
628	62	1.5 (11)	3.8	10	703,796
1073	72	...	...	7	821,863
1084	27	2.1 (10)	0.6	7	821,1808
1637	56	2.7 (10)	4.2	7	373,450
2903	22	5.0 (10)	2.7	7	265,707
4321	62	9.0 (10)	1.6	7	686,777
5194	55	8.1 (10)	1.5	7	373,455

References for rotation curves and/or total masses:

NGC 628: Epstein (1964); Rogstad, Rougoor, and Whiteoak (1967)
NGC 1084: Burbidge, Burbidge, and Prendergast (1963)
NGC 1637: Roberts (1969)
NGC 2903: Burbidge, Burbidge, and Prendergast (1960); Simkin (1975)
NGC 4321: van der Kruit (1973)
NGC 5194: Burbidge and Burbidge (1964); Rogstad et al. (1967); Tully (1974)

FIGURE 1.

Short-exposure direct photographs of the nuclear regions of the program galaxies, reproduced from plates from the Hale Observatories files. All prints are shown at a uniform scale as indicated. NGC numbers are given on each print, and in the case of NGC 2903 the knot observed is indicated by an arrow. North is at the top, east is to the left.

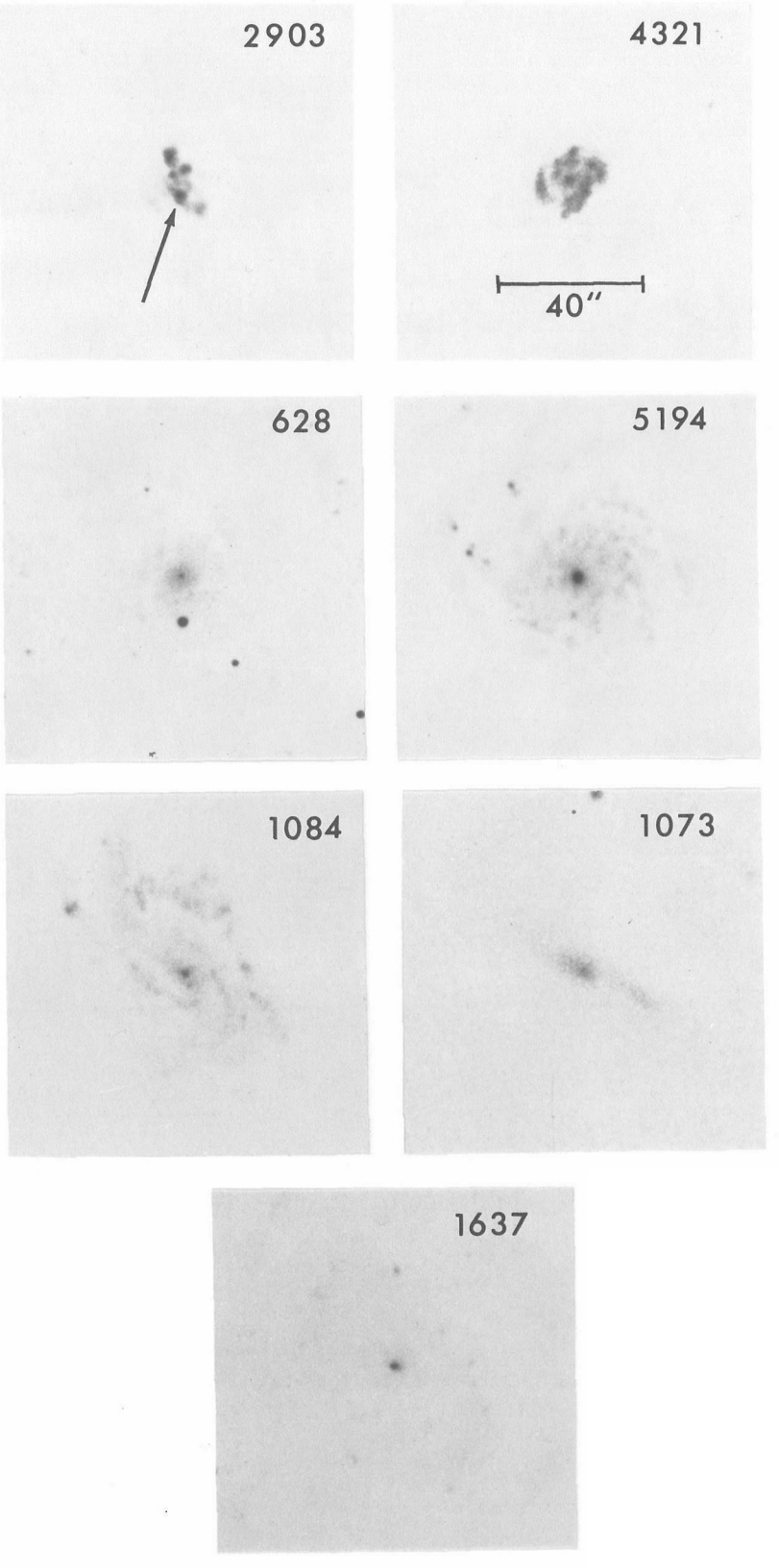

FIGURE 1

FIGURE 2

Absolute spectral energy distributions of the program galaxies: log f_ν (ergs cm^{-2} sec^{-1} Hz^{-1}) versus log ν in Hz. The data have been corrected for galactic reddening and referred to the individual rest frames by means of the color excesses and observed radial velocities in Table 3. The zero points in log f_ν have been marked at the left-hand margin for each galaxy. The positions of prominent absorption features and the Hα + [NII] emission lines are marked at the bottom of the figure for reference. Strong telluric H_2O absorption is visible in the λ9300 region for most galaxies.

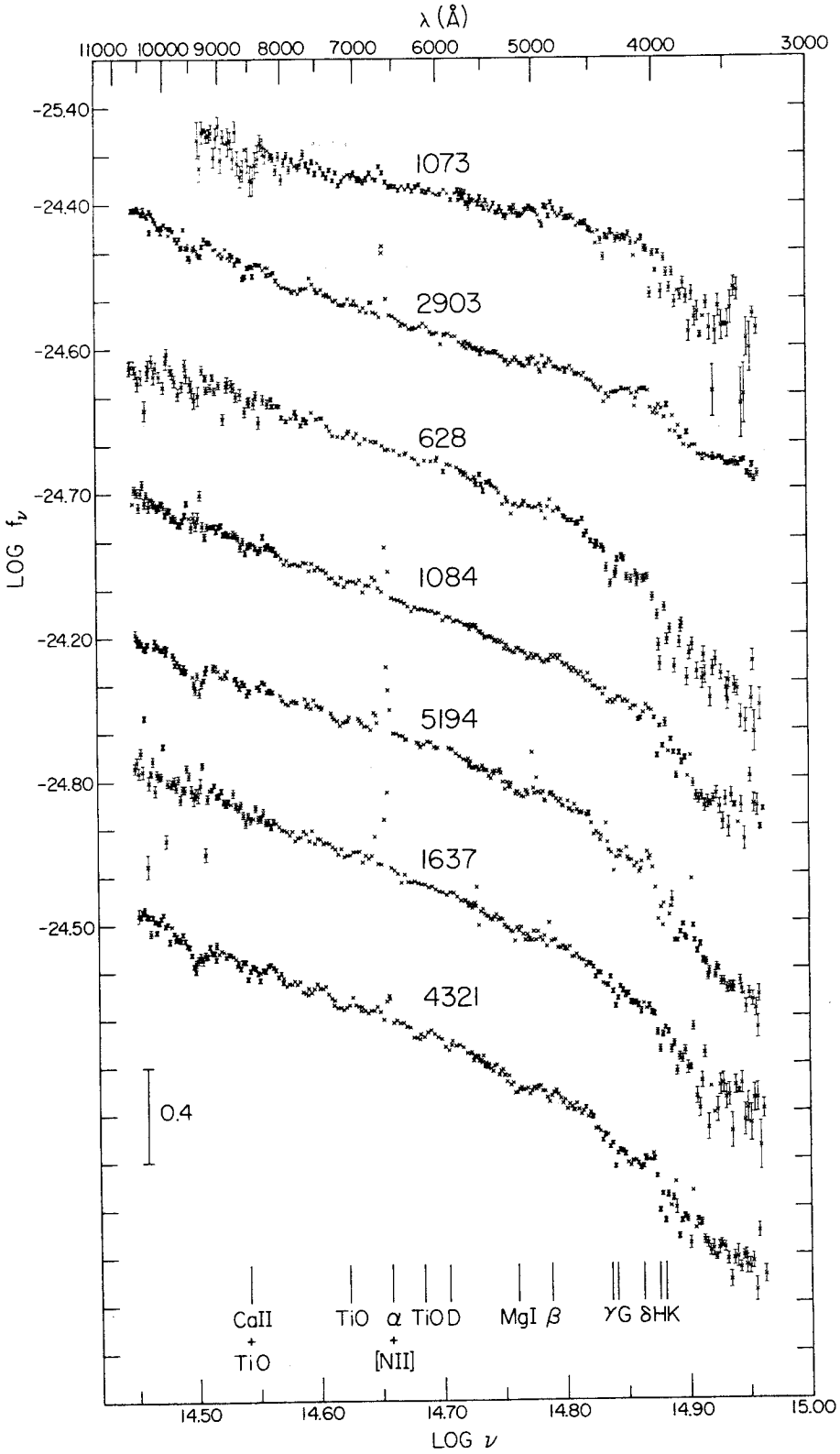
λ (Å)
11000 10000 9000 8000 7000 6000 5000 4000 3000
-25.40
-24.40
-24.60
-24.70
-24.20
-24.80
-24.50
LOG f_ν
1073
2903
628
1084
5194
1637
4321
0.4
CaII + TiO
TiO
α + [NII]
TiO
D
MgI
β
γG
δHK
14.50
14.60
14.70
14.80
14.90
15.00
LOG ν

FIGURE 2

V-magnitude within the 7 arc sec aperture of about 16.0 is the faintest galaxy in the program, the statistical uncertainties in the flux measurements are approximately 1 percent over the range $5000\text{Å} \leq \lambda \leq 8000\text{Å}$ and somewhat larger as the ends of the observed spectral region are approached (see Figure 2). The best points for NGC 1073 are uncertain by 2-3 percent; the extreme ultraviolet and red regions for this galaxy have very large uncertainties and have been excluded.

NGC 1084 was observed in the normal star/sky chopper mode, which provides the advantage of simultaneous sky subtraction. The small (40 arc sec E-W) separation of the two MCSP apertures, however, prohibited the use of the chopping system in the larger galaxies, and for all others separate sky measurements were made by offset to a region well outside the galaxy. Such a procedure is unfortunately subject to some inherent inaccuracies, as the energy distribution of NGC 1637 illustrates: the four pairs of isolated points appearing substantially above and below the actual flux levels occur in regions where the airglow spectrum is strong (see Turnrose 1974) and are caused by a change in that spectrum between the time of the "galaxy" and the "sky" measurements, a period of less than ten minutes. Imperfect sky subtraction is also apparent at the wavelengths of the ultraviolet artificial Hg lines near λ3660.

In several instances, systematic changes in the sensitivity of one or two MCSP channels were apparent. These drifts were usually easily detectable and could be well compensated by small ($\leq$ 0.10 mag.) corrections applied to the affected channels. Such corrections have been applied to the wavelength region $4200\text{Å} \lesssim \lambda \lesssim 4370\text{Å}$ for NGC 2903, NGC 4321, and NGC 5194, and to the wavelength region $5600\text{Å} \lesssim \lambda \lesssim 6000\text{Å}$ for NGC 1084, NGC 1637, and NGC 2903.

Table 4 lists the galaxy synthesis-wavelength magnitudes ($-2.5 \log f_\nu$ + const.) normalized to 0.0 at λ5450 and corrected for galactic reddening, along with the estimated fractional accuracies. All wavelengths have been referred to the galaxy restframes. Also listed is the observed flux at λ5450, expressed as an AB magnitude: $AB \equiv -2.5 \log f_\nu - 48.60$. The constant is such that $AB(\lambda 5450) \simeq V$ magnitude (see Oke and Schild 1970). For each of the galaxies except NGC 5194, the contribution to the observed energy distribution from gaseous continuum radiation has been removed as described in Section IIIc.

None of the galaxies has measurements at all of the 66 stellar wavelengths: because of the galaxy redshifts, it is impossible to center all the synthesis bandpasses without prohibitively long observing times, and a practical limit of about 5Å in the case of 20Å bandpasses (10Å for the first-order 40Å bandpasses) was set on the allowable centering error for points containing absorption features. Thus,

TABLE 4

NORMALIZED MAGNITUDES AT SYNTHESIS WAVELENGTHS FOR PROGRAM GALAXIES, CORRECTED FOR GALACTIC ABSORPTION

	NGC 628		NGC 1073		NGC 1084	
λ (Å)	MAG.	σ	MAG.	σ	MAG.	σ
3300	...	...	...	...	...	...
3350	2.44	0.15	...	...	...	...
3400	2.10	0.10	...	..	2.06	0.15
3450	2.01	0.10	1.37	0.15	1.78	0.15
3570	2.04	0.10	1.14	0.15	1.83	0.07
3620	1.85	0.10	1.35	0.15	1.90	0.07
3780	1.45	0.06	0.99	0.10	1.30	0.10
3800	...	...	1.10	0.08	...	...
3820	...	...	...	...	...	...
3830	1.86	0.06	0.95	0.05	1.48	0.03
3840	...	...	...	...	...	...
3860	1.47	0.05	...	...	...	...
3870	...	...	0.64	0.05	1.10	0.03
3890	...	...	1.00	0.04	1.23	0.03
3910	1.24	0.07	0.59	0.04	0.92	0.03
3930	1.84	0.04	0.78	0.04	1.17	0.03
3970	...	...	1.01	0.04	1.27	0.03
4020	0.93	0.04	0.49	0.04	0.78	0.02
4100	0.99	0.04	0.64*	0.06	0.90*	0.05
4170	0.94	0.04	0.42	0.04	0.77	0.02
4200	0.74	0.04	0.43	0.04	0.68	0.02
4230	...	...	0.45	0.04	0.69	0.02
4270	0.90	0.04	0.37	0.03	0.64	0.02
4300	1.00	0.04	...	...	0.70	0.04
4340	0.83	0.04	0.65*	0.08	0.70*	0.04
4360	0.64	0.03	0.36	0.03	0.55	0.02
4380	0.61	0.03	0.49	0.05	0.61	0.03
4400	0.59	0.03	0.38	0.03	0.56	0.02
4430	0.61	0.03	0.35	0.03	0.56	0.02
4500	0.45	0.03	0.28	0.03	0.39	0.02
4530	...	...	0.28	0.03	0.47	0.05
4620	0.33	0.02	0.22	0.03	0.34	0.02
4780	0.24	0.02	...	...	0.20	0.02
4860	0.31	0.03	0.32*	0.06	0.25*	0.02
4900	0.18	0.02	0.17	0.03	0.26	0.02

TABLE 4 (continued)

	NGC 628		NGC 1073		NGC 1084	
λ (Å)	MAG.	σ	MAG.	σ	MAG.	σ
5050	0.13	0.02	0.18	0.03	0.20	0.02
5180	0.26	0.02	...	...	0.16	0.02
5250	0.09	0.03	0.10	0.02	0.08	0.03
5270	0.16	0.04	0.16	0.02	...	...
5300	0.04	0.02	0.06	0.02	0.04	0.01
5330	-0.02	0.02	0.10	0.02	...	...
5400	...	...	0.11	0.03	-0.01	0.01
5450	0.00	0.04	0.00	0.03	0.00	0.01
5820	-0.26	0.02	-0.08	0.03	-0.21	0.01
5900	-0.18	0.04	0.00	0.05	-0.18	0.01
6100	-0.30	0.02	-0.12	0.03	-0.30	0.01
6180	-0.26	0.04	-0.07	0.03	-0.30	0.01
6380	-0.36	0.02	-0.12	0.03	-0.39	0.01
6560	-0.41*	0.02	-0.27*	0.03	...	...
6620	-0.47	0.02	-0.19	0.03	-0.49	0.01
6800	-0.53	0.03	-0.17	0.05	-0.55	0.02
7040	-0.59	0.02	-0.22	0.03	-0.60	0.01
7100	-0.54	0.01	-0.14	0.03	-0.55	0.01
7400	-0.75	0.01	-0.35	0.04	-0.73	0.01
8060	-0.88	0.02	-0.45	0.04	-0.90	0.03
8180	-0.90	0.10	...	...	-0.99	0.10
8400	-0.90	0.05	...	...	-0.99	0.03
8540	-0.81	0.05	...	...	-0.91	0.03
8800	-1.11	0.06	-0.59	0.15	-1.11	0.03
8880	...	...	...	...	-1.11	0.03
9200	-1.17	0.10	...	...	-1.08	0.10
9880	-1.37	0.20	-0.74	0.25	-1.36	0.04
9920	-1.33	0.20	...	...	-1.32	0.04
9960	...	...	-0.77	0.25	-1.41	0.04
10400	-1.17	0.10	-0.82	0.25	-1.55	0.04
10680	...	...	...	...	...	...
AB(λ5450) =	14.37		15.87		14.70	

TABLE 4 (continued)

	NGC 1637		NGC 2903		NGC 4321	
λ (Å)	MAG.	σ	MAG.	σ	MAG.	σ
3300	...	...	1.41	0.04	...	...
3350	...	...	1.24	0.04	2.19	0.08
3400	...	...	1.27	0.04	2.14	0.08
3450	...	...	1.29	0.02	2.11	0.08
3570	2.32	0.15	1.22	0.02	2.10	0.06
3620	...	...	1.22	0.02	1.98	0.06
3780	1.47	0.05	0.83	0.02	1.62	0.06
3800	1.55	0.05	0.89	0.02	...	...
3820	1.53	0.05	0.72	0.03	...	...
3830	...	...	...	...	1.82	0.03
3840	1.68	0.05	0.88	0.03	...	...
3860	1.38	0.04	0.61*	0.10	1.23*	0.03
3870	...	...	...	...	1.41*	0.03
3890	...	...	...	...	1.50	0.03
3910	1.21	0.05	0.60	0.03	1.38	0.03
3930	...	...	0.70	0.02	1.65	0.09
3970	...	...	...	...	1.54	0.03
4020	1.05	0.03	0.44	0.02	0.99	0.03
4100	1.04*	0.03	0.62*	0.02	...	...
4170	0.95	0.03	0.44	0.03	1.01	0.02
4200	0.85	0.03	0.43	0.03	1.04	0.02
4230	...	...	0.46	0.03	0.91	0.05
4270	0.84	0.03	0.47	0.03	0.90	0.05
4300	0.98	0.03	0.53	0.03	1.07	0.05
4340	0.67*	0.03	0.57*	0.03	0.86*	0.05
4360	0.76	0.03	0.42	0.03	0.73	0.02
4380	0.75	0.02	0.46	0.01	0.73	0.03
4400	0.74	0.02	0.43	0.01	0.79	0.03
4430	0.62	0.02	0.39	0.03	0.69	0.02
4500	0.53	0.02	0.27	0.01	0.51	0.02
4530	0.55	0.04	...	...	0.54	0.02
4620	0.42	0.02	0.19	0.01	0.43	0.02
4780	0.35	0.02	0.15	0.01	0.30	0.01
4860	0.09*	0.02	0.08*	0.01	0.38*	0.03
4900	0.23	0.02	0.15	0.01	0.26	0.01

TABLE 4 (continued)

	NGC 1637		NGC 2903		NGC 4321	
λ(Å)	MAG.	σ	MAG.	σ	MAG.	σ
5050	0.23	0.02	0.18	0.01	0.29	0.01
5180	0.27	0.02	0.17	0.01	0.28	0.01
5250	0.13	0.01	0.08	0.01	0.10	0.01
5270	...	...	...	...	0.16	0.02
5300	0.05	0.01	0.03	0.01	0.03	0.01
5330	0.05	0.01	...	...	...	...
5400	0.05	0.01	0.04	0.01	0.05	0.01
5450	0.00	0.01	0.00	0.02	0.00	0.01
5820	-0.24	0.01	-0.17	0.01	-0.28	0.01
5900	-0.22	0.03	-0.06	0.01	-0.18	0.05
6100	-0.32	0.02	-0.26	0.02	-0.37	0.01
6180	-0.34	0.02	-0.22	0.02	-0.31	0.02
6380	-0.40	0.04	-0.32	0.02	-0.47	0.01
6560	-1.31*	0.01	-1.08*	0.01	-0.76*	0.01
6620	-0.54	0.02	-0.36	0.01	-0.51	0.01
6800	-0.61	0.02	-0.42	0.03	-0.60	0.02
7040	-0.64	0.01	-0.49	0.01	-0.68	0.03
7100	-0.63	0.01	-0.47	0.01	-0.64	0.01
7400	-0.77	0.01	-0.61	0.01	-0.84	0.02
8060	-0.97	0.02	-0.81	0.02	-0.96	0.02
8180	...	...	...	...	-1.09	0.10
8400	-1.05	0.04	-0.89	0.02	-1.03	0.03
8540	-1.00	0.05	-0.76	0.05	-0.95	0.03
8800	-1.21	0.04	-1.07	0.03	-1.20	0.03
8880	-1.20	0.04	-1.03	0.03	-1.18	0.04
9200	-1.26	0.10	-1.10	0.12	...	...
9880	-1.41	0.04	-1.33	0.03	-1.52	0.04
9920	-1.43	0.04	-1.30	0.03	...	...
9960	...	...	-1.29	0.03	-1.51	0.03
10400	-1.55	0.05	-1.50	0.03	-1.66	0.03
10680	...	...	...	...	...	...
AB(λ5450) =	14.86		13.96		14.18	

TABLE 4 (continued)

NGC 5194		
λ (Å)	MAG.	σ
3300	2.52	0.07
3350	2.36	0.07
3400	2.28	0.06
3450	2.30	0.06
3570	2.17	0.06
3620	2.11	0.05
3780	1.64	0.03
3800	1.72	0.03
3820	1.74†	0.05
3830	1.87†	0.05
3840	1.87†	0.05
3860	1.38*	0.03
3870	1.43†*	0.05
3890	1.53	0.05
3910	1.38†	0.05
3930	1.65	0.02
3970	1.58	0.04
4020	1.92	0.02
4100	1.09*	0.02
4170	0.96	0.02
4200	0.88	0.04
4230	0.94†	0.05
4270	0.86	0.04
4300	1.07	0.04
4340	0.85*	0.04
4360	0.57*	0.04
4380	0.73†	0.05
4400	0.70	0.01
4430	0.68	0.01
4500	0.46	0.01
4530	0.51†	0.05
4620	0.37	0.01
4780	0.31	0.01
4860	0.36†*	0.05
4900	0.23	0.01

TABLE 4 (continued)

λ(Å)	NGC 5194 MAG.	σ
5050	0.23	0.01
5180	0.38†	0.05
5250	0.13	0.01
5270	0.23†	0.03
5300	0.03	0.01
5330	0.03†	0.05
5400	0.08	0.01
5450	0.00	0.01
5820	-0.22	0.01
5900	-0.16†	0.05
6100	-0.31	0.02
6180	-0.27	0.02
6380	-0.37	0.02
6560	-1.09*	0.01
6620	-0.43	0.02
6800	-0.47	0.02
7040	-0.57	0.01
7100	-0.52	0.01
7400	-0.67	0.01
8060	...	...
8180	...	...
8400	-0.92	0.03
8540	-0.81	0.03
8800	-1.03	0.03
8880	-1.04	0.03
9200	-1.10	0.12
9880	...	...
9920	-1.30	0.03
9960	-1.32	0.03
10400	-1.35	0.03
10680	...	...

AB(λ5450) = 13.32

† Taken from photographic spectra of Williams (1975).

* Not used in synthesis fitting procedure.

feature bandpasses miscentered by more than this amount were rejected, and those miscentered by more than about 2Å in a 20Å bandpass (4Å in the first-order) were assigned progressively larger uncertainties. Considerably more latitude was granted in the case of continuum wavelengths, where even short-range interpolations were permitted with only slight increases in assigned uncertainty. The assigned fractional accuracies listed in Table 4 as σ have been estimated both from the smoothed random uncertainties of photon statistics (which are recoverable from the general trends with wavelength) and the systematic uncertainties introduced by bandpass miscentering.

In Table 4 we have indicated by an asterisk those data points omitted from the synthesis fitting procedure to be described in Section IV. In all cases, the reason for omission of a point was the apparent, or in the case of higher Balmer-series members, expected, presence of a gaseous emission line. Aside from the Balmer lines Hα through Hδ, these emission lines include [NeIII] λ3869 in several galaxies and apparent [OIII] λ4363 in NGC 5194 (see Section IIIb). The NGC 5194 points marked by a dagger have been derived differentially with respect to neighboring points from calibrated image-tube spectra obtained with the Palomar 1.5-meter telescope by T. Williams (1975) and very kindly made available to the author in advance of publication. These points fill in omissions in the MCSP data and in some cases have been

used to estimate corrections for large bandpass miscenterings. They have uniformly been assigned fractional errors of 5 percent, in view of the inherent photographic uncertainties and with allowance for possible additional uncertainties due to the fact that the spectrograph slit in this case accepted light from a region only about one-half the linear size of the scanner aperture. The NGC 1073 points at wavelengths larger than 8400Å represent average extrapolations based on a comparison with a MCSP scan with a 14 arc sec aperture kindly obtained for the author by J. E. Gunn; accordingly, large uncertainties have been assigned these 4 points.

b) Gaseous Emission Lines

Gaseous emission lines of the elements H, N, O, and S are observed in each of the nuclear regions studied, with the exception of NGC 628. Given the broad spectral coverage of the MCSP data, it is possible to measure the absolute intensities of most of the prominent emission lines. The line strengths so determined are listed in Table 5 in absolute flux units along with their estimated uncertainties and the equivalent widths of the emission lines in Å. The energy distributions from which these strengths are determined have been corrected only for the (small) assumed Galactic reddenings listed in Table 3 of Section IIIa. It is clear both from the listed equivalent widths and Figure 2 that many of the lines are very weak relative to the underlying stellar continuum. As a result, the uncertainties in line strengths

TABLE 5

OBSERVED EMISSION-LINE STRENGTHS CORRECTED FOR GALACTIC ABSORPTION

LINE		NGC 1073 7 arcsec f*	EW(Å)	NGC 1084[1] 7 arcsec f	EW(Å)	NGC 1637 7 arcsec f	EW(Å)
λ9532	[SIII]	...	...	...	...	73.7 ±18	15.5
λ9069	[SIII]	...	...	...	...	17.6 ±11	3.5
λλ6731+6717	[SII]	3.0 ±2.3	2.3	33.1[4]± 5.0	6.2	56.2[6]± 2.8	11.7
Hα+[NII]		12.3 ±3.1	9.1	169.0 ± 8.5	32.8	303.0 ± 9.1	64.0
λ6583	[NII]	...	...	31.8[5]± 8.0	6.2	107.0[2]±11	22.6
λ6583	Hα	12.3[2]±3.1	9.1	127.0[5]±32.0	24.6	160.0[2]±16	33.8
λ6548	[NII]	...	...	10.6[5]± 2.7	2.0	36.0[2]± 3.6	7.6
λ5007	[OIII]	...	...	3.8 ± 2.1	0.8	7.0 ± 1.7	1.8
λ4959	[OIII]	...	...	...	...	5.1[3]± 1.8	1.2
λ4861	Hβ	...	...	...	...	16.2 ± 1.6	3.9
λ4340	Hγ	...	...	...	...	7.3 ± 2.2	2.2
λ3727	[OII]	7.2[3]±4.3	5.7	13.9 ± 2.8	5.4	23.5[3]± 5.9	12.8

*All fluxes are measured in units of 10^{-15} ergs $cm^{-2}sec^{-1}$ and are the observed strengths corrected only for absorption within the Galaxy. Dotted lines indicate that emission was not detected; solid lines indicate that the appropriate observations were not made. (NGC 628 is excluded from the table since no emission was detected in the observed bandpasses; λλ9532, 6731, 6717, 5007, and 4959 were not observed in this galaxy, however.)

TABLE 5 (continued)

LINE		NGC 2903 7 arcsec f	EW(Å)	NGC 4321 7 arcsec f	EW(Å)	NGC 5194 7 arcsec f	EW(Å)
λ9532	[SIII]	62.8 ±16.0	7.2	...	...	—	—
λ9069	[SIII]	15.6 ±11.0	1.6	...	...	...	...
λλ6731+6717	[SII]	36.2[7]± 5.4	4.0	40.3 ± 8.1	4.7	171.0 [8]±17.0	10.1
Hα+[NII]		412.0 ±12.0	44.2	156.0 ± 9.4	18.4	766.0 [9]±38.0	43.8
λ6583	[NII]	107.0[2]±11.0	11.4	41.8[2]± 5.0	5.0	425.0[10]±64.0	24.4
λ6563	Hα	269.0[2]±27.0	28.8	100.0[2]±12.0	11.8	170.0[10]±26.0	9.7
λ6548	[NII]	36.0[2]± 3.6	3.8	13.9[2]± 1.7	1.7	170.0[10]±26.0	9.7
λ5007	[OIII]	8.4[3]± 5.9	0.8	4.1[3]± 3.1	0.6	168.0 ±17.0	10.2
λ4959	[OIII]	6.4[3]± 5.7	0.6	...	...	49.8 ± 5.0	3.0
λ4861	Hβ	29.7 ± 5.9	3.0	...	...	—	—
λ4340	Hγ	...	...	...	...	...	...
λ3727	[OII]	23.1[3]± 4.6	2.9	34.0[3]± 3.4	10.6	113.0 [9]±11.3	15.8

Notes:

1. Observed with star/sky chopping system.
2. Photographic resolution of Hα and [NII] from calibrated spectra by the author.
3. Placement of continuum level uncertain.
4. I(λ6731)/I(λ6717) = 1.0±0.3 from photographic spectra by the author.
5. Photographic resolution of Hα and [NII] from uncalibrated spectrum (Searle 1974).
6. I(λ6731)/I(λ6717) = 0.94±0.1 from photographic spectra by the author.
7. I(6731)/I(6717) = 1.2±0.2 from photographic spectra by the author.
8. I(6731)/I(6717) = 0.83±.08 for central 2.5 arcsec from Warner (1973) and 0.96±0.1 from spectra by Williams (1975).
9. Lower limit to line flux due to incomplete spectral coverage.
10. Photoelectric resolution of Hα and [NII] from Peimbert (1968).

are often rather large.

In the cases of the closely-spaced lines of [SII] at λλ6717 and 6731 and the Hα + [NII] λ6548,6563,6583 group, the MCSP resolution is sufficient to measure only the total intensity of emission. Wherever possible, these groupings have been resolved by means of calibrated image-tube slit spectra obtained by the author at the Palomar 1.5-meter telescope or by means of measurements from other sources. In such cases the total intensity of the group of lines is better determined than the intensities of the individual components.

The Hα + [NII] combination is the strongest emission feature present in each case. With the exception of NGC 5194, which is considered separately below, the overall run of line strengths in the galaxies studied is similar to that in low-excitation HII regions (see Peimbert and Costero 1969; Searle 1971). In particular, [OIII] λ5007 + λ4959 is very weak or absent. The total strength of the [SII] lines tends to be somewhat greater relative to Hα ($I([SII])/I(H\alpha) \sim 0.13$ to 0.40) than in galactic HII regions ($I([SII])/I(H\alpha) \lesssim 0.1$) (Peimbert and Costero 1969), but not so large as in the supernova remnants of shockwave ionization models discussed by Mathewson and Clarke (1973) and Osterbrock and Dufour (1973) in which $I([SII])/I(H\alpha) \sim 1.0$. [OI] λ6300 is not detected at all, whereas this line is expected to be of significant strength in shockwave models (Osterbrock 1971; Osterbrock

and Dufour 1973). The [SII] and [OI] intensities would thus appear in general to be incompatible with collisional-ionization models. In these respects, the Sc nuclei are rather similar to the peculiar emission-line galaxies discussed by Osmer, Smith, and Weedman (1974), and so for the same reasons cited in their analysis we conclude with regard to the Sc nuclei (excluding NGC 5194) that ultraviolet radiation from hot stars is the most likely principal ionization source.

Given the observed Hα intensities, Hβ is noticeably weak compared to the normal Case B radiative decrement at $T_e \sim 10^4$ °K (Pengelly 1964). In only two cases (for which $(I(H\alpha)/I(H\beta) \sim 10)$ is there any net Hβ emission visible above the local continuum at all. These small Hβ strengths are interpreted here as being primarily a result of the superposition of the Hβ emission over a significant underlying stellar Hβ absorption feature--note the considerable Balmer absorption strengths in Figure 2. This point is considered quantitatively in the discussion of the stellar-population models in Section Vd.

The emission spectrum of NGC 5194 is clearly unlike that of any of the other galaxies in the present program. The observed intensities for NGC 5194 in Table 5, while in some cases incomplete or only lower limits due to missing data, are similar to the published intensities of Peimbert (1968, 1971) with the major exception that the present

observed absolute intensity of Hα is some 20 percent greater than Peimbert's value for the same nuclear region. The present study uses Peimbert's (1968) Hα/[NII] ratio to infer the Hα strength from the total observed intensity of Hα + [NII]. The agreement of Peimbert's measurement of the continuum flux density at λ5360 with the present study rules out an overall absolute calibration discrepancy.

NGC 5194 is the only galaxy in the present program in which I([NII]) > I(Hα), and it has by far the strongest [OIII] intensities: EW (λ5007) ∿ 10Å . We measure I([SII]) ∿ I(Hα), and Peimbert (1968) has observed strong [OI] λ6300 emission. Together with the results of the stellar-population models to be discussed in Section Vc, which rule out the presence of significant numbers of unobscured O-B stars and appear to confirm Warner's (1973) detection of the [OIII] λ4363 line, these data suggest that a simple hot-star ionization model is unlikely in the case of NGC 5194.

c) Gaseous Continuum Emission

As mentioned in Section IIIa, the contribution to the observed energy distribution from gaseous continuum radiation was estimated from the observed Hα flux and subtracted for all galaxies except NGC 5194. (No corrections were attempted in the case of NGC 5194 because of the ambiguities regarding the conditions of ionization and excitation.) The expressions of Seaton (1960) for the radiative

recombination intensity of Hα emission were combined with the formulae of Brown and Mathews (1970) for the hydrogen recombination, free-free, and two-photon continuum emission to relate the expected hydrogen continuum flux density F_ν (ergs cm^{-2} sec^{-1} Hz^{-1}) for those processes to the observed Hα flux J_α (ergs cm^{-2} sec^{-1}) under the assumed average conditions of $T_e = 10^4$ °K and electron density $n_e = 10^3 cm^{-3}$:

$$F_\nu = 2.81 \times 10^{24} J_\alpha \gamma_{tot}(\nu) \text{ ergs } cm^{-2} sec^{-1} Hz^{-1} \qquad (1)$$

where $\gamma_{tot}(\nu)$ is an interpolated emission coefficient defined in Brown and Mathews (1970) and where we have used an effective Hα recombination coefficient $\alpha_{3,2} = 1.17 \times 10^{-13}$ $cm^3 sec^{-1}$ (Pengelly 1964).

The inferred corrections to the galaxy energy distributions are important only in the region below the Balmer jump and they are largest relative to the observed continuum when no reddening intrinsic to the galaxies is presumed. In this case, the correction is greatest for NGC 1637, where at λ3620 the observed flux density is revised downward by 25 percent (20 percent at λ3570). NGC 1084 has a correction of 11 percent at λ3620, and NGC 2903 has a correction of 7 percent at λ3620. (This last correction is roughly one-third of the amount suggested by Alloin (1973) for the central 3" of NGC 2903. The reasons for this discrepancy are unclear, however, inasmuch as the Hα emission equivalent width and continuum energy distribution observed by Alloin (1973) are

similar to our results.) For all other galaxies, the largest inferred corrections at $\lambda 3620$ are $\lesssim$ 5 percent.

IV. SYNTHESIS PROCEDURE

a) General Approach

The actual methods of synthesis used in previous stellar-content investigations have ranged from simple trial and error to the more objective quadratic-programming approach of Faber (1972), who has demonstrated the advantages of the latter procedure over earlier techniques. In the present work we have used a linear-programming approach to the synthesis problem similar to that employed by O'Connell (1974). The reasons for this choice are briefly outlined below.

It is clear from the work of previous authors that in order to obtain physically meaningful solutions to stellar-population-synthesis problems, it is necessary to impose continuity constraints on the resulting distribution of stars in the H-R diagram (Spinrad and Taylor 1971; Faber 1972). Analytical methods of solution fail because they cannot deal properly with either these continuity constraints, or with the fundamental restriction to nonnegative numbers of stars, or both. Hybrid trial-and-error semi-automatic synthesis methods to find the "best-fit" solutions (Christensen 1972; Joly 1974) suffer from the fact that the investigator must choose an initial solution. Because there apparently may be a number of local minima of the function chosen to represent the deviation of the synthetic model from

the observations (Christensen 1972), the final "best" solution is in general dependent on the exact initial solution chosen (Joly 1974); i.e., one seldom ends up very far from one's starting point. There is consequently no guarantee that a global minimization has been achieved. Pure trial and error methods are of course even more limited in this respect (Faber 1972).

Solution schemes using either quadratic or linear programming have the advantage of yielding best-fitting solutions which are global within the context of the assigned continuity constraints and the restriction to nonnegative variables. We have adopted a linear fitting criterion (described in Section IVb) in favor of the quadratic approach of Faber (1972). The usual motivations for a least-squares type of fitting procedure are largely historical and may in fact be called into question in instances like the present where the unknown variables are subject to constraints which can severely restrict the allowable solution space. Additionally, the intrinsically lower weight given to discrepant points by the linear approach (compared to a quadratic treatment) was considered to be an overall advantage in the present context.

b) Linear Programming

As the means of selecting the "best-fitting" synthetic model stellar population for each galaxy in the sample studied, we use linear programming to minimize the sum over

the synthesis wavelengths of the weighted absolute values of the percentage residuals between the model and observed energy distributions.

$$\sum_{i=1}^{m} \rho_i \left| \frac{\sum_{j=1}^{n} a_{ij} x_j - g_i}{g_i} \right| = \text{minimum} \qquad (2)$$

is solved for the x_j where m is the number of synthesis wavelengths to be fitted, n is the number of allowable stellar groups, g_i is the observed absolute flux density at wavelength i of the galaxy in question, a_{ij} is similarly the observed absolute flux density from a single mean star of type j at wavelength i, x_j is the (nonnegative) number of mean stars of type j, and ρ_i is a nonnegative weight factor for wavelength i. The g_i and the a_{ij} are both scaled to a common distance so that the x_j are actual, not just relative, numbers of stars of each mean type present in the model. The ρ_i are taken in all cases to be proportional to $1/\sigma_i$, where the σ_i are the fractional uncertainties given in Table 4. In this way, the actual percentage residuals are scaled so that points with equal ratios of deviation-to-uncertainty contribute equally to the sum in equation (2).

Appendix E contains the details of the linear-programming methods used in the present work.

c) Astrophysical Continuity Constraints

The minimization problem in equation (2) must be solved subject to astrophysical constraints on the x_j, as has been emphasized in Section IVa. Faber (1972) has illustrated how these may be expressed within the framework of quadratic (or linear) programming. Of greatest importance are the group-ratio constraints interrelating the population of various points of the H-R diagram. We have already indicated in the introduction that simple single-generation models are clearly inappropriate for the type of composite system being studied here. A set of physically-consistent constraints describing a multiple-generation system is required.

To produce the necessary constraints we have adopted a simple theoretical model for the history of star formation and have computed the expected present-day (i.e., at an age of 12×10^9 years) distributions of stars in the H-R diagram corresponding to various model histories. The calculations are patterned after those of Tinsley (1972b) and Searle, Sargent, and Bagnuolo (1973). A separable, analytic stellar birthrate function is assumed: the number of stars formed in the interval dm about mass m and in the interval dt about time t is written

$$B(m,t) = C\, m^{-\alpha}\, e^{-t/\tau} \qquad (3)$$

where C, α, and τ are constants. The time t, measured

in units of 10^9 years, runs from 0 to 12, and the mass m ranges from 0.05 $m_\odot$ to 50.0 $m_\odot$; outside of these limits the birthrate is presumed to be zero. In support of the simple form of equation (3), we might point out that the power-law representation of the initial mass function (IMF) is a well-established convention (see, e.g., Salpeter 1955; Limber 1960; Tinsley 1968, 1972a)and that Tinsley (1972b) has shown that evolutionary galaxy models with stellar birthrates proportional to a power of the mass of residual gas often approximate an exponential time dependence.

Through the use of equation (3) and stellar evolutionary theory, the number of stars expected to populate any given region of the theoretical H-R diagram (log L, log T_e) at any time t = 0 to 12 may be calculated. In general, we have adopted the evolutionary tracks and time scales given in a series of papers by Iben (1965, 1966a,b, c, 1967a,b) and in Tinsley (1972b). For He-burning stages the data of Tinsley's (1972b) "case B" are used. We consider only the time t = 12 and only the domains in the (log L, log T_e) plane corresponding to the 34 distinct synthesis groups. The domains of the evolved synthesis-star groups were estimated from their B-V and spectral-type limits, using the log T_e calibrations of Johnson (1966) and Lee (1970). In the case of subgiants, since Tinsley's empirical giant-branch effective temperatures are higher than the theoretical temperatures (Iben 1967a), the domains are regarded as uncertain. For unevolved stars, the domains

are considered to extend approximately 1 magnitude above the initial main sequence, and the appropriate time scales have been estimated from Iben (1965, 1966a,b,c, 1967a,b) and from the compilation by Thuan, Hart, and Ostriker (1975).

Appendix D contains a description of the equations and adopted time scales used to compute the expected population of each synthesis group of luminosity classes V-III according to the present model, for any specified α and τ. In the case of supergiant stars, the evolutionary time scales are so short that their total numbers depend only on the birthrate of their upper-main-sequence progenitors during the last $\sim 10^7$ years. For these luminosity-class I stars, we have adopted a semi-empirical scheme combining observations of young clusters and stellar-evolutionary theory to estimate both their distribution over spectral type and their total numbers relative to the present main-sequence population from O5 V to B3 V (Wildey 1962; Iben 1966b; Stothers 1969, 1972b; Schild(1970).

It is clearly desirable that the constraints one applies on the basis of these simple evolutionary histories be as unrestrictive as possible within the context of providing the necessary continuity of stellar groups. Consequently, in an effort to let the linear-programming solution be as <u>empirical</u> as possible, the constraints adopted were derived from the population densities appropriate to what were considered to be reasonable <u>extremes</u> to plausible

histories. Thus, the constraints actually applied are consistent with all possible model histories with values of α ranging from 0.75 to 3.50 and time dependence ranging from a steeply-decreasing exponential (time constant 10^9 years) on up to a constant rate. As a further gesture of independence from the exact details of stellar evolution beyond the main sequence, the allowable populations of all evolved-star groups have been relaxed by ±50 percent relative to the strict model values, and the total number of all MIII stars has been allowed to float freely.

We have found that group-ratio constraints relating entire blocks of stars (i.e., several synthesis groups) to other blocks of stars can be very useful in preserving overall proportions of evolved stars without unnecessarily restricting any particular group. Thus, the total numbers of type IV, III and I stars can be separately related to appropriate groups of type-V stars. This option is particularly useful in leaving the choice of normal or strong-lined KIII stars open to the linear-programming algorithm: the total number of KIII stars is constrained, but any combination of normal or strong-lined stars within that total is allowed.

The basic population-density constraints derived as explained above and applied in identical form to each of the seven galaxies are summarized in Table 6. In general, the final optimal solutions found by the linear-programming

TABLE 6

STANDARD CONTINUITY CONSTRAINTS

APPLIED TO SYNTHESIS GROUPS

SYNTHESIS GROUP(S) A	SYNTHESIS GROUP(S) B	CONSTRAINED RATIO OF NUMBERS OF STARS IN GROUPS A and B A/B
1	2	0.05 - 0.65
2	3	0.13 - 0.62
3	4	0.16 - 0.54
4	5	0.22 - 0.60
5	6	0.49 - 1.03
6	7	0.36 - 0.69
7	8	0.10 - 0.37
8	9	0.03 - 0.58
9	10	0.07 - 0.94
10	11	0.02 - 0.80
11	12	0.89 - 1.18
12	13	0.50 - 0.70
13	14	0.86 - 1.23
14	15	0.27 - 0.47
15	16	0.19 - 0.59
16	17	0.00* - 0.93
17	18	0.00* - 0.74
19	20	0.03 - 1.73
20	21	0.86 - 4.19
21	22	0.45 - 2.21
24	23	0.23 - 0.86
26	25	0.26 - 0.87
27	26	0.26 - 0.89
29	28	0.22 - 1.10
32	31	0.75 - 1.25
33	32	0.75 - 1.25
19+20+21+22	10+11+12	0.02 - 0.26
23+24+25+26+27	10+11+12	0.01 - 0.14
31+32+33	1+2	0.09 - 0.26
34	31+32+33	0.20 - 1.00

*No upper limit was set on the numbers of stars in the last two M V groups relative to the remainder of the main sequence, in order to allow the possibility of late-dwarf-star enrichment.

algorithm using these constraints will not correspond to any particular "pure" (single α and τ) evolutionary history, due to the considerable freedom allowed by the constraints. This is considered to be an advantage rather than a drawback--the simplistic models described by equation (3) are regarded largely as a means to our end, rather than that end itself.

d) Intrinsic Reddening

The work of Holmberg (1969) on a large sample of spiral galaxies has shown that there is no systematic dependence of photographic nuclear colors on galaxy inclination until the galaxies are viewed close to edge-on. One may not, however, conclude from this that there is no intrinsic nuclear absorption: Holmberg (1969) has pointed out, for example, that a spherical distribution of absorbing matter could not be ruled out, and there is in fact some evidence for significant reddening and absorption in individual galaxy nuclei (see Warner 1973). Therefore, the possibility of absorption intrinsic to the nuclear regions studied in the present work demands consideration.

Lacking any suitable means of determining a priori whether or in what amounts any absorption should be present, we have used the following approach to infer intrinsic reddening. A number of possible discrete intrinsic

color excesses E(B-V) were tested for each galaxy by subjecting the appropriately de-reddened energy distribution to the linear-programming algorithm described in the above Sections. Whereas one can achieve satisfactorily good fits to the continuum points of arbitrarily de-reddened energy distributions through the use in the solution of stars of the appropriate temperature, a simultaneous good fit to the absorption features is obtained only when the solution contains a mix of stars which is also appropriate to those features. The reddening-independent character of the absorption features thus provides the leverage by which one can infer that the proper intrinsic reddening is that for which the overall residual sum is least.

To the extent that only a finite number of color excesses are tested, the method suffers the drawbacks of trial and error. However, the set of all physically reasonable color excesses has for any galaxy practical limits, and in fact in all seven cases here the fit improves as the assumed color excess is increased from zero, peaks in most cases at a well-defined value, and thereafter grows worse as increasing amounts of reddening are presumed. Encouraging also is the fact that in most cases totally unconstrained models have their best overall fits at the same presumed reddening as do the physically constrained models, indicating that the choice of actual reddening is not an artifact of the particular constraint system employed. A source of uncertainty

in the inferred actual reddening is the discreteness of the color excesses tested (the presumed reddening is incremented in steps of 0.05 or 0.10 mag.); it was not felt, however, that meaningful discrimination of smaller increments would be possible.

Most of the test cases for intrinsic reddening are of the standard Whitford type (Miller and Mathews 1972) describing the effect of a screen of absorbing matter overlying the emitting matter and for which $R = A_V/E(B-V) = 2.97$, where A_V is the total absorption at V , in magnitudes. Such cases are said to refer to external reddening. One test case for internal reddening, in which the emitting and obscuring matter are well mixed, is included. This case has been calculated along the lines of the simple model neglecting scattering used by O'Connell (1970) and Liebowitz (1973), assuming that the extinctive properties of the obscuring matter are given by the wavelength dependence of the Whitford law. Only a single such case, for internal $E(B-V) = 0.30$ mag., is considered inasmuch as for smaller color excesses such models are too similar to purely external models to be distinguishable, and the limiting internal color excess (see Mathis 1970) for infinite internal optical depth is less than 1 percent greater. In this case, $A_V/E(B-V) \sim 5$, but because of the limiting behavior of the reddening, the actual total optical depth (and hence A_V) appropriate to a model with reddening similar to this is very uncertain.

V. RESULTS OF THE SYNTHESIS

a) Optimal Solutions

The linear-programming algorithm described in Section IV has been applied to each of the seven program-galaxy nuclear regions. Although a number of various constraints were used experimentally to test certain features of the solution, the fundamental optimal solution for each galaxy has been calculated on the basis of the standard constraints listed in Table 6, with the following exception: for NGC 5194 the presence of upper-main-sequence stars in proportions consistent with the standard constraints introduces systematic residuals in the continuum below the Balmer jump, so the optimal model has been calculated with the numbers of stars in groups 1-4 left completely free.

In Figure 3 we show for each galaxy the optimal-model percentage flux residuals in the sense (model-observed) / (observed) for all wavelengths which were used in the fitting procedure. Thus, the lower Balmer-series lines and the specific emission-line bandpasses flagged in Table 4 as deleted are not included in the figure. Points measuring the continuum and those measuring absorption features are differentiated in the figure by separate symbols. Note that the actual, not weighted, percentage residuals are shown in Figure 3. Since it is the weighted percentage residuals which are minimized by the fitting algorithm, a numerical

FIGURE 3

Percentage flux residuals (model-observed)/(observed) for the optimal stellar-population models discussed in the text. Only points used in the fitting algorithm are shown, with bandpasses containing prominent stellar absorption features shown as filled circles and continuum bandpasses shown as open circles. The parameter $<\delta>$ is a measure of the average quality of the fit and is defined in the text.

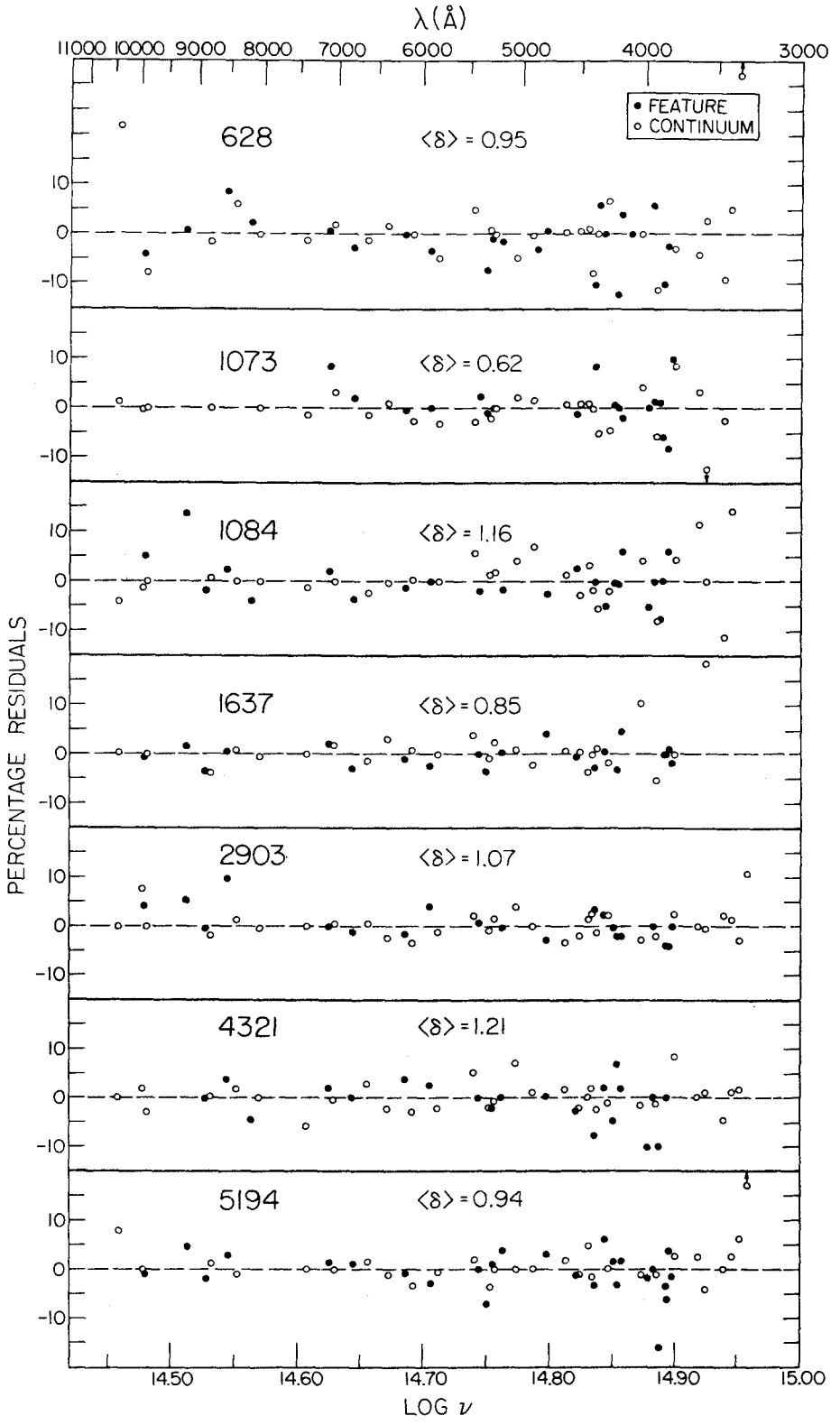
λ(Å)
11000 10000 9000 8000 7000 6000 5000 4000 3000
• FEATURE
○ CONTINUUM
628 ⟨δ⟩ = 0.95
1073 ⟨δ⟩ = 0.62
1084 ⟨δ⟩ = 1.16
1637 ⟨δ⟩ = 0.85
2903 ⟨δ⟩ = 1.07
4321 ⟨δ⟩ = 1.21
5194 ⟨δ⟩ = 0.94
PERCENTAGE RESIDUALS
10
0
-10
14.50 14.60 14.70 14.80 14.90 15.00
LOG ν

FIGURE 3

measure of the character of the fit, $\langle\delta\rangle$, has been included in the diagram. The quantity $\langle\delta\rangle$ is the average over all fitted points of the quantity $|r_i|/\sigma_i$, where r_i is the percentage residual, and σ_i the estimated uncertainty, at wavelength i . Note that since the weights used in the fitting algorithm are proportional to $1/\sigma_i$, the minimization performed is equivalent to the minimization of $\langle\delta\rangle$. The fact that $\langle\delta\rangle \sim$ unity for the adopted optimal models means that the observations have been fitted to about the level of the inherent uncertainties. Together with the absence of significant systematic trends in the residuals, this is interpreted as indicating that satisfactory models have been obtained for each of the seven galaxies.

Several further remarks can be made concerning the general nature of the optimal solutions. Comparison with totally unconstrained (and thus unphysical) models shows that the overall character of the residual diagrams are very similar; in particular, the "worst" points in the optimal fit are in general also the worst points in the unconstrained model and thus are not artificially induced by the constraints. The fact that these worst points show no preference for particular wavelengths (aside from occurring most often in the far-red or UV where uncertainties are large) suggests that random observational errors, not model deficiencies, are the cause of the highly discrepant points. In addition, we note that the application of the standard constraints results in

an increase in $\langle\delta\rangle$ of only about 10 percent over that for the unconstrained models. Finally, the overall proportions of large blocks of stellar groups considered as a whole are similar for the unconstrained and the optimal models. Apparently, the standard constraints do not place unreasonable restrictions on the solutions.

b) Stellar Populations: General Remarks

Table 7 summarizes the stellar properties of the optimal solution for each galaxy. Quantities listed include the model mass/luminosity ratio in λ5450 light (∿ V band) in solar units, the total model stellar mass in solar units, the inferred intrinsic reddening expressed as a color excess E(B-V), the numbers of stars in each group, and the percentage contributions for each group to the total model mass and to the total model light at six wavelengths spanning the spectral range studied.

Several features of the stellar models are immediately apparent from Table 7. 1) The lower main sequence is comparatively sparsely populated in all optimal solutions, with the result that model mass-luminosity ratios are low, of order unity. This result stands in contrast to the late-dwarf-star-enriched model for M31 by Spinrad and Taylor (1971), but is similar to the recent results of Whitford (1972), Baldwin et al. (1973), and O'Connell (1974) which indicate late-giant-star dominance in the red and infrared

TABLE 7

SYNTHESIZED MODEL

NGC 628

INTRINSIC E(B-V) = 0.10 MAG.

MODEL M/L = 0.67 MODEL STELLAR MASS = 2.81D 08

PERCENTAGE CONTRIBUTIONS

TOTAL NO. STARS	MASS	3620	4500	5450	7400	8800	10400	GROUP	
3.86D 01	0.0	0.9	0.2	0.1	0.0	0.0	0.0	O5-9	V
7.72D 02	0.0	1.3	0.4	0.2	0.1	0.0	0.0	B1-3	V
1.40D 03	0.0	0.3	0.1	0.1	0.0	0.0	0.0	B5	V
8.78D 03	0.0	0.4	0.3	0.1	0.1	0.0	0.0	B8-9	V
3.99D 04	0.0	0.5	0.4	0.2	0.1	0.1	0.1	A0-3	V
8.14D 04	0.1	0.4	0.4	0.2	0.1	0.1	0.1	A4-5	V
2.26D 05	0.1	0.7	0.6	0.4	0.2	0.2	0.1	A7-F0	V
2.26D 06	1.1	3.4	2.5	2.0	1.2	0.9	0.7	F1-5	V
2.21D 07	8.7	13.5	10.9	9.2	6.2	4.8	4.0	F6-8	V
2.36D 07	8.4	7.1	6.3	5.6	4.0	3.1	2.7	G0-5	V
2.94D 07	8.9	3.7	3.9	3.7	2.8	2.3	2.0	G8	V
2.50D 07	7.1	1.0	1.5	1.6	1.4	1.2	1.1	K0-2	V
3.57D 07	8.9	0.4	0.9	1.0	1.1	0.9	0.9	K3-5	V
2.90D 07	6.2	0.1	0.3	0.3	0.5	0.5	0.5	K7	V
6.17D 07	12.1	0.1	0.2	0.3	0.5	0.5	0.5	M0	V
1.05D 08	13.0	0.0	0.1	0.1	0.3	0.3	0.4	M1-4	V
1.12D 08	8.0	0.0	0.0	0.0	0.1	0.1	0.1	M5-6	V
1.52D 08	5.4	0.0	0.0	0.0	0.0	0.0	0.1	M7-8	V
1.03D 07	4.8	28.2	21.5	17.0	10.2	7.8	6.4	F5-8	IV
5.94D 06	2.3	7.6	7.3	6.9	4.9	3.9	3.4	G0-4	IV
1.42D 06	0.6	1.2	1.4	1.5	1.2	1.1	0.9	G5-8	IV
2.62D 06	1.0	1.6	2.3	2.7	2.5	2.3	2.1	K0-2	IV
4.74D 06	2.5	17.3	23.4	25.6	22.3	20.0	16.9	G5-K1	III
1.09D 06	0.6	2.9	9.2	13.1	16.3	16.4	15.7	K2-5	III
5.90D-03	0.0	0.0	0.0	0.0	0.0	0.0	0.0	K0-1	III SL
0.0	0.0	0.0	0.0	0.0	0.0	0.0	0.0	K2-3	III SL
0.0	0.0	0.0	0.0	0.0	0.0	0.0	0.0	K4-5	III SL
1.42D 05	0.1	0.5	2.2	3.8	8.4	9.4	10.5	M0-1	III
6.14D 04	0.0	0.3	1.0	2.2	13.3	21.1	27.7	M2-5	III
0.0	0.0	0.0	0.0	0.0	0.0	0.0	0.0	M6-8	III
5.53D 01	0.0	3.1	0.7	0.4	0.1	0.1	0.0	B0	I
6.91D 01	0.0	2.2	0.8	0.4	0.2	0.1	0.1	B5-7	I
8.64D 01	0.0	1.3	0.9	0.6	0.3	0.2	0.1	A2	I
2.11D 02	0.0	0.1	0.3	0.7	1.8	2.4	2.8	M1-4	I

TABLE 7 (CONTINUED)

SYNTHESIZED MODEL

NGC 1073

INTRINSIC E(B-V) = 0.20 MAG.

MODEL M/L = 1.32 MODEL STELLAR MASS = 4.74D 08

PERCENTAGE CONTRIBUTIONS

TOTAL NO. STARS	MASS	3620	4500	5450	7400	8800	10400	GROUP	
4.44D 02	0.0	5.7	1.9	1.2	0.6	0.4	0.2	C5-9	V
8.89D 03	0.0	8.1	3.9	2.7	1.4	1.0	0.7	B1-3	V
6.84D 04	0.1	8.6	5.4	3.9	2.2	1.6	1.2	B5	V
3.17D 05	0.2	8.6	8.1	6.0	3.6	2.9	2.0	B8-9	V
1.44D 06	0.7	9.2	12.5	10.0	6.3	5.2	4.0	A0-3	V
1.40D 06	0.6	3.5	5.4	4.6	3.3	2.8	2.3	A4-5	V
3.80D 06	1.4	6.3	8.6	8.1	6.3	5.3	4.4	A7-F0	V
1.03D 07	3.0	8.3	9.6	10.5	9.4	8.1	7.1	F1-5	V
1.77D 07	4.1	5.9	7.5	8.6	8.6	7.6	6.9	F6-8	V
1.88D 07	4.0	3.1	4.3	5.2	5.5	5.0	4.7	G0-5	V
2.35D 07	4.2	1.6	2.6	3.4	3.9	3.7	3.5	G8	V
2.00D 07	3.4	0.4	1.1	1.5	2.0	1.9	1.9	K0-2	V
3.99D 07	5.9	0.3	0.8	1.3	2.0	2.1	2.1	K3-5	V
4.64D 07	5.9	0.1	0.4	0.6	1.3	1.5	1.6	K7	V
1.72D 08	20.0	0.1	0.5	1.0	2.4	2.8	3.0	M0	V
2.91D 08	21.5	0.0	0.1	0.3	1.3	1.8	2.1	M1-4	V
3.13D 08	13.2	0.0	0.0	0.0	0.3	0.6	0.7	M5-6	V
4.23D 08	8.9	0.0	0.0	0.0	0.1	0.2	0.3	M7-8	V
6.07D 06	1.7	9.1	10.9	11.8	10.5	9.2	8.1	F5-8	IV
3.51D 06	0.8	2.4	3.7	4.8	5.0	4.6	4.3	G0-4	IV
8.38D 05	0.2	0.4	0.7	1.0	1.3	1.2	1.2	G5-8	IV
3.79D 05	0.1	0.1	0.3	0.4	0.6	0.7	0.7	K0-2	IV
6.54D-03	0.0	0.0	0.0	0.0	0.0	0.0	0.0	G5-K1	III
0.0	0.0	0.0	0.0	0.0	0.0	0.0	0.0	K2-5	III
2.62D 05	0.1	0.3	0.8	1.3	1.7	1.8	1.7	K0-1	III SL
2.28D 05	0.1	0.2	1.0	1.9	3.2	3.6	3.8	K2-3	III SL
1.33D 05	0.0	0.1	0.7	1.6	3.4	4.0	4.5	K4-5	III SL
1.51D 04	0.0	0.0	0.2	0.5	1.5	2.0	2.4	M0-1	III
1.66D 04	0.0	0.0	0.2	0.7	6.2	11.3	16.1	M2-5	III
1.38D 02	0.0	0.0	0.0	0.0	0.1	0.6	1.5	M6-8	III
3.63D 02	0.0	11.1	4.0	2.7	1.3	1.0	0.7	B0	I
2.72D 02	0.0	4.8	2.7	2.1	1.2	1.0	0.7	B5-7	I
2.04D 02	0.0	1.6	1.8	1.6	1.0	0.9	0.7	A2	I
1.68D 02	0.0	0.0	0.2	0.6	2.5	3.8	4.8	M1-4	I

TABLE 7 (CONTINUED)

SYNTHESIZED MODEL

NGC 1084

INTRINSIC E(B-V) = 0.40 MAG.

MODEL M/L = 0.72 MODEL STELLAR MASS = 1.44D 09

PERCENTAGE CONTRIBUTIONS

TOTAL NO. STARS	MASS	3620	4500	5450	7400	8800	10400	GROUP		
1.16D 03	0.0	3.1	1.0	0.6	0.3	0.2	0.1	O5-9	V	
2.32D 04	0.0	4.4	1.9	1.3	0.6	0.4	0.3	B1-3	V	
1.78D 05	0.1	4.7	2.7	1.8	1.0	0.7	0.5	B5	V	
8.74D 05	0.2	5.0	4.3	3.0	1.7	1.3	0.8	B8-9	V	
3.97D 06	0.6	5.3	6.6	5.0	2.9	2.3	1.7	A0-3	V	
8.11D 06	1.1	4.3	6.1	4.8	3.2	2.6	2.0	A4-5	V	
2.25D 07	2.7	7.9	9.8	8.6	6.2	5.0	3.9	A7-F0	V	
6.19D 07	6.0	10.6	11.2	11.4	9.4	7.8	6.4	F1-5	V	
1.07D 08	8.1	7.5	8.7	9.3	8.6	7.3	6.3	F6-8	V	
1.14D 08	7.9	4.0	5.0	5.7	5.5	4.8	4.2	G0-5	V	
1.42D 08	8.3	2.1	3.1	3.7	3.9	3.5	3.2	G8	V	
1.20D 08	6.7	0.6	1.2	1.6	2.0	1.8	1.7	K0-2	V	
1.72D 08	8.3	0.2	0.7	1.0	1.5	1.4	1.4	K3-5	V	
1.40D 08	5.8	0.1	0.2	0.4	0.7	0.7	0.7	K7	V	
2.97D 08	11.3	0.0	0.2	0.3	0.7	0.8	0.8	M0	V	
5.04D 08	12.2	0.0	0.0	0.1	0.4	0.5	0.5	M1-4	V	
5.41D 08	7.5	0.0	0.0	0.0	0.1	0.2	0.2	M5-6	V	
7.32D 08	5.1	0.0	0.0	0.0	0.0	0.1	0.1	M7-8	V	
3.17D 07	2.9	10.0	10.9	11.0	9.2	7.6	6.3	F5-8	IV	
1.83D 07	1.4	2.7	3.7	4.5	4.4	3.8	3.4	G0-4	IV	
1.48D 07	1.1	1.4	2.4	3.2	3.7	3.5	3.1	G5-8	IV	
3.28D 07	2.5	2.3	4.8	7.0	9.1	9.2	8.6	K0-2	IV	
0.0	0.0	0.0	0.0	0.0	0.0	0.0	0.0	G5-K1	III	
0.0	0.0	0.0	0.0	0.0	0.0	0.0	0.0	K2-5	III	
2.83D 06	0.2	0.6	1.7	2.4	3.1	3.0	2.8	K0-1	III	SL
7.36D 05	0.1	0.1	0.6	1.1	1.7	1.9	1.8	K2-3	III	SL
1.91D 05	0.0	0.0	0.2	0.4	0.8	0.9	1.0	K4-5	III	SL
6.11D 04	0.0	0.0	0.2	0.3	1.0	1.3	1.4	M0-1	III	
6.72D 04	0.0	0.0	0.2	0.5	4.2	7.3	9.7	M2-5	III	
6.42D 03	0.0	0.0	0.0	0.1	1.1	4.6	10.6	M6-8	III	
1.66D 03	0.0	10.7	3.6	2.3	1.0	0.7	0.4	B0	I	
2.08D 03	0.0	7.7	4.0	2.8	1.6	1.2	0.8	B5-7	I	
2.60D 03	0.0	4.3	4.3	3.6	2.2	1.9	1.3	A2	I	
3.32D 03	0.0	0.2	0.8	2.2	8.3	12.0	14.1	M1-4	I	

TABLE 7 (CONTINUED)

SYNTHESIZED MODEL

NGC 1637

INTRINSIC E(B-V) = 0.40 MAG.

MODEL M/L = 1.52 MODEL STELLAR MASS = 5.32D 08

PERCENTAGE CONTRIBUTIONS

TOTAL NO. STARS	MASS	3620	4500	5450	7400	8800	10400	GROUP		
1.47D 02	0.0	2.7	0.7	0.4	0.2	0.1	0.1	O5-9	V	
2.95D 03	0.0	3.9	1.5	0.9	0.4	0.3	0.2	B1-3	V	
2.05D 04	0.0	3.7	1.9	1.2	0.6	0.4	0.3	B5	V	
1.28D 05	0.1	5.0	3.9	2.5	1.3	1.0	0.7	B8-9	V	
5.82D 05	0.3	5.3	6.0	4.2	2.3	1.8	1.3	A0-3	V	
8.93D 05	0.3	3.2	4.1	3.0	1.9	1.5	1.2	A4-5	V	
1.30D 06	0.4	3.1	3.5	2.8	1.9	1.6	1.2	A7-F0	V	
3.50D 06	0.9	4.1	3.9	3.7	2.8	2.4	1.9	F1-5	V	
4.63D 07	9.7	22.4	23.5	23.3	20.2	17.2	14.8	F6-8	V	
4.98D 07	9.4	11.9	13.6	14.2	12.9	11.3	10.0	G0-5	V	
6.23D 07	10.0	6.2	8.3	9.3	9.1	8.4	7.5	G8	V	
5.28D 07	7.9	1.7	3.3	4.1	4.6	4.3	4.1	K0-2	V	
7.54D 07	9.9	0.7	1.9	2.5	3.4	3.3	3.3	K3-5	V	
6.13D 07	6.9	0.2	0.6	0.9	1.6	1.7	1.7	K7	V	
1.30D 08	13.5	0.1	0.5	0.8	1.6	1.8	1.8	M0	V	
2.21D 08	14.6	0.0	0.1	0.3	0.9	1.2	1.3	M1-4	V	
2.38D 08	8.9	0.0	0.0	0.0	0.2	0.4	0.4	M5-6	V	
3.21D 08	6.0	0.0	0.0	0.0	0.1	0.1	0.2	M7-8	V	
8.81D 05	0.2	1.9	1.9	1.8	1.4	1.1	0.9	F5-8	IV	
5.09D 05	0.1	0.5	0.6	0.7	0.6	0.6	0.5	G0-4	IV	
5.92D 05	0.1	0.4	0.6	0.7	0.8	0.7	0.7	G5-8	IV	
1.32D 06	0.3	0.6	1.2	1.6	2.0	2.0	1.9	K0-2	IV	
0.0	0.0	0.0	0.0	0.0	0.0	0.0	0.0	G5-K1	III	
0.0	0.0	0.0	0.0	0.0	0.0	0.0	0.0	K2-5	III	
9.00D 05	0.2	1.4	3.3	4.4	5.3	5.2	4.8	K0-1	III	SL
7.83D 05	0.2	1.0	3.9	6.7	9.7	10.7	10.5	K2-3	III	SL
2.04D 05	0.0	0.2	1.3	2.4	4.7	5.3	5.6	K4-5	III	SL
6.49D 03	0.0	0.0	0.1	0.2	0.6	0.7	0.8	M0-1	III	
7.13D 03	0.0	0.0	0.1	0.3	2.4	4.2	5.6	M2-5	III	
1.26D 03	0.0	0.0	0.0	0.1	1.2	4.9	11.2	M6-8	III	
2.11D 02	0.0	9.3	2.8	1.6	0.7	0.5	0.3	B0	I	
2.64D 02	0.0	6.6	3.1	2.0	1.1	0.8	0.6	B5-7	I	
3.30D 02	0.0	3.8	3.4	2.6	1.5	1.3	0.9	A2	I	
1.61D 02	0.0	0.0	0.2	0.6	2.1	3.1	3.7	M1-4	I	

TABLE 7 (CONTINUED)

SYNTHESIZED MODEL

NGC 2903

INTRINSIC E(B-V) = 0.30 MAG. (INTERNAL)

MODEL M/L = 1.18 MODEL STELLAR MASS = 6.39D 08

PERCENTAGE CONTRIBUTIONS

TOTAL NO. STARS	MASS	3620	4500	5450	7400	8800	10400	GROUP	
8.02D 02	0.0	5.6	2.2	1.4	0.7	0.4	0.3	G5-9	V
1.60D 04	0.0	8.0	4.6	3.2	1.6	1.1	0.7	B1-3	V
5.02D 04	0.0	3.5	2.6	1.9	1.0	0.7	0.5	B5	V
3.14D 05	0.2	4.7	5.2	4.0	2.3	1.7	1.2	B8-9	V
1.43D 06	0.5	5.0	8.1	6.6	4.0	3.2	2.3	A0-3	V
2.91D 06	0.9	4.0	7.4	6.4	4.4	3.6	2.7	A4-5	V
4.22D 06	1.1	3.9	6.2	5.9	4.5	3.6	2.8	A7-F0	V
1.14D 07	2.5	5.1	7.0	7.7	6.7	5.5	4.5	F1-5	V
1.97D 07	3.4	3.6	5.4	6.3	6.2	5.2	4.4	F6-8	V
4.56D 07	7.1	4.2	6.9	8.4	8.6	7.4	6.4	G0-5	V
5.70D 07	7.6	2.2	4.2	5.5	6.1	5.5	4.8	G8	V
4.83D 07	6.0	0.6	1.7	2.4	3.1	2.8	2.6	K0-2	V
6.89D 07	7.5	0.3	1.0	1.5	2.3	2.2	2.1	K3-5	V
5.61D 07	5.3	0.1	0.3	0.5	1.0	1.1	1.1	K7	V
2.08D 08	17.9	0.1	0.4	0.8	1.9	2.1	2.1	M0	V
3.52D 08	19.3	0.0	0.1	0.3	1.0	1.3	1.4	M1-4	V
3.78D 08	11.8	0.0	0.0	0.0	0.2	0.4	0.5	M5-6	V
5.11D 08	8.0	0.0	0.0	0.0	0.1	0.1	0.2	M7-8	V
8.05D 05	0.2	0.7	0.9	1.0	0.9	0.7	0.6	F5-8	IV
4.66D 05	0.1	0.2	0.3	0.4	0.4	0.4	0.3	G0-4	IV
5.41D 05	0.1	0.1	0.3	0.4	0.5	0.5	0.4	G5-8	IV
1.20D 06	0.2	0.2	0.6	0.9	1.3	1.3	1.2	K0-2	IV
0.0	0.0	0.0	0.0	0.0	0.0	0.0	0.0	G5-K1	III
0.0	0.0	0.0	0.0	0.0	0.0	0.0	0.0	K2-5	III
7.00D 05	0.1	0.4	1.4	2.2	3.0	2.9	2.6	K0-1	III SL
6.09D 05	0.1	0.3	1.7	3.3	5.5	5.9	5.8	K2-3	III SL
5.42D 05	0.1	0.2	1.9	4.2	9.1	10.0	10.6	K4-5	III SL
3.18D 03	0.0	0.0	0.0	0.1	0.2	0.3	0.3	M0-1	III
3.50D 03	0.0	0.0	0.0	0.1	0.8	1.5	1.9	M2-5	III
2.38D 03	0.0	0.0	0.0	0.1	1.6	6.6	15.0	M6-8	III
1.53D 03	0.0	25.9	11.1	7.7	3.5	2.6	1.6	B0	I
1.63D 03	0.0	15.7	10.5	8.2	4.8	3.7	2.5	B5-7	I
1.22D 03	0.0	5.3	6.9	6.2	4.0	3.4	2.4	A2	I
8.76D 02	0.0	0.1	0.7	2.2	8.4	12.2	14.2	M1-4	I

TABLE 7 (CONTINUED)

SYNTHESIZED MODEL

NGC 4321

INTRINSIC E(B-V) = 0.30 MAG.

MODEL M/L = 0.86 MODEL STELLAR MASS = 1.46D 09

PERCENTAGE CONTRIBUTIONS

TOTAL NO. STARS	MASS	3620	4500	5450	7400	8800	10400	GROUP		
7.19D 02	0.0	3.3	0.8	0.4	0.2	0.1	0.1	G5-9	V	
1.44D 04	0.0	4.7	1.7	0.9	0.4	0.2	0.1	B1-3	V	
2.41D 04	0.0	1.1	0.5	0.3	0.1	0.1	0.1	B5	V	
1.51D 05	0.0	1.5	1.0	0.6	0.3	0.2	0.1	B8-9	V	
6.86D 05	0.1	1.6	1.6	1.0	0.5	0.4	0.2	A0-3	V	
1.40D 06	0.2	1.3	1.5	1.0	0.6	0.4	0.3	A4-5	V	
3.89D 06	0.5	2.3	2.4	1.7	1.1	0.8	0.6	A7-F0	V	
3.89D 07	3.7	11.3	9.9	8.4	6.0	4.6	3.4	F1-5	V	
1.20D 08	9.0	14.3	13.7	12.4	9.8	7.7	6.0	F6-8	V	
1.28D 08	8.7	7.6	8.0	7.6	6.3	5.1	4.0	G0-5	V	
1.60D 08	9.3	4.0	4.8	4.9	4.4	3.8	3.0	G8	V	
1.36D 08	7.4	1.1	1.9	2.2	2.2	1.9	1.7	K0-2	V	
1.94D 08	9.3	0.5	1.1	1.3	1.7	1.5	1.3	K3-5	V	
1.58D 08	6.5	0.1	0.3	0.5	0.8	0.7	0.7	K7	V	
3.35D 08	12.6	0.1	0.3	0.4	0.8	0.8	0.7	M0	V	
5.68D 08	13.6	0.0	0.1	0.1	0.4	0.5	0.5	M1-4	V	
6.11D 08	8.3	0.0	0.0	0.0	0.1	0.2	0.2	M5-6	V	
8.25D 08	5.6	0.0	0.0	0.0	0.0	0.1	0.1	M7-8	V	
9.93D 06	0.9	5.3	4.8	4.1	2.9	2.3	1.7	F5-8	IV	
1.29D 07	1.0	3.2	3.7	3.7	3.1	2.5	2.0	G0-4	IV	
3.08D 06	0.2	0.5	0.7	0.8	0.8	0.7	0.6	G5-8	IV	
6.57D 06	0.5	0.8	1.4	1.6	1.8	1.7	1.5	K0-2	IV	
6.54D-03	0.0	0.0	0.0	0.0	0.0	0.0	0.0	G5-K1	III	
0.0	0.0	0.0	0.0	0.0	0.0	0.0	0.0	K2-5	III	
2.36D 07	1.9	9.0	19.7	24.0	26.1	23.8	19.8	K0-1	III	SL
6.14D 06	0.5	2.0	7.0	10.8	14.3	14.7	13.0	K2-3	III	SL
1.60D 06	0.1	0.4	2.3	4.0	7.0	7.2	7.0	K4-5	III	SL
0.0	0.0	0.0	0.0	0.0	0.0	0.0	0.0	M0-1	III	
0.0	0.0	0.0	0.0	0.0	0.0	0.0	0.0	M2-5	III	
1.92D 04	0.0	0.1	0.1	0.2	3.4	13.0	27.1	M6-8	III	
1.03D 03	0.0	11.3	3.1	1.6	0.6	0.4	0.2	B0	I	
1.29D 03	0.0	8.1	3.4	2.1	1.0	0.7	0.4	B5-7	I	
1.61D 03	0.0	4.6	3.8	2.6	1.4	1.1	0.7	A2	I	
7.85D 02	0.0	0.1	0.3	0.6	2.0	2.7	2.8	M1-4	I	

TABLE 7 (CONTINUED)

SYNTHESIZED MODEL

NGC 5194

INTRINSIC E(B-V) = 0.10 MAG.

MODEL M/L = 1.82 MODEL STELLAR MASS = 1.13D 09

PERCENTAGE CONTRIBUTIONS

TOTAL NO. STARS	MASS	3620	4500	5450	7400	8800	10400	GROUP		
0.0	0.0	0.0	0.0	0.0	0.0	0.0	0.0	O5-9	V	
1.86D 02	0.0	0.2	0.1	0.0	0.0	0.0	0.0	B1-3	V	
0.0	0.0	0.0	0.0	0.0	0.0	0.0	0.0	B5	V	
0.0	0.0	0.0	0.0	0.0	0.0	0.0	0.0	B8-9	V	
9.39D 05	0.2	8.6	6.5	3.8	1.7	1.2	0.8	A0-3	V	
1.92D 06	0.3	6.9	5.9	3.7	1.8	1.3	0.9	A4-5	V	
5.32D 06	0.8	12.7	9.5	6.6	3.6	2.6	1.8	A7-F0	V	
1.44D 07	1.8	16.7	10.7	8.5	5.3	4.0	2.9	F1-5	V	
3.05D 07	3.0	14.5	10.2	8.6	6.0	4.5	3.5	F6-8	V	
3.24D 07	2.9	7.7	5.9	5.2	3.8	3.0	2.4	G0-5	V	
8.96D 07	6.8	8.9	8.0	7.6	6.0	4.9	3.9	G8	V	
1.01D 08	7.2	3.2	4.2	4.4	4.0	3.4	2.8	K0-2	V	
2.02D 08	12.5	1.9	3.4	3.8	4.2	3.6	3.2	K3-5	V	
1.64D 08	8.7	0.4	1.0	1.3	1.9	1.8	1.7	K7	V	
3.49D 08	17.0	0.4	0.8	1.2	2.0	2.0	1.8	M0	V	
5.91D 08	18.4	0.1	0.2	0.4	1.1	1.3	1.3	M1-4	V	
6.35D 08	11.3	0.0	0.0	0.1	0.3	0.4	0.4	M5-6	V	
8.58D 08	7.6	0.0	0.0	0.0	0.1	0.1	0.2	M7-8	V	
2.80D 04	0.0	0.1	0.0	0.0	0.0	0.0	0.0	F5-8	IV	
9.33D 05	0.1	0.9	0.8	0.7	0.5	0.4	0.3	G0-4	IV	
1.09D 06	0.1	0.7	0.7	0.8	0.7	0.6	0.4	G5-8	IV	
2.41D 06	0.2	1.1	1.5	1.7	1.6	1.5	1.2	K0-2	IV	
0.0	0.0	0.0	0.0	0.0	0.0	0.0	0.0	G5-K1	III	
0.0	0.0	0.0	0.0	0.0	0.0	0.0	0.0	K2-5	III	
4.55D 06	0.5	7.0	11.1	12.6	12.1	10.6	8.8	K0-1	III	SL
3.95D 06	0.4	5.0	13.3	19.0	22.2	21.9	19.4	K2-3	III	SL
1.08D 06	0.1	1.2	4.6	7.3	11.3	11.3	10.8	K4-5	III	SL
9.36D 04	0.0	0.2	1.0	1.7	3.9	4.3	4.4	M0-1	III	
2.06D 04	0.0	0.1	0.2	0.5	3.1	4.9	5.9	M2-5	III	
6.46D 03	0.0	0.1	0.1	0.2	2.8	10.2	21.0	M6-8	III	
1.27D 01	0.0	0.6	0.1	0.1	0.0	0.0	0.0	B0	I	
1.59D 01	0.0	0.4	0.1	0.1	0.0	0.0	0.0	B5-7	I	
1.98D 01	0.0	0.2	0.1	0.1	0.0	0.0	0.0	A2	I	
9.67D 00	0.0	0.0	0.0	0.0	0.1	0.1	0.1	M1-4	I	

spectral regions of elliptical, SO, and similar galaxies, including M31. Substantial contributions from evolved M stars at long wavelengths are a feature of all of the present models. We note that this is consistent with the observations made at the wavelengths of the luminosity-sensitive CaII + TiO λ8542 feature and the λ9920 Wing-Ford band. The λ8190 NaI feature and the λ9190 CN feature are weak in all stars and fall in bands of telluric absorption, the effects of which cannot be adequately estimated without special observing procedures. These features thus carry little weight in the present solutions.

2) The upper main sequence is substantially populated in most of the models, the fractional light contributions in the UV from the earliest type-V groups and associated supergiants totaling 20 percent or more in all galaxies except NGC 628 and NGC 5194.

3) Intrinsic reddening is inferred to be present in each nuclear region. Values for the intrinsic E(B-V) range from $\sim$0.10 to $\sim$0.40 mag. (By way of contrast, trial syntheses using exactly the same procedures for unpublished elliptical-galaxy data by Gunn indicate the absence of intrinsic reddening: i.e., for those data, $\langle\delta\rangle$ grows progressively larger as increasing amounts of intrinsic reddening are presumed.)

We might make the following additional remarks regarding the inferred solutions as a whole. We have tested

the sensitivity of the optimal solutions to random observational errors in the galaxy data by means of model calculations with perturbed input data. These tests indicate that the significant properties of the model are not affected by random observational error, an encouraging result similar to the findings of Faber (1972) regarding quadratic-programming methods. The kinds of changes one does see as the result of perturbations include the interchanging of the relative contributions of closely-similar groups (for example F V and F IV stars). The joint contribution of these groups remains nearly unchanged, however. Also, groups which contribute to the solution in only small amounts are understandably subject to larger changes. Specifically, the perturbed models imply that the numbers of stars on the lower main sequence relative to G0-5 V are clearly uncertain by at least a factor of two.

We have also tested the significance of the inferred mass-luminosity ratios in a direct way by means of models with additional constraints on allowable values of M/L. We find that whereas M/L is rather severely limited on the low side (values of $M/L \lesssim 0.3$ generally result in models which are too bright in both the ultraviolet and far-red regions; see Figure 4), upper limits to M/L are less well defined. This is due largely to the small luminosity contributions made by the late M V stars in the optimal solutions--their numbers can be significantly increased

FIGURE 4

Percentage flux residuals (model-observed)/(observed) for a selection of non-optimal stellar population models. The symbol usage in Figure 3 also applies to Figure 4. The NGC 5194 and NGC 2903 models shown are discussed in the text. The NGC 1084 models illustrate the effects of imposing high and low mass-to-light ratio constraints: high M/L = 20, low M/L = 0.18. The NGC 4321 cases illustrate the typical deficiencies of models constrained to represent the present-day distribution of stars for star formation histories with initial mass functions characterized by values of $\alpha = 3$ and $\alpha = 2$. (See equation (3) and the discussion on p. 86 of the text.)

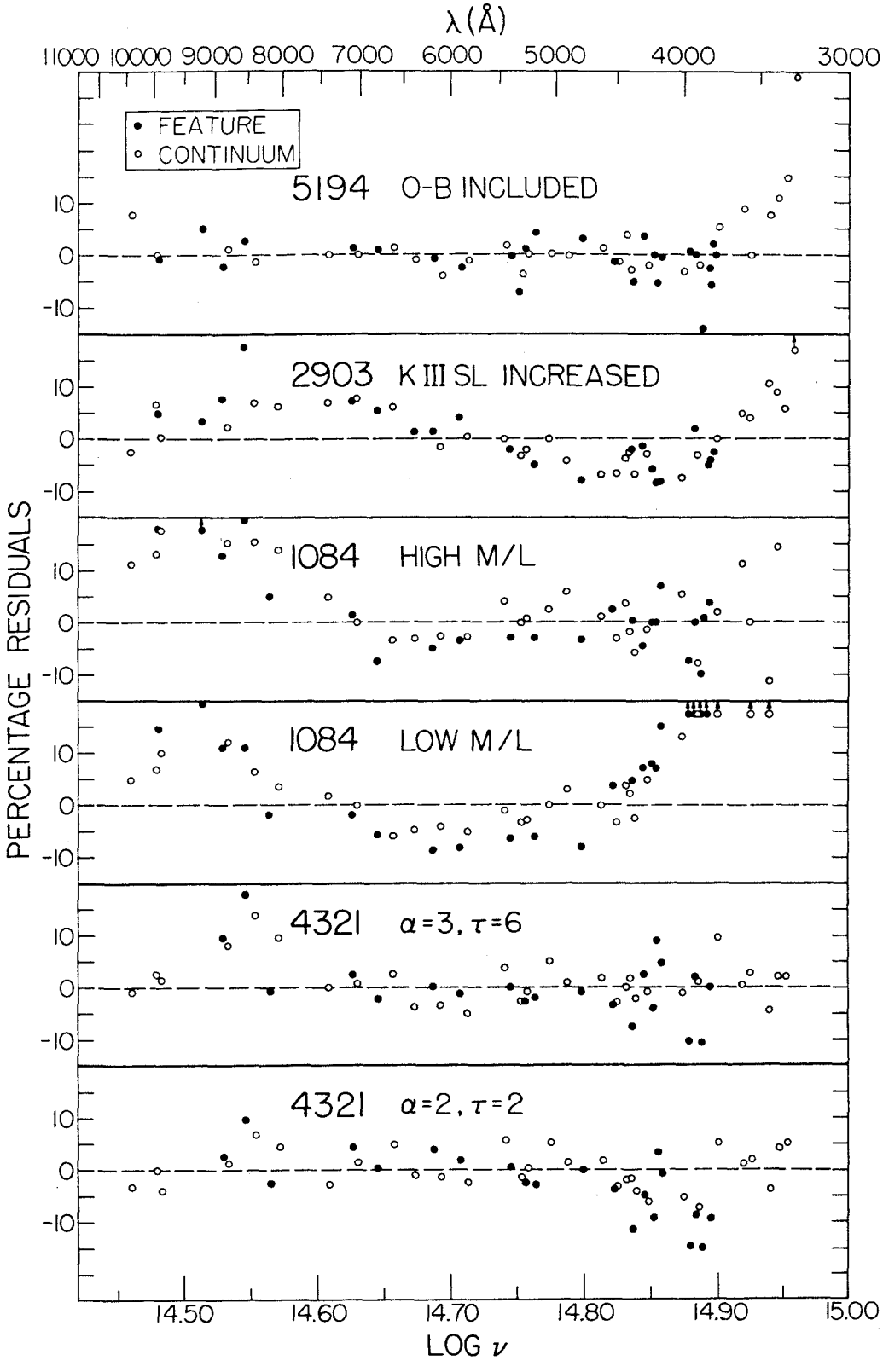
λ(Å)
11000 10000 9000 8000 7000 6000 5000 4000 3000
FEATURE
CONTINUUM
5194 O-B INCLUDED
2903 K III SL INCREASED
1084 HIGH M/L
1084 LOW M/L
4321 α=3, τ=6
4321 α=2, τ=2
PERCENTAGE RESIDUALS
10
0
-10
14.50 14.60 14.70 14.80 14.90 15.00
LOG ν

FIGURE 4

without severely compromising the overall fit. As increasingly larger M/L values are demanded, however, the substitution of M dwarfs for M giant stars gradually and systematically increases the residuals at the long-wavelength feature bandpasses. Particularly sensitive is the λ8542 feature, where the model flux becomes too bright at high values of M/L . In this way, we infer that M/L cannot be as large as 10 in any of the nuclear regions studied here, and that it is likely to be substantially lower in all except NGC 628 and NGC 5194.

Finally, we note from Table 7 that all optimal models but that for NGC 628 use strong-lined KIII groups exclusively. However, because the observations of NGC 628 were made with an entrance aperture of 10 arc sec (all other galaxies with 7 arc sec) the greater spectral degradation (which weakens spectral features) may mean that this result is artificial. We have tested the various galaxies with regard to this property and find that the overall sensitivity to the interchange of the normal and SL groups is low. Residuals at features such as CaII + TiO λ8542 and CN λ4200 do increase slightly when the optimally-chosen type of K giant is arbitrarily suppressed, but the differences are slight enough that the exclusive use of normal or SL groups in any given galaxy (particularly those in which the total K-giant contribution is small) is probably not highly significant. Considering that physical regions of several

hundred parsecs or more have been observed in these galaxies, this relative insensitivity may not be surprising if the strong-lined phenomenon such as that found in M31 is closely confined to the extreme nuclear regions of galaxies (see Spinrad, Smith, and Taylor 1972).

c) Stellar Population: Specifics

In this section we summarize the salient features of the individual models not already discussed in Section Vb.

i) NGC 628

This model contains a large G-KIII population, which contributes substantially to the luminosity at all wavelengths observed. The upper main sequence is very weak (note the sharp cutoff in population above F6-8 V). The need for any stars hotter than A7 V was tested by computing a model with the first 6 main-sequence groups deleted. The residual sum was virtually identical for this model, but all residuals for $\lambda < 4000\text{Å}$, with the exception of the point at $\lambda 3350$ which is presumably a bad datum, became negative (model too faint), introducing a systematic skew in the residual diagram. Because the observational uncertainties in the ultraviolet are large for NGC 628, the interpretation of this is somewhat ambiguous, but certainly the evidence is consistent with a lack of significant numbers of O-B stars in the nucleus. Interestingly, this confirms the inference made by Pronik (1973) that the lack

of Hα emission in the nucleus of this galaxy (see Section IIIb) is due to a lack of excitation.

The subgiant F contribution is particularly strong in the NGC 628 model. Our experience with the behavior of perturbed models (Section Vb) has indicated, however, that these stars are very often interchangeable with the main-sequence F groups. It is probably safest, therefore, to consider the early subgiant groups only in conjunction with their close-lying main-sequence neighbors.

Finally, we note that the intrinsic reddening is only poorly determined for this galaxy. The optimal value of E(B-V) = 0.10 mag. is probably uncertain by ±0.10 mag.

ii) NGC 1073

NGC 1073 is the only unambiguously barred spiral in the present sample, and its reddening-uncorrected energy distribution is the bluest of the seven program galaxies (see Figure 2). Unfortunately, because of its faintness, the observational uncertainties are large over a substantial portion of the spectrum, and in particular, no spectral features for $\lambda > 7000\text{Å}$ are measured. The Balmer lines other than Hα are strong in absorption.

Unlike the previous galaxy, NGC 1073 has very little KIII luminosity contributions, and the upper main sequence and supergiant stars are important contributors over a large wavelength range. Note the importance of the AO-3 V group.

iii) NGC 1084, NGC 1637

The models for these two galaxies are sufficiently alike that they are discussed together. Like NGC 1073, these galaxies show only minimal KIII contributions, with a significant upper-main-sequence population present, although there is more emphasis on the F and G dwarfs in these models. Models testing the need for O-B stars in these galaxies indicate that they may not be deleted without inducing systematic deficiencies in the ultraviolet residuals.

The inferred intrinsic reddening for these two nuclei is large; however, we regard them as well established. The residual sums for bandpasses measuring line features alone are very clearly larger for significantly greater or less amounts of presumed intrinsic reddening. Also, the Yerkes form classifications for these galaxies (see Table 3) are consistent with substantial proportions of early-type stars, implying the rather red observed energy distributions are due to the effects of reddening and not stellar temperature.

iv) NGC 2903

NGC 2903 is a remarkable galaxy with a peculiar nuclear complex of "hot spots" (see Figure 1). It has been the subject of dynamical, spectroscopic, and photometric investigations by a number of authors. Analyses of the nuclear stellar content have been made by means of broadband

photometry (Tifft 1963) and slit spectra plus scanner photometry (Alloin 1973). O'Connell (1974) has pointed out the large strength of the λ8542 absorption feature in NGC 2903 and the fact that relative to normal Sc galaxies, NGC 2903 has both a near-infrared and an ultraviolet excess of flux. The latter point is confirmed by the energy distribution in Figure 2, and the great strength of the λ8542 feature is apparent in terms of the nearly 10 percent positive residual for the optimal model in Figure 3.

Given the unusual continuum shape for this galaxy, the fact that the internal intrinsic reddening case was inferred is not surprising, as internal-type reddening would act in just such a way as to produce excess infrared and ultraviolet flux relative to that from external models. The visual appearance of the nuclear region (Figure 1) is also such as to suggest that large amounts of dust are present.

The stellar-content model for NGC 2903 is singular among the present samples for the dominating role of supergiant stars--nearly half of the total ultraviolet flux is from the B-A I groups. O-B main-sequence stars are of course also present in large numbers. The suggestion by Tifft (1963) on the basis of spectroscopic data that large numbers of supergiants must be present is strikingly confirmed by the present model.

The model for NGC 2903 by Alloin (1973) contains no B supergiants and many more G and K stars than the present model. We have tested the significance of the lack of substantial K-giant light in our model by calculating a model where the K4-5III SL contribution in λ5450 light was constrained to be 15 percent--roughly 3 times its "optimal" value. The resulting solution was clearly unacceptable: $\langle\delta\rangle$ increased by a factor of 2.5 and the residuals were systematically deficient (see Figure 4).

The large number of O-B stars in the present model, indicative of currently active star formation in the nuclear region, does not necessarily stand in contradiction to the absence of HeI λ3820 absorption on Simkin's (1975) slit spectra: this feature is strong only in early B V stars (O'Connell 1973)--in particular, it is not strong in the B I stars providing the bulk of the ultraviolet luminosity in the present model.

v) NGC 4321

The stellar-population model for this galaxy has a large K-giant luminosity contribution over a wide spectral range, and a main-sequence which decreases sharply at the transition from F V to A V . In these respects it resembles NGC 628. Unlike that galaxy, however, the model for NGC 4321 incorporates a significant O-B V and I population. Relative to the number of F1-5 V stars, NGC 4321 has 10

times as many O5-9 V stars as does NGC 628. These O-B stars are apparently not an artifact, since a model with the first two main-sequence groups deleted has clear deficiencies: $\langle\delta\rangle$ increases by about 12 percent and the blue and ultraviolet residuals bear the systematic mark of stars which have Balmer jumps that are too large to match the observations in that region. The intrinsic reddening inferred for the NGC 4321 nucleus is E(B-V) = 0.30 mag. The case E(B-V) = 0.20 mag. is a close second choice with, in fact, an insignificantly smaller $\langle\delta\rangle$. This case was rejected since the residual diagram possessed a small but distinct tilt extending over the whole spectral range. Larger amounts of intrinsic reddening can be more securely rejected, but there is some ambiguity about the lower acceptable limit.

Finally, we note that the present model is consistent with the F8 blue-violet spectral type and the inferred presence of substantial numbers of K stars quoted by Morgan and Osterbrock (1969).

vi) NGC 5194

NGC 5194 possesses the strong K-giant and F-dwarf contributions characteristic of NGC 628 and NGC 4321. However, as stated in Section Va, the basic model for NGC 5194 has been calculated with the numbers of O5-B9 V stars left completely unconstrained. This procedure was necessitated by the excessive ultraviolet flux in the model with normal

constraints on these stars (see Figure 4). That these high points are not just due to observational errors is established by the unconstrained models we have tested for NGC 5194. With the exception of the highly discrepant λ3300 point, which is regarded as a bad datum, the points below the Balmer jump do not systematically diverge unless constraints forcing O-B stars into the solution are used. This behavior is not observed for any of the other galaxies, including NGC 628. We note that had a gaseous continuum-emission contribution inferred from the Hα strength been subtracted in the case of NGC 5194, the problem of excessive ultraviolet flux in models containing O-B stars would be compounded (∿ additional 6 percent residual at λ3620).

Since the main-sequence groups are constrained in a serial-ratio fashion, it appears that it may be largely a need for a substantial A V component which causes the standard-constraint model to have too many O-B V stars in NGC 5194. A model like the standard one but with the group 2 / group 3 ratio left free, and which is constrained to include only enough O5-O9 V stars to contribute 0.005 of the λ3300 light,actually uses 17 such stars and improves, but does not in fact completely cure, the ultraviolet discrepancy. Our conclusion then is that unobscured O-B stars cannot be present in NGC 5194 in significant proportions relative to the numbers of A and F dwarf stars in the model, and that the data are not inconsistent with their complete

absence. This apparent selective exclusion of O-B stars is not seen in the models for any of the other galaxies.

The final note in regard to our NGC 5194 stellar model concerns the likely presence of the auroral emission line λ4363 of [OIII]. Warner (1973) has noted the probable detection of this line in the central 2.5 arc sec of the nuclear region. The image-tube spectra of Williams (1975) refer to a similar region and also indicate an emission feature at the expected wavelength. On the basis of these spectra and the excess flux observed in the MCSP bandpass centered at λ4363 (rest frame), we consider the detection likely. (The possibility of imperfect sky subtraction at the wavelengths of strong night-sky features, such as is seen in the case of NGC 1637, raises a question in regard to the influence of the λ4359 artificial Hg line. However, there are no indications of particular difficulties with the sky subtraction for NGC 5194, and furthermore, λ4359 is separated from redshifted λ4363 by 10Å, and thus the Hg line should not be strongly present in the relevant MCSP bandpass.)

An estimate of the strength of the observed [OIII] λ4363 emission may be obtained from the flux residual with respect to the stellar model at the λ4360 synthesis wavelength, which was omitted from the fitting process. The literal residual flux is 11.3 percent, but with due regard for the scatter of the residuals at neighboring wavelengths,

a fair estimate for the excess is ∿8 percent of the synthesis model flux, or approximately 3×10^{-14} ergs $cm^{-2} sec^{-1}$. The [OIII] λ5007 intensity, corrected for the inferred intrinsic nuclear reddening, is 2.3×10^{-13} ergs $cm^{-2} sec^{-1}$ so that $I(\lambda 4363)/I(\lambda 5007) \sim 0.1$ with an estimated uncertainty of about a factor of 2. This measurement, although uncertain, suggests that the ionization mechanism in NGC 5194 may be collisional (Osterbrock 1971; Warner 1973).

d) O-B Stars and the Ultraviolet Radiation Field

The presence of significant numbers of O-B stars has arisen in a natural and consistent way in the optimal models for all of the nuclear regions studied here except those for NGC 628 (which has no emission lines) and NGC 5194. In the case of NGC 5194, there are suggestions from the emission-line spectrum that the ionization process may be collisional (Sections IIIb and Vc vi).

For the remaining five nuclear regions, presumed to be radiatively ionized (Section IIIb), we must ask whether the ultraviolet radiation field associated with the model O-B stars is sufficient to provide the ionization inferred from Balmer-line emission strengths. There are at least two conflicting precedents regarding this question in other galaxies: Pronik (1973) has concluded from a sample of 16 nearby normal galaxies that the ionizing stars are in fact the same stars which determine the ultraviolet and blue colors of the galaxies, whereas Osmer, Smith, and Weedman (1974) have concluded in the case of six Sersic-Pastoriza galaxies that the ionizing stars contribute negligibly to the integrated colors, due to large amounts of dust absorption selectively associated with the HII complexes.

Our calculations of the number of ionizing photons required in the nuclear regions studied closely parallel those of Osmer, Smith, and Weedman (1974), except we use

the Hα flux as corrected for the intrinsic reddening and underlying Hα stellar absorption determined from the model stellar population. (Model Hα absorption equivalent widths are typically $\sim$1.5Å - 3Å). Equating the number of ionizations to the number of recombinations onto excited levels, we find the production rate of ultraviolet photons to be $N_{u\ell} = 7.25 \times 10^{11}$ L(Hα) photons sec^{-1} where L(Hα) is the Hα luminosity in ergs sec^{-1}, and where we have used a recombination coefficient to excited levels at $T_e = 10^4$ °K of $2.58 \times 10^{-13} cm^3 sec^{-1}$ (Seaton 1960).

To estimate the production rate of Lyman continuum photons from the O-B stars of synthesis groups 1 and 2, we use the quantity $N_L/\pi F_V$ ($\equiv f(T_{eff})$, a function of stellar effective temperature) derived by Morton (1969) from model atmospheres of O-B stars. Thus, $N_{u\ell} = 1.23 \times 10^{35} f(T_{eff}) 10^{-.4M_V}$ photons sec^{-1}, where $N_{u\ell}$ is the Lyman continuum photon production rate for a star of absolute magnitude M_V and effective temperature T_{eff}. The constant coefficient here differs slightly from that given by Osmer, Smith and Weedman (1974) because we have referred Morton's numbers to the more recent absolute calibration of α Lyr by Oke and Schild (1970). The effective temperature scale adopted for spectral types O5 V to BO V is a mean of the scales given by Hjellming (1968), Morton (1969) and Peterson and Scholz (1971); for B1 V to B3 V, the scale of Morton and Adams

(1968) is adopted. The absolute-magnitude scale of Blaauw (1963) is then used to compute $N_{u\ell}$ for each spectral type. Means of $N_{u\ell}$ over the first two synthesis groups, obtained by weighting each spectral type in accordance with the "local" initial mass function for large masses $\sim m^{-2.55}$ (Limber 1960), are $\langle N_{u\ell}(1)\rangle = 9.5 \times 10^{48}$ photons sec^{-1} per star and $\langle N_{u\ell}(2)\rangle = 4.7 \times 10^{45}$ photons sec^{-1} per star. Group 1 (O5-O9 V) stars are clearly far more effective ionizing agents.

In Table 8 we compare the number of O5-O9 V stars required to produce the Hα luminosity with the numbers of such stars actually present in the model solutions. The overall agreement within the inherent uncertainties is very good, indicating that with the exception of NGC 5194 the numbers of O stars arising naturally in the stellar-population models are sufficient to explain the observed Hα intensities. This lends credibility to the radiative-ionization scheme presumed for these nuclear regions.

Note that the numbers of O stars required to ionize these nuclear regions are much smaller than the numbers of ionizing-stars inferred by Osmer, Smith, and Weedman (1974) in six Sersic-Pastoriza galaxies. Their inferred numbers are large primarily because of large absorption corrections for the young stars and gas ($E(B-V) \sim 1.0$ mag.) derived from the observed Hα/Hβ emission decrements. However, we find from our work that the observed Hα/Hβ decrements can be

TABLE 8

COMPARISON OF THE NUMBER OF O5-O9V STARS REQUIRED TO PRODUCE OBSERVED IONIZATION WITH NUMBERS PRESENT IN POPULATION MODELS

NGC	Corrected Hα Lumimosity $L(H\alpha)^{*}$ (ergs sec^{-1})	Ultraviolet photon rate N_{ul} (sec^{-1})	Predicted N(O5-O9V)	Actual N(O5-O9V)
628	...	...	...	39
1073	1.8 (39)	1.3 (51)	140	444
1084	2.3 (40)	1.7 (52)	1800	1160
1637	5.8 (39)	4.2 (51)	440	147
2903	6.9 (39)	5.0 (51)	530	802
4321	1.1 (40)	7.9 (51)	830	719
5194	3.6 (39)	2.6 (51)	280	0

*Hα luminosities are corrected for the intrinsic reddening and underlying stellar absorption implied by the stellar-content models.

The numbers in columns 2 and 3 are written in exponential notation - the parentheses contain the appropriate powers of 10.

rather misleading if the underlying Hβ stellar absorption is neglected. For example, NGC 1637 and NGC 2903 both have observed decrements $I(H\alpha)/I(H\beta) \sim 10$, yet when the correction for underlying Balmer-line absorption is taken into account, as well as the (comparatively modest) intrinsic reddening implied by the model-fitting process, the decrements are close to normal within the uncertainties: for NGC 1637, the corrected intensity ratios α/β, γ/β, δ/β are 3.6 ± 0.4, 0.6 ± 0.1, 0.3 ± 0.1; and for NGC 2903 3.7 ± 0.4, 0.3 ± 0.1, 0.3 ± 0.1, to be compared to theoretical Case B values at $T_e = 10^4$ °K of 2.87, 0.47, 0.26 (Pengelly 1964). In these two galaxies, there is apparently no need to presume large amounts of differential gas/star absorption and reddening, and we suggest that it is dangerous to attribute large emission decrements solely to the effects of reddening in cases where the emission equivalent widths of Hβ are small enough to be significantly affected by underlying stellar absorption (Hβ absorption equivalent widths in our population models are $\sim$2.2Å - 4.5Å). In particular, since the analysis of Osmer, Smith and Weedman (1974) makes no explicit reference to allowance for underlying absorption and the Hβ emission strengths correspond, except for NGC 1808, to equivalent widths from $\sim$2.3Å to 5.5Å, it seems possible that somewhat less extreme interpretations may be compatible with their data.

Finally, we should note in connection with the other galaxies in the present sample that accurate corrected decrements are not recoverable: the uncertainties are large due to the weakness of Hβ which is not seen at all except as a residual with respect to the stellar-model flux. This is likely a result of the overall relative weakness of the Balmer emission system--see the Hα equivalent widths in Table 5--rather than evidence for additional reddening. A possible exception is NGC 1084, for which EW(Hα) $\sim$ 25Å and for which the model-corrected decrement $I(H\alpha)/I(H\beta) \sim 6 \pm 1.7$. The Hα intensity for this galaxy is uncertain, however, since the Hα/[NII] ratio is an estimate from an uncalibrated photographic spectrum.

e) Electron Densities and HII Masses

For the nuclei of NGC's 1084, 1637, and 2903 we have measured the density-dependent intensity ratio of the [SII] emission lines at λ6717 and λ6731 from calibrated photographic slit spectra obtained by the author. For NGC 5194 the ratio is given by Warner (1973) and measurable on the slit spectra of Williams (1975). One can estimate the electron density appropriate to the region emitting the [SII] lines by means of the data in Krueger, Aller, and Czyzak (1970). The "forbidden line" electron densities so inferred are denoted $n_e(f\ell)$ and are given in Table 9. In the case of the galaxies for which the [SII] intensity ratio has not

been measured, for the purposes of the present discussion we have assumed that the density $n_e(f\ell)$ can be approximated by the mean of that for the four other galaxies: $\langle n_e(f\ell)\rangle = 2.3 \times 10^3 cm^{-3}$.

From the absolute intensities of the absorption-corrected Hα emission (Table 8), it is possible to measure an r.m.s. electron density since the Hα intensity is proportional to $n_e^2 V$, where V is the volume of the emitting region. In each of the nuclear regions with Hα present, the emission extends over a region larger than that defined by the scanner aperture used (this is determined from the slit spectra) so that V is assumed to be a spherical volume with angular diameter equal to the scanner aperture. The $n_e^2 V$ and the V and $n_e(rms)$ calculated in this way (see Piembert 1968 for equations) are also listed in Table 9 for each galaxy. (We have computed these quantities for NGC 5194 even though the exact conditions of excitation and ionization are uncertain). As is often found, $n_e(rms) << n_e(f\ell)$, implying the probable existence of large density fluctuations in the emitting material. Following Piembert (1968), it is possible to reconcile $n_e(rms)$ with $n_e(f\ell)$ if one assumes an extreme model of density fluctuations where a fraction α of the total volume is filled at density $n_e(f\ell)$ and the density is zero throughout the remaining volume; in this case, $\alpha \equiv n_e^2(rms)/n_e^2(f\ell)$. One may

then set upper and lower limits on the mass of ionized hydrogen M(HII) in the emitting region: $M(HII) \leq n_e(rms)V\, m_H \equiv M(rms)$ where m_H is the mass of a hydrogen atom. At the same time, $M(HII) \geq (n_e^2 V) m_H / n_e(f\ell) \equiv M(\alpha)$. (One may easily verify that this is equal to the total mass contained in filaments occupying a volume αV with density $n_e(f\ell)$ and thus is identical with Piembert's (1968) $M(\alpha)$). The quantities α , M(rms), and $M(\alpha)$ are listed in Table 9. Note that very small filling factors α are implied by the data.

In the mean, the HII mass limits indicate that the mass in ionized hydrogen is between $\sim 5 \times 10^{-6}$ and 10^{-2} of the total stellar mass of the adopted synthesis model. There appears to be no clear-cut correlation of the ratio M(HII)/M(stellar) with other properties of the nucleus such as indications of recent star-formation activity. Although the interpretation of this is somewhat ambiguous, especially in view of the uncertainties in both M(HII) and M(stellar), it <u>may</u> indicate that some gas-replenishment mechanism is required to maintain continued star-formation processes in the nuclear regions.

TABLE 9

ELECTRON DENSITIES AND IONIZED HYDROGEN MASSES

NGC	$n_e^2 V$ (cm^{-3})	V (cm^3)	n_e(rms) (cm^{-3})	$n_e(f\ell)$ (cm^{-3})	Filling Factor α	HII Masses M(rms) $m_\odot$	M(α) $m_\odot$
628	...	5.34 (63)	...	...	...	...	...
1073	5.1 (63)	8.51 (63)	0.8	2.3 (3)*	1.1 (-7)	5.5 (6)	1.8 (3)
1084	6.5 (64)	8.51 (63)	2.8	2.2 (3)	1.6 (-6)	2.0 (7)	2.5 (4)
1637	1.6 (64)	7.99 (62)	4.5	1.8 (3)	6.4 (-6)	3.1 (6)	7.7 (3)
2903	1.9 (64)	2.85 (62)	8.3	4.1 (3)	4.1 (-6)	2.0 (6)	4.0 (3)
4321	3.1 (64)	4.95 (63)	2.5	2.3 (3)*	1.2 (-6)	1.0 (7)	1.1 (4)
5194	1.0 (64)	7.99 (62)	3.6	1.1 (3)	1.1 (-5)	2.4 (6)	7.8 (3)

* Mean value for the galaxies in which $n_e(f\ell)$ was directly measured.

For all data columns except n_e(rms), the numbers are written in exponential notation - the parentheses contain the appropriate powers of 10.

VI. DISCUSSION

a) Evolutionary Interpretation

The stellar-population models presented in Section V understandably share some common characteristics but also exhibit a large degree of diversity. All the models calculated have weak lower-main-sequence populations, some intrinsic reddening, and a much stronger population of "young" stars (main sequence more massive than 1 $m_{\odot}$) than is found in k-nuclei galaxies. This last characteristic, however, is shared to considerably varying degrees. In galaxies like NGC 628 and NGC 5194, the extreme upper main sequence plays no essential role and these systems are characterized by very significant G-K III contributions. In systems such as NGC 1073, NGC 1084, NGC 1637, and NGC 2903, on the other hand, massive young stars are very important and the G-K III stars contribute relatively little. NGC 4321 appears, interestingly, to represent an intermediate, or "transition" object between these two broad categories--it possesses both the strong K-giant contribution characteristic of the first category and a significant O-B star contribution such as is characteristic of the second category.

The question of the origin of this diversity among the Sc nuclei studied immediately suggests itself. Several recent investigations of the evolutionary histories of

various stellar systems have suggested that the present-day characteristics of the stellar populations in diverse galaxies are explicable in terms of the time dependence of a star-formation process with a constant, universal mass spectrum (Searle, Sargent, and Bagnuolo 1973; Larson and Tinsley 1974; Ostriker and Thuan 1975). Within the framework of the simple models used in Section IVc to construct evolutionarily-consistent constraints for the synthesis procedure, it is possible to subject the present results to tests of various evolutionary histories. The results of any such procedure should of course be viewed with caution: the model histories are highly schematic, and all one can ever hope to demonstrate in any case is compatibility with one or another particular history.

Extensive tests of models highly constrained to correspond to various combinations of α and τ (see equation (3)) have been conducted for the seven galaxies in the present sample. Because of its possible special significance (see references above), an initial mass function (relative number of stars formed per unit mass) approximating the "local" IMF (Limber 1960) has been given particular emphasis. Limber's data shows, and Larson and Tinsley (1974) have pointed out, that for masses less than 1 $m_\odot$, the local IMF is considerably shallower (smaller α) than the Salpeter mass function $\sim m^{-2.4}$. We have consequently approximated the local IMF by fitting the Limber (1960)

data with a two-part power law joined smoothly at $m = .75\ m_\odot$ such that $\alpha = 2.55$ for $m \geq .75\ m_\odot$ and $\alpha = 1.5$ for $m < .75\ m_\odot$. Additionally, tests have been made with single-α IMF's and a second two-part IMF similar to the local function but with $\alpha = 3$ for $m \geq .75\ m_\odot$. All total ages have been taken to be 12×10^9 years.

Without exception, each of the nuclear regions studied here seems most compatible, among the possibilities tried, with initial mass functions approximating either the "local" IMF or the two-part IMF with $\alpha = 3$ at high masses, with some indications that even larger α values may be appropriate in the very high mass range. The discriminating characteristic between galaxies is the birthrate time dependence, which appears to range from exponential with time constant $\tau \simeq 3 \times 10^9$ years (NGC 628) to a completely constant rate (NGC 2903). Not surprisingly, the two broad categories of stellar population mentioned above correspond to two broad classes of time dependence: the NGC 628-5194 group is most compatible with time constants in the range $3\text{-}6 \times 10^9$ years, and the NGC 1073-1084-1637-2903 group is most compatible with very large time constants ($\sim 12 \times 10^9$ years) or even constant birthrates. Also, as before, NGC 4321 seems to be intermediate, characterized by time constants $\sim 6\text{-}12 \times 10^9$ years.

Single-α IMF's as steep as $\alpha = 3$ or as shallow as $\alpha = 2$ are not as compatible with the galaxy data in any of

the cases. In general, the $\alpha = 3$ models are much too red at $\lambda > 5000\text{Å}$ for the bluest galaxies and they provide too much flux in the $\lambda 8500$ region for the redder galaxies (see Figure 4). NGC 628 is unique among the present galaxies in that it is the one least compromised by an $\alpha = 3$ model. Additionally, the nuclear-region masses for the $\alpha = 3$ models are extremely high, often $\gtrsim 10^{10}\ m_\odot$, due to the very large number of faint M dwarfs present. Nothing like the steep mass function found by Spinrad and Taylor (1971) for M31 ($\alpha \sim 3.5$) seems allowable in the present galaxies. Models with $\alpha = 2$ are generally too bright at ultraviolet wavelengths. When time constants short enough to reduce this ultraviolet flux ($\tau \sim 2 \times 10^9$ years) are used, the region $3800\text{Å} \leq \lambda \leq 4500\text{Å}$ then typically becomes too faint (see Figure 4). This presumably happens because when numbers of O-B stars small enough to be consistent with the ultraviolet luminosity are used, the shallow mass function does not provide sufficient numbers of F and G dwarf stars.

The conclusion we make with respect to the initial mass functions characterizing the galaxies studied is that, whereas it is obviously not possible to consider <u>all</u> combinations of IMF and time dependence, there is apparently no <u>need</u> to invoke a <u>large variety</u> of IMF's: the overall observed stellar properties are best reproduced by IMF's resembling the local function with a variety of time dependences. This result is thus similar to that found by

Searle, Sargent, and Bagnuolo (1973) and Larson and Tinsley (1974) in reference to other stellar systems.

b) Final Considerations

One particularly interesting aspect of the broad categorization of stellar populations made in the preceding section is revealed in Figure 5, where the intrinsic nuclear energy distributions (i.e., corrected for the intrinsic reddening implied by the model-fitting process) have been grouped according to the van den Bergh luminosity classification (Table 3). Those galaxies classified as Sc I have the intrinsically reddest nuclei (those with significant K-giant contributions); the other luminosity classes have intrinsically bluer nuclear regions. (It should be noted that two of the intrinsically "blue" nuclear regions (NGC 1084, NGC 1637) have observed colors as red as the Sc I group (see Figure 2). The separation of luminosity classes in terms of color is thus not evident until the intrinsic colors are recovered. NGC 4321 is the bluest of the Sc I group, consistent with its "transition object" nature cited in Section VIa. However, inasmuch as the choice of intrinsic reddening for this galaxy is uncertain and may be too large, as explained in Section Vcv, the significance of its assigned intrinsic color is ambiguous.) By the results of Section VIa, we may interpret these intrinsic colors and corresponding stellar populations as reflecting the overall time dependence of star formation in each nuclear region.

FIGURE 5

Intrinsic energy distributions of the nuclear regions studied (observed energy distributions corrected for the intrinsic reddening implied by the model-fitting process as described in the text), grouped according to van den Bergh luminosity classifications. Note that only the observed synthesis wavelengths are shown and that the Hα point has been deleted to avoid confusing overlap. The Sc I group has been normalized to provide overall agreement in the region from λ7000 to λ10000, and likewise the remaining galaxies have been so normalized and arbitrarily displaced from the Sc I group to avoid overlap. The Sc I group is comprised of (in order of increasing flux at λ3570) NGC 5194, NGC 628, and NGC 4321. In similar order, the other galaxies are NGC 1637, NGC 1084, NGC 2903, and NGC 1073. (Note the local crossover of NGC 2903 and NGC 1073 at the λ3570 point.)

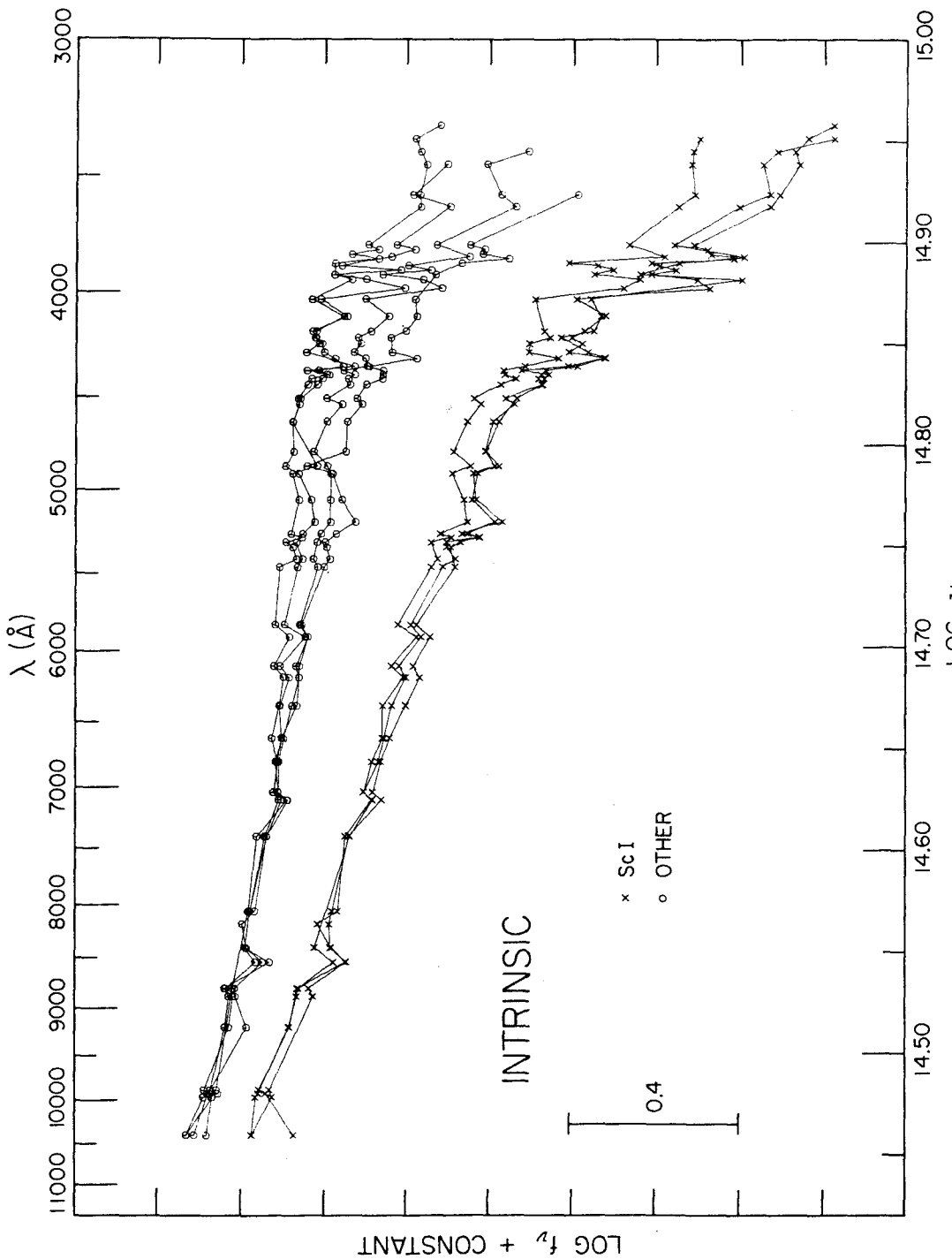
λ (Å)
3000
4000
5000
6000
7000
8000
9000
10000
11000
LOG ν
15.00
14.90
14.80
14.70
14.60
14.50
LOG f_ν + CONSTANT
INTRINSIC
× Sc I
○ OTHER
0.4

FIGURE 5

Taken literally, this implies that among the present sample, star formation has in recent times been less active in the nuclear regions of the Sc I galaxies than it has been in the nuclear regions of the lower-luminosity class galaxies.

This result is intriguingin that it relates a nuclear property of the galaxies to a more global property (luminosity class, which essentially measures the degree of development of the spiral arms; van den Bergh 1960a,b). Suggestions have been made that overall characteristics such as luminosity class are largely determined by more fundamental dynamical properties of spiral galaxies (Roberts, Roberts, and Shu 1975). If this is so, then one might ask whether the nuclear-color luminosity-class correlation seen here is also simply a manifestation of some more fundamental property or properties.

In this connection the available rotation-curve data for the program galaxies have been consulted (see the references in Table 3). Four galaxies in all, two in each of the main groups differentiated here, have published rotation curves. The rotation curves for NGC 4321 and NGC 5194 show strong differential rotation indicative of high central mass concentrations. The two blue galaxies with rotation curves, NGC 1084 and NGC 2903, have relatively more extensive regions of solid-body rotation, indicative of lower central mass concentrations. Under the density-wave theory of spiral structure, galaxies with rotation properties of the former type

are in general expected to have inner Lindblad resonances (see, e.g., Lin 1971; Shu, Stachnik, and Yost 1971). Shu et al. (1971) and Tully (1974) have discussed the existence of an inner Lindblad resonance in NGC 5194; Tully (1974) finds it to be coincident with the termination of spiral structure at an angular radius of about 30 arc sec. On the other hand, galaxies with more nearly solid-body rotation properties do not in general possess the inner resonance. Can it be that a typical "blue" nucleus of the present sample has been able to continue star-formation processes over a large portion of its history because of interactions with its surrounding galaxy as a whole, and that the "red" nuclei have been largely denied these interactions by damping in dynamical resonances? Our data can only be suggestive on this point; interestingly, however, Simkin (1975) has found evidence for streaming motions of gas into the nucleus of NGC 2903 at small radii along the optical spiral arms. If our speculation is correct, then the nuclear-color rotation-curve correlation is the more general one, and we should expect, for example, that a galaxy like NGC 157 with a large solid-body radius and no indications of an inner resonance (Roberts et al. 1975) would fall into the intrinsically-blue-nucleus category, despite its Sc I classification. A test of this would need to be able to infer the intrinsic reddening or be based on reddening-independent parameters.

We note that Saslaw (1971) has previously addressed the question of the relation between the dynamical properties of spiral galaxies and the stellar content of their nuclei. His data led to the conclusion that no correlation exists, which is largely inconsistent with the present results for the four galaxies with adequate dynamical data. We suggest the possibility that the uncorrected effects of Balmer-line emission and intrinsic reddening (both shown to be significant in the present sample) may have reduced the usefulness of the $H\delta$ and $H\gamma$ absorption indices and the "blueness" continuum index employed by Saslaw (1971). His two remaining indices, measuring CN and G-band strengths, are by themselves probably inadequate guides to the overall stellar content.

VII. SUMMARY

The present work has reported a means of studying the stellar content of the nuclear regions of seven nearby Sc galaxies, utilizing the methods of linear programming to carry out detailed stellar-population syntheses. The guidelines for the syntheses were provided by simple model evolutionary histories and are believed to have resulted in physically consistent stellar-content models incorporating the effects of multiple generations of stars.

The principal conclusions to be drawn from these synthesis models include the existence of substantial intrinsic reddening in most of the nuclear regions studied, the existence of significant upper-main-sequence populations in most cases, and the lack of a very heavily-populated lower main sequence in all cases. In addition, with the exception of NGC 5194, for which there is evidence for collisional influences, the O-B stars in the model population are sufficient to provide the observed nuclear ionization. No evidence for significant amounts of differential gas/star absorption has been found, and the possible effects of underlying stellar absorption on observed Balmer decrements have been emphasized.

Reference to the simple evolutionary models used to constrain the synthesis solutions has indicated that the properties of the observed nuclear regions are consistent

with the existence of a common initial mass function for star formation (∿"local" IMF) and a variety of time dependences for the star-formation process ranging from exponential decays with time constants of 3-6 billion years to a constant rate. Finally, attention has been drawn to a possibly significant correlation of stellar content and dynamical properties among four of the program galaxies.

APPENDIX A

STELLAR SINGLE-CHANNEL SCANNER PHOTOMETRY

A program of spectrophotometry of local stars was carried out using single-channel photoelectric spectrum scanners attached to the Mount Wilson 1.5-meter and 2.5-meter telescopes, and the Palomar 1.5-meter telescope. Originally intended to supplement the scanner photometry of O'Connell (1970), this program measures the absolute flux density f_ν (ergs $cm^{-2}sec^{-1}Hz^{-1}$) at 35 wavelengths between 3570Å and 10800Å corresponding to most of those measured by O'Connell and with the following bandpasses: for $\lambda \leq 3620$Å, $\Delta\lambda = 40$Å; for $3860\text{Å} \leq \lambda \leq 4862\text{Å}$, $\Delta\lambda = 20$Å; for $5050\text{Å} \leq \lambda \leq 7400\text{Å}$, $\Delta\lambda = 30$Å; for $8050\text{Å} \leq \lambda \leq 10800\text{Å}$, $\Delta\lambda = 40$Å. Since several of the program stars were observed only with an earlier version of this bandpass sequence measuring the Hβ line at λ4862 with a 30Å bandpass, a correction to an effective bandpass of 20Å was computed as a function of spectral type from data for stars having both 30Å and 20Å measurements. This correction was applied to those stars with only 30Å Hβ measurements. (Near type AOV this correction ≃+0.08 mag.) Stars with the Hβ point so "rectified" are identified in the list of Table A1 (described below) by an asterisk at the λ4862 point.

Wavelengths shorter than 8000Å were measured with an S-20 photocathode; at longer wavelengths, an S-1

photocathode was employed. Separation of spectral orders was achieved by means of glass filters. Stars redder than $B-V \simeq +0.40$ could not be accurately measured in the ultraviolet region with the Mount Wilson scanner using the standard Schott BG-38 filter. Excess flux (relative to Palomar-scanner measurements or other sources) in the ultraviolet for these stars persisted even when the contribution from the monochromatic first-order redleak was removed, suggesting that scattered light was the chief contaminant. Because of this problem, no Mount Wilson ultraviolet data for stars redder than $B-V = +0.40$ are used.

Reliable data for 35 bright stars of predominantly early spectral type are available. Most stars were observed more than once, and the standard deviations of the multiple scans suggest that the photometric accuracy is of the order of 1 or 2 percent over most of the observed spectral range, and up to several times larger in the ultraviolet. The observed scans have been corrected for reddening by the Whitford law using color excesses determined in one of two ways. For class V and class IV stars, the intrinsic two-color relation and reddening trajectories given by Wildey (1962) were combined with published UBV colors (Blanco, Demers, Douglass, and Fitzgerald 1968) to infer the color excess E(B-V). For higher-luminosity stars, the intrinsic colors as a function of spectral type and luminosity class (Johnson 1963, 1966) and published UBV colors were used to

estimate E(B-V). Spectral types given by Hoffleit (1964) were adopted.

Table A1 lists the reddening-corrected scans (some of which are only partial) for the 35 program stars. The quantities listed are the wavelength and the magnitude per unit frequency interval (-2.5 log f_ν + const.) normalized to 0.0 at λ5050. Entries of 0.0 at wavelengths other than λ5050 indicate the absence of data. Stars are identified by their HR number or, in the case of the last 3 stars in the table, by their HD number.

The overall agreement with the spectrophotometry of O'Connell (1970, 1973) is good except for wavelengths greater than about 7000Å in the O and early B stars, where the present magnitudes become increasingly fainter than those of O'Connell with increasing wavelength. Individual stars are fainter by up to ∿ 20 percent at the λ10800 point. The origin of the discrepancy is unclear and not traceable to differences in the absolute calibrations. Comparisons with hot-star model atmospheres (Mihalas 1965; Hickok and Morton 1968) favor the present results.

TABLE A1

NORMALIZED MAGNITUDES

	8023	8622	6353	6588	7171	7174
	O6	O9V	B1V	B3V	B6V	B6V
LAMBDA	MAG	MAG	MAG	MAG	MAG	MAG
3570	-0.64	-0.64	-0.40	0.08	0.47	0.50
3620	-0.61	-0.61	-0.37	0.07	0.43	0.49
3860	-0.53	-0.53	-0.47	-0.34	-0.25	-0.18
3910	-0.52	-0.52	-0.48	-0.37	-0.28	-0.21
3933	-0.49	-0.50	-0.44	-0.36	-0.30	-0.22
4015	-0.43	-0.44	-0.36	-0.32	-0.31	-0.22
4101	-0.28	-0.26	-0.14	-0.03	0.08	0.21
4200	-0.34	-0.35	-0.34	-0.30	-0.28	-0.20
4270	-0.34	-0.34	-0.29	-0.26	-0.25	-0.17
4305	-0.33	-0.33	-0.27	-0.27	-0.22	-0.15
4340	-0.19	-0.15	-0.04	0.05	0.15	0.26
4400	-0.29	-0.28	-0.24	-0.22	-0.20	-0.15
4470	-0.23	-0.19	-0.15	-0.13	-0.16	-0.09
4500	-0.23	-0.22	-0.20	-0.20	-0.18	-0.11
4786	-0.10	-0.11	-0.11	-0.08	-0.08	-0.07
4862	0.06	0.07	0.11	0.19	0.27*	0.29
5050	0.0	0.0	0.0	0.0	0.0	0.0
5176	0.04	0.03	0.03	0.04	0.03	0.03
5300	0.10	0.09	0.09	0.07	0.04	0.06
5820	0.32	0.31	0.29	0.25	0.19	0.19
5892	0.40	0.41	0.35	0.30	0.25	0.23
6100	0.39	0.39	0.37	0.31	0.24	0.24
6562	0.66	0.71	0.67	0.58	0.53	0.56
7050	0.71	0.73	0.65	0.54	0.48	0.44
7100	0.69	0.73	0.67	0.54	0.48	0.44
7400	0.78	0.82	0.75	0.63	0.57	0.51
8050	0.95	0.98	0.89	0.76	0.73	0.60
8190	0.96	1.02	0.94	0.77	0.75	0.61
8400	1.03	1.06	0.99	0.82	0.79	0.66
8542	1.07	1.10	1.01	0.87	0.84	0.68
8800	1.19	1.24	1.12	0.90	0.77	0.70
9190	1.23	1.28	1.14	0.94	0.86	0.68
9950	1.34	1.37	1.22	1.04	0.92	0.77
10400	1.45	1.44	1.31	1.11	1.03	0.84
10800	1.53	1.48	1.37	1.21	1.09	0.85

TABLE A1 (CONTINUED)

NORMALIZED MAGNITUDES

	6281	6826	7773	5567	6533	7710
	B3V	B8V	B9V	B9.5V	B9.5V	B9.5II
LAMBDA	MAG	MAG	MAG	MAG	MAG	MAG
3570	0.58	0.81	1.02	1.00	1.04	0.94
3620	0.58	0.76	1.01	0.98	0.99	0.92
3860	-0.25	-0.13	-0.11	-0.11	-0.06	-0.20
3910	-0.28	-0.17	-0.18	-0.12	-0.09	-0.24
3933	-0.30	-0.20	-0.16	-0.17	-0.15	-0.25
4015	-0.28	-0.26	-0.19	-0.25	-0.25	-0.25
4101	0.25	0.29	0.43	0.41	0.53	0.36
4200	-0.23	-0.25	-0.16	-0.20	-0.21	-0.21
4270	-0.20	-0.21	-0.14	-0.18	-0.19	-0.19
4305	-0.17	-0.18	-0.09	-0.14	-0.13	-0.16
4340	0.32	0.33	0.51	0.45	0.55	0.41
4400	-0.17	-0.15	-0.11	-0.15	-0.14	-0.15
4470	-0.12	-0.13	-0.07	-0.12	-0.13	-0.11
4500	-0.13	-0.14	-0.08	-0.14	-0.15	-0.12
4786	-0.08	-0.07	-0.06	-0.05	-0.06	-0.08
4862	0.30	0.40	0.37	0.51 *	0.59 *	0.37
5050	0.0	0.0	0.0	0.0	0.0	0.0
5176	0.03	0.03	0.03	0.05	0.05	0.03
5300	0.07	0.04	0.07	0.06	0.06	0.06
5820	0.23	0.16	0.19	0.17	0.18	0.19
5892	0.26	0.21	0.23	0.19	0.23	0.23
6100	0.27	0.19	0.22	0.20	0.23	0.22
6562	0.62	0.0	0.60	0.58	0.66	0.60
7050	0.48	0.38	0.38	0.41	0.40	0.41
7100	0.48	0.39	0.39	0.41	0.41	0.41
7400	0.54	0.47	0.44	0.50	0.48	0.48
8050	0.66	0.0	0.54	0.60	0.59	0.0
8190	0.66	0.0	0.54	0.64	0.57	0.0
8400	0.73	0.0	0.57	0.63	0.63	0.0
8542	0.76	0.0	0.62	0.64	0.69	0.0
8800	0.70	0.0	0.59	0.56	0.61	0.0
9190	0.76	0.0	0.57	0.72	0.66	0.0
9950	0.85	0.0	0.64	0.65	0.70	0.0
10400	0.89	0.0	0.67	0.76	0.76	0.0
10800	1.00	0.0	0.70	0.81	0.80	0.0

TABLE A1 (CONTINUED)

NORMALIZED MAGNITUDES

	8541	4789	8573	4033	7826	4738
	B9IAB	A0IV	A0IV	A2IV	A3V	A4V
LAMBDA	MAG	MAG	MAG	MAG	MAG	MAG
3570	0.0	1.13	0.99	1.21	0.0	1.31
3620	0.0	1.11	0.95	1.18	0.0	1.27
3860	0.0	-0.03	-0.09	0.04	0.0	0.14
3910	0.0	-0.04	-0.13	-0.00	0.0	0.10
3933	0.0	-0.09	-0.19	-0.03	0.0	0.14
4015	0.0	-0.20	-0.25	-0.19	0.0	-0.13
4101	0.0	0.53	0.43	0.59	0.0	0.60
4200	0.0	-0.16	-0.23	-0.15	0.0	-0.12
4270	0.0	-0.14	-0.20	-0.13	0.0	-0.09
4305	0.0	-0.10	-0.16	-0.06	0.0	-0.01
4340	0.0	0.55	0.48	0.59	0.0	0.60
4400	0.0	-0.11	-0.17	-0.11	0.0	-0.07
4470	0.0	-0.11	-0.14	-0.11	0.0	-0.08
4500	0.0	-0.11	-0.15	-0.12	0.0	-0.09
4786	0.0	-0.03	-0.07	-0.04	0.0	-0.02
4862	0.0	0.58*	0.49	0.61	0.0	0.61
5050	0.0	0.0	0.0	0.0	0.0	0.0
5176	0.0	0.05	0.04	0.06	0.0	0.06
5300	0.0	0.06	0.04	0.05	0.0	0.05
5820	0.0	0.16	0.16	0.14	0.0	0.12
5892	0.0	0.19	0.21	0.18	0.0	0.15
6100	0.0	0.20	0.20	0.17	0.0	0.14
6562	-0.01	0.64	0.63	0.0	0.24	0.58
7050	-0.05	0.38	0.43	0.35	-0.03	0.29
7100	-0.05	0.39	0.44	0.35	-0.04	0.30
7400	0.0	0.45	0.50	0.42	0.0	0.35
8050	0.09	0.56	0.60	0.0	0.07	0.41
8190	0.12	0.57	0.61	0.0	0.11	0.42
8400	0.13	0.58	0.64	0.0	0.13	0.45
8542	0.13	0.63	0.66	0.0	0.16	0.49
8800	0.15	0.53	0.65	0.0	0.16	0.42
9190	0.15	0.58	0.68	0.0	0.15	0.44
9950	0.20	0.62	0.69	0.0	0.15	0.45
10400	0.24	0.65	0.74	0.0	0.20	0.49
10800	0.31	0.76	0.75	0.0	0.19	0.54

TABLE A1 (CONTINUED)

NORMALIZED MAGNITUDES

	5333	5291	6332	2820	1740	3975
	A8V	A0III	A3III	A4III	A5II	A0IB
LAMBDA	MAG	MAG	MAG	MAG	MAG	MAG
3570	1.25	1.05	1.17	1.28	1.62	0.89
3620	1.21	1.03	1.14	1.23	1.59	0.87
3860	0.31	-0.10	0.03	0.17	0.09	-0.09
3910	0.27	-0.13	0.01	0.09	0.09	-0.14
3933	0.42	-0.18	-0.01	0.21	0.25	-0.13
4015	0.03	-0.24	-0.18	-0.11	-0.04	-0.18
4101	0.64	0.43	0.56	0.57	0.35	0.07
4200	0.01	-0.19	-0.15	-0.09	-0.03	-0.16
4270	0.01	-0.16	-0.13	-0.07	-0.02	-0.13
4305	0.13	-0.13	-0.06	0.04	0.05	-0.11
4340	0.62	0.47	0.60	0.56	0.39	0.12
4400	0.02	-0.13	-0.09	-0.05	0.03	-0.12
4470	-0.00	-0.12	-0.08	-0.05	-0.01	-0.09
4500	-0.03	-0.12	-0.10	-0.08	-0.02	-0.10
4786	-0.01	-0.04	-0.06	-0.03	-0.04	-0.05
4862	0.46	0.53 *	0.54	0.41	0.29 *	0.18
5050	0.0	0.0	0.0	0.0	0.0	0.0
5176	0.04	0.05	0.06	0.05	0.05	0.04
5300	0.01	0.06	0.05	0.04	0.01	0.05
5820	0.05	0.17	0.15	0.11	0.03	0.13
5892	0.09	0.21	0.17	0.13	0.08	0.16
6100	0.08	0.22	0.19	0.15	0.06	0.17
6562	0.43	0.58	0.64	0.53	0.0	0.40
7050	0.15	0.38	0.36	0.27	0.15	0.33
7100	0.16	0.38	0.37	0.29	0.16	0.34
7400	0.18	0.44	0.44	0.33	0.21	0.40
8050	0.23	0.53	0.54	0.0	0.0	0.0
8190	0.26	0.55	0.57	0.0	0.0	0.0
8400	0.25	0.58	0.60	0.0	0.0	0.0
8542	0.30	0.60	0.67	0.0	0.0	0.0
8800	0.28	0.53	0.56	0.0	0.0	0.0
9190	0.35	0.57	0.63	0.0	0.0	0.0
9950	0.31	0.62	0.64	0.0	0.0	0.0
10400	0.31	0.68	0.66	0.0	0.0	0.0
10800	0.43	0.75	0.72	0.0	0.0	0.0

TABLE A1 (CONTINUED)

NORMALIZED MAGNITUDES

	4090 F0V	5634 F5V	382 F0IA	7387 F2IB	7770 F5IB	7368 G8V
LAMBDA	MAG	MAG	MAG	MAG	MAG	MAG
3570	1.32	1.15	0.0	1.79	1.71	2.08
3620	1.28	1.09	0.0	1.71	1.63	1.73
3860	0.33	0.51	0.0	0.20	0.52	1.92
3910	0.30	0.51	0.0	0.27	0.66	1.29
3933	0.58	0.95	0.0	0.83	1.46	1.88
4015	0.05	0.30	0.0	0.09	0.33	0.75
4101	0.53	0.53	0.0	0.43	0.51	0.75
4200	0.04	0.23	0.0	0.11	0.30	0.71
4270	0.03	0.22	0.0	0.07	0.21	0.71
4305	0.15	0.33	0.0	0.19	0.35	0.95
4340	0.52	0.43	0.0	0.42	0.43	0.50
4400	0.04	0.15	0.0	0.12	0.22	0.49
4470	0.03	0.12	0.0	0.07	0.17	0.28
4500	-0.04	0.08	0.0	0.03	0.09	0.20
4786	-0.03	0.02	0.0	0.00	0.01	0.03
4862	0.40	0.29	0.0	0.34	0.28	0.16
5050	0.0	0.0	0.0	0.0	0.0	0.0
5176	0.07	0.04	0.0	0.05	0.07	0.17
5300	0.02	-0.04	0.0	-0.00	-0.01	-0.15
5820	0.04	-0.09	0.0	-0.01	-0.08	-0.31
5892	0.08	-0.04	0.0	0.07	-0.01	-0.20
6100	0.08	-0.09	0.0	0.01	-0.06	-0.33
6562	0.37	0.08	0.04	0.25	0.09	-0.36
7050	0.15	-0.11	-0.07	0.07	-0.05	-0.49
7100	0.17	-0.13	-0.05	0.07	-0.05	-0.50
7400	0.20	-0.10	0.0	0.11	0.0	-0.49
8050	0.0	-0.11	0.04	0.13	0.0	-0.55
8190	0.0	-0.08	0.08	0.18	0.04	-0.55
8400	0.0	-0.11	-0.00	0.15	0.0	-0.59
8542	0.0	-0.01	0.00	0.19	0.11	-0.49
8800	0.0	-0.05	-0.01	0.10	0.04	-0.50
9190	0.0	-0.02	-0.01	0.10	0.00	-0.56
9950	0.0	-0.06	-0.02	0.08	-0.01	-0.67
10400	0.0	-0.05	0.03	0.11	0.02	-0.69
10800	0.0	0.00	0.10	0.13	0.02	-0.67

TABLE A1 (CONTINUED)

NORMALIZED MAGNITUDES

	7429 K3III	8248 K1IB	130705 K3III	161817 HBA	219615 G8III
LAMBDA	MAG	MAG	MAG	MAG	MAG
3570	3.29	0.0	3.60	0.0	0.0
3620	2.68	0.0	2.91	0.0	0.0
3860	2.95	0.0	3.27	0.0	0.0
3910	2.12	0.0	2.33	0.0	0.0
3933	2.85	0.0	3.01	0.0	0.0
4015	1.28	0.0	1.42	0.0	0.0
4101	1.30	0.0	1.52	0.0	0.0
4200	1.29	0.0	1.50	0.0	0.0
4270	1.08	0.0	1.15	0.0	0.0
4305	1.30	0.0	1.27	0.0	0.0
4340	0.71	0.0	0.74	0.0	0.0
4400	0.77	0.0	0.81	0.0	0.0
4470	0.50	0.0	0.52	0.0	0.0
4500	0.37	0.0	0.41	0.0	0.0
4786	0.09	0.0	0.09	0.0	0.0
4862	0.15	0.0	0.18	0.0	0.0
5050	0.0	0.0	0.0	0.0	0.0
5176	0.18	0.0	0.14	0.0	0.0
5300	-0.26	0.0	-0.29	0.0	0.0
5820	-0.55	0.0	-0.61	0.0	0.0
5892	-0.43	0.0	-0.39	0.0	0.0
6100	-0.63	0.0	-0.67	0.0	0.0
6562	-0.73	0.16	-0.77	0.16	0.19
7050	-0.88	0.01	-0.92	-0.04	0.04
7100	-0.88	0.08	-0.89	-0.08	0.04
7400	-0.93	0.0	-0.96	0.0	0.0
8050	-1.06	-0.06	0.0	0.05	-0.09
8190	-1.04	-0.04	0.0	0.02	-0.07
8400	-1.09	-0.07	0.0	0.06	-0.12
8542	-1.03	0.03	0.0	0.09	-0.05
8800	-1.08	-0.06	0.0	0.05	-0.06
9190	-1.12	-0.01	0.0	0.07	-0.13
9950	-1.31	-0.23	0.0	0.08	-0.25
10400	-1.38	-0.27	0.0	0.07	-0.30
10800	-1.43	-0.29	0.0	0.10	-0.30

APPENDIX B

SYNTHESIS-STAR SPECTROPHOTOMETRY

Since the MCSP stellar survey by Gunn (1974) includes no data for early spectral types or supergiants, spectrophotometry from other sources has been adapted to the MCSP system for these stellar types. The survey by O'Connell (1973) provides the basic required data, although several modifications to these data have been made. Since for O and early B stars there is a systematic discrepancy between the spectrophotometry of O'Connell (1973) and that of the author (Appendix A), data from the two sources have been averaged for these stars and wavelengths. Also, through the use of the individual stellar scans comprising the O'Connell survey (kindly furnished by Dr. R. W. O'Connell), it was possible to eliminate some small peculiarities in the group-averaged energy distributions as published (O'Connell 1973). These anomalies (such as unusual strengths of some Balmer absorption lines and unexpected "bumps" in the energy distribution below the Balmer jump) apparently resulted from the occasional use of incomplete scans in the averaging process. All such instances in the group data used here have been rectified by continuity arguments or by the elimination of partial scans from the averages.

The mean AO-3 V energy distribution of O'Connell (1973) was combined with MCSP data for HD 190849A (A1 V)

to provide the adopted data for the A0-3 V synthesis group. Energy distributions for earlier spectral types and blue supergiants were generated differentially: the magnitude differences between successive groups in the O'Connell survey (modified as above) were applied to successive adopted group energy distributions on the MCSP system, with A0-3 V as the starting point. Because hot stars contain relatively few strong absorption lines, this differential technique can be used successfully even though the O'Connell survey does not include all MCSP synthesis bandpasses. In the instances where lines or line wings do fall in synthesis bandpasses not in the O'Connell survey, the uncertainties in the adopted energy distributions are increased somewhat. Examples of wavelengths affected by these uncertainties are λ3780, λ3830, λ3870, λ3970, λ4360, and λ6560.

The M1-4 I synthesis-group energy distribution was generated in a similar differential fashion from the MCSP M0-1 III synthesis group data and the O'Connell (1973) survey. Here the luminosity-sensitive λ6800 flux was inferred differentially from the λ6620 flux, using the data of Fäy, Stein, and Warren (1974).

In Table B1 we list the constituent stars defining the synthesis groups taken from the Gunn (1974) survey. Groups defined wholly or in part by the O'Connell (1973) data are marked by an asterisk.

TABLE B1

SYNTHESIS GROUP MEMBERS

NO.	NAME		CONSTITUENTS
1	O5-9	V	*
2	B1-3	V	*
3	B5	V	*
4	B8-9	V	*
5	A0-3	V	HD 190849A,*
6	A4-5	V	HD 187754 Praesepe 276 HD 192285
7	A7-F0	V	Praesepe 114 Praesepe 154 HD 190192 Praesepe 37 Praesepe 226 HD 5132
8	F1-5	V	Praesepe 332 Praesepe 222 BD +29° 3891
9	F6-8	V	HD 122693 Hyades 1 Praesepe 418 HD 13391
10	G0-5	V	Hyades 2 HD 154760 HD 227547 Hyades 15 HD 190605
11	G8	V	HD 150205 Hyades 26 HD 136274 Hyades 21
12	K0-2	V	Hyades 183 HD 190470
13	K3-5	V	HD 154712 Hyades 185 BD +38° 2457
14	K7	V	Hyades 189 GL 40 Hyades 173
15	M0	V	HD 132683 HD 151288 HD 157881
16	M1-4	V	GL 49 GL 15A GL 109
17	M5-6	V	GL 15B GL 83.1
18	M7-8	V	GL 65
19	F5-8	IV	BD +63° 0013 HD 7331
20	G0-4	IV	HD 192344
21	G5-8	IV	M67 F143 HD 173399A BD -02° 4018 HD 190571
22	K0-2	IV	HD 199580 HD 191615 HD 4744 HD 7010
23	G5-K1	III	HD 227693 HD 199191

TABLE B1 (continued)

NO.	NAME	CONSTITUENTS
24	K2-5 III	BD +30° 2344 BD +28° 2165 HD 166780
25	K0-1 III SL	HD 113439 M67 F141
26	K2-3 III SL	M67 F170 HD 158885 NGC 188 1-69
27	K4-5 III SL	M67 IV-202 (= BD +12° 1919) HD 127227
28	M0-1 III	BD +2° 2884 BD -2° 3873
29	M2-5 III	BD -2° 4025 BD -1° 3097 BD +1° 3133 BD -2° 3886 Z CYG
30	M6-8 III	W HER RZ HER
31	B0-1 I	*
32	B5-7 I	*
33	A2 I	*
34	M1-4 I	*

* From O'Connell (1973) data as described in the text.

References: Hyades stars - Johnson and Knuckles (1955)
Praesepe stars - Johnson (1952)
GL stars - Gliese (1957, 1969)
M67 stars - Fagerholm (1906)
NGC 188 stars - Sandage (1962)

Table B2 gives the adopted energy distributions for each of the 34 synthesis groups. Listed with the wavelengths are the normalized magnitudes per unit frequency (-2.5 log f_ν + const.). For each group, the normalization is such that

$$\left(\int_{-\infty}^{\infty} S_V(\nu) f_\nu \, d\nu \right) \Big/ \int_{-\infty}^{\infty} S_V(\nu) \, d\nu = 1$$

where $S_V(\nu)$ is the single-airmass V-band response function (Matthews and Sandage 1963). For the groups derived from the O'Connell (1973) data, the normalization integrals are performed assuming a linearly-interpolated f_ν between the 66 synthesis bandpasses. The other groups (Gunn survey) are normalized by means of the actual measurements of f_ν at all intermediate wavelengths. This normalization is particularly convenient in that the overall group luminosities can be accurately ranked by the absolute V-magnitude.

Because of very large observational uncertainties in the blue and ultraviolet spectral regions for the latest two M V synthesis groups, the data have been deleted and replaced by entries of 0.0 in Table B2.

Note that for each synthesis group Table B2 also gives the mean (over all wavelengths) standard deviation of the adopted average energy distribution, in magnitude units. This quantity is denoted <sigma>.

TABLE B2

MEAN NORMALIZED MAGNITUDES

	O5-9 V	B1-3 V	B5 V	B8-9 V	A0-3 V	A4-5 V
LAMBDA	MAG	MAG	MAG	MAG	MAG	MAG
3300	-0.85	-0.34	0.04	0.61	1.16	1.38
3350	-0.86	-0.36	0.02	0.59	1.16	1.40
3400	-0.83	-0.36	0.03	0.57	1.13	1.36
3450	-0.81	-0.32	0.04	0.57	1.08	1.33
3570	-0.74	-0.26	0.07	0.57	1.06	1.25
3620	-0.72	-0.25	0.09	0.56	1.04	1.24
3780	-0.68	-0.42	-0.21	0.03	0.41	0.63
3800	-0.64	-0.31	-0.10	0.17	0.53	0.72
3820	-0.68	-0.44	-0.34	-0.20	0.11	0.34
3830	-0.63	-0.33	-0.15	0.10	0.45	0.61
3840	-0.63	-0.31	-0.12	0.17	0.55	0.74
3860	-0.69	-0.54	-0.44	-0.34	-0.13	0.14
3870	-0.68	-0.53	-0.43	-0.33	-0.12	0.13
3890	-0.59	-0.31	-0.10	0.17	0.52	0.70
3910	-0.68	-0.54	-0.45	-0.33	-0.14	0.16
3930	-0.65	-0.52	-0.45	-0.36	-0.15	0.10
3970	-0.54	-0.26	-0.08	0.15	0.50	0.61
4020	-0.62	-0.47	-0.41	-0.37	-0.27	-0.17
4100	-0.46	-0.21	-0.05	0.18	0.48	0.48
4170	-0.54	-0.45	-0.39	-0.33	-0.25	-0.09
4200	-0.51	-0.45	-0.39	-0.33	-0.25	-0.12
4230	-0.51	-0.43	-0.38	-0.32	-0.24	-0.10
4270	-0.51	-0.42	-0.37	-0.31	-0.23	-0.11
4300	-0.50	-0.41	-0.36	-0.30	-0.17	-0.01
4340	-0.36	-0.13	0.02	0.23	0.50	0.48
4360	-0.45	-0.36	-0.27	-0.15	-0.04	0.05
4380	-0.45	-0.37	-0.32	-0.26	-0.17	-0.06
4400	-0.44	-0.36	-0.32	-0.27	-0.18	-0.07
4430	-0.40	-0.34	-0.30	-0.27	-0.20	-0.11
4500	-0.42	-0.34	-0.30	-0.26	-0.19	-0.12
4530	-0.42	-0.34	-0.30	-0.26	-0.19	-0.10
4620	-0.37	-0.32	-0.28	-0.25	-0.18	-0.13
4780	-0.28	-0.25	-0.21	-0.18	-0.14	-0.14
4860	-0.10	0.03	0.16	0.32	0.52	0.45
4900	-0.22	-0.19	-0.18	-0.15	-0.12	-0.07

TABLE B2 (CONTINUED)

MEAN NORMALIZED MAGNITUDES

	O5-9 V	B1-3 V	B5 V	B8-9 V	A0-3 V	A4-5 V
LAMBDA	MAG	MAG	MAG	MAG	MAG	MAG
5050	-0.17	-0.14	-0.13	-0.11	-0.09	-0.04
5180	-0.14	-0.11	-0.11	-0.08	-0.05	-0.01
5250	-0.12	-0.10	-0.10	-0.08	-0.06	-0.02
5270	-0.09	-0.07	-0.06	-0.05	-0.03	0.04
5300	-0.08	-0.06	-0.05	-0.05	-0.04	-0.02
5330	-0.06	-0.05	-0.02	-0.02	-0.01	0.02
5400	-0.03	-0.03	-0.03	-0.03	-0.02	0.00
5450	-0.00	-0.01	-0.02	-0.01	-0.02	-0.01
5820	0.13	0.11	0.08	0.08	0.06	-0.03
5900	0.20	0.16	0.13	0.11	0.09	0.03
6100	0.22	0.20	0.18	0.14	0.11	0.06
6180	0.27	0.24	0.20	0.17	0.14	0.08
6380	0.32	0.28	0.25	0.21	0.18	0.10
6560	0.45	0.45	0.43	0.44	0.44	0.36
6620	0.44	0.39	0.33	0.28	0.22	0.13
6800	0.49	0.43	0.37	0.31	0.25	0.14
7040	0.55	0.49	0.42	0.36	0.29	0.17
7100	0.55	0.48	0.42	0.35	0.29	0.18
7400	0.65	0.55	0.46	0.39	0.33	0.20
8060	0.80	0.67	0.62	0.50	0.42	0.26
8180	0.77	0.65	0.58	0.55	0.43	0.27
8400	0.78	0.66	0.59	0.50	0.41	0.25
8540	0.80	0.69	0.63	0.54	0.44	0.27
8800	0.91	0.74	0.61	0.48	0.37	0.21
8880	0.96	0.81	0.69	0.60	0.55	0.37
9200	1.06	0.86	0.73	0.63	0.48	0.24
9880	1.06	0.85	0.73	0.62	0.46	0.27
9920	1.04	0.83	0.71	0.58	0.41	0.24
9960	1.08	0.86	0.74	0.61	0.43	0.25
10400	1.23	0.92	0.79	0.68	0.49	0.28
10680	1.25	0.97	0.83	0.75	0.54	0.37
<SIGMA> =	0.01	0.04	0.02	0.03	0.02	0.02

TABLE B2 (CONTINUED)

MEAN NORMALIZED MAGNITUDES

	A7-F0 V	F1-5 V	F6-8 V	G0-5 V	G8 V	K0-2 V
LAMBDA	MAG	MAG	MAG	MAG	MAG	MAG
3300	1.30	1.32	1.48	1.59	1.89	2.39
3350	1.32	1.29	1.51	1.61	1.93	2.47
3400	1.31	1.27	1.47	1.57	1.89	2.40
3450	1.29	1.32	1.52	1.70	2.03	2.62
3570	1.21	1.21	1.42	1.55	1.93	2.63
3620	1.19	1.17	1.34	1.50	1.74	2.29
3780	0.70	0.80	0.96	1.06	1.33	1.82
3800	0.76	0.86	1.05	1.19	1.50	2.11
3820	0.50	0.78	1.16	1.30	1.84	2.51
3830	0.74	1.01	1.35	1.56	2.08	2.78
3840	0.80	1.00	1.22	1.49	1.88	2.58
3860	0.33	0.66	1.01	1.20	1.76	2.50
3870	0.34	0.66	1.02	1.21	1.73	2.42
3890	0.74	0.87	1.07	1.23	1.55	2.08
3910	0.34	0.62	0.90	1.04	1.34	1.85
3930	0.48	0.98	1.33	1.48	1.83	2.25
3970	0.72	0.97	1.19	1.38	1.61	1.99
4020	0.02	0.31	0.49	0.61	0.76	1.09
4100	0.48	0.52	0.60	0.64	0.78	1.05
4170	0.08	0.31	0.47	0.55	0.77	1.11
4200	0.05	0.29	0.46	0.57	0.76	1.10
4230	0.06	0.31	0.49	0.61	0.80	1.17
4270	0.02	0.27	0.45	0.58	0.79	1.07
4300	0.10	0.40	0.63	0.77	1.05	1.27
4340	0.46	0.45	0.48	0.54	0.63	0.73
4360	0.09	0.22	0.32	0.39	0.55	0.68
4380	0.04	0.24	0.38	0.49	0.68	0.90
4400	0.04	0.23	0.35	0.48	0.61	0.81
4430	0.01	0.17	0.30	0.37	0.48	0.67
4500	-0.03	0.12	0.19	0.25	0.33	0.44
4530	0.00	0.17	0.24	0.31	0.39	0.53
4620	-0.06	0.07	0.15	0.18	0.24	0.32
4780	-0.08	0.01	0.07	0.09	0.14	0.23
4860	0.36	0.26	0.25	0.24	0.26	0.29
4900	-0.04	0.03	0.08	0.10	0.14	0.21

TABLE B2 (CONTINUED)

MEAN NORMALIZED MAGNITUDES

	A7-F0 V	F1-5 V	F6-8 V	G0-5 V	G8 V	K0-2 V
LAMBDA	MAG	MAG	MAG	MAG	MAG	MAG
5050	-0.01	0.05	0.08	0.11	0.14	0.25
5180	0.02	0.09	0.15	0.20	0.29	0.53
5250	-0.01	0.02	0.06	0.05	0.07	0.08
5270	0.06	0.09	0.13	0.15	0.19	0.26
5300	-0.01	0.02	0.04	0.03	0.04	0.05
5330	0.03	0.04	0.07	0.07	0.08	0.12
5400	0.01	0.02	0.06	0.05	0.08	0.11
5450	-0.03	-0.04	-0.03	-0.03	-0.02	-0.01
5820	0.01	-0.04	-0.11	-0.09	-0.14	-0.21
5900	0.02	-0.02	-0.08	-0.05	-0.09	-0.07
6100	0.00	-0.06	-0.11	-0.14	-0.14	-0.24
6180	0.04	-0.03	-0.11	-0.11	-0.15	-0.23
6380	0.03	-0.07	-0.14	-0.17	-0.22	-0.32
6560	0.22	0.04	-0.08	-0.12	-0.20	-0.34
6620	0.04	-0.07	-0.17	-0.21	-0.26	-0.37
6800	0.05	-0.09	-0.19	-0.22	-0.28	-0.42
7040	0.06	-0.08	-0.18	-0.21	-0.29	-0.42
7100	0.07	-0.08	-0.19	-0.23	-0.30	-0.43
7400	0.08	-0.07	-0.18	-0.23	-0.31	-0.45
8060	0.11	-0.08	-0.26	-0.28	-0.39	-0.53
8180	0.12	-0.06	-0.23	-0.26	-0.40	-0.56
8400	0.12	-0.10	-0.26	-0.31	-0.43	-0.60
8540	0.14	-0.05	-0.16	-0.23	-0.37	-0.54
8800	0.09	-0.08	-0.21	-0.29	-0.43	-0.59
8880	0.19	-0.08	-0.23	-0.31	-0.42	-0.66
9200	0.12	-0.10	-0.27	-0.35	-0.43	-0.66
9880	0.11	-0.07	-0.25	-0.32	-0.47	-0.67
9920	0.10	-0.09	-0.27	-0.33	-0.48	-0.70
9960	0.09	-0.10	-0.27	-0.35	-0.51	-0.69
10400	0.14	-0.10	-0.29	-0.38	-0.54	-0.76
10680	0.23	-0.03	-0.24	-0.31	-0.51	-0.75
<SIGMA> =	0.02	0.02	0.01	0.01	0.02	0.02

TABLE B2 (CONTINUED)

MEAN NORMALIZED MAGNITUDES

	K3-5 V	K7 V	M0 V	M1-4 V	M5-6 V	M7-8 V
LAMBDA	MAG	MAG	MAG	MAG	MAG	MAG
3300	2.86	3.58	3.87	4.29	0.0	0.0
3350	2.85	3.38	3.62	4.03	0.0	0.0
3400	2.77	3.28	3.43	3.82	0.0	0.0
3450	2.97	3.49	3.67	3.83	0.0	0.0
3570	2.98	3.38	3.58	3.55	0.0	0.0
3620	2.68	3.17	3.31	3.36	0.0	0.0
3780	2.25	2.72	2.88	2.97	0.0	0.0
3800	2.43	2.88	2.96	2.92	0.0	0.0
3820	2.90	3.16	3.25	3.13	0.0	0.0
3830	2.97	3.28	3.31	3.18	0.0	0.0
3840	2.78	3.05	3.10	3.10	0.0	0.0
3860	2.73	3.09	3.11	3.01	0.0	0.0
3870	2.68	2.96	3.03	2.93	0.0	0.0
3890	2.45	2.89	3.00	2.91	0.0	0.0
3910	2.27	2.73	2.82	2.78	3.24	0.0
3930	2.60	2.89	3.01	2.84	3.22	0.0
3970	2.25	2.69	2.73	2.63	2.56	0.0
4020	1.45	1.91	2.08	2.11	2.61	0.0
4100	1.34	1.73	1.90	2.02	2.50	0.0
4170	1.34	1.66	1.80	1.86	2.44	0.0
4200	1.32	1.68	1.79	1.95	2.76	0.0
4230	1.52	2.11	2.30	2.40	3.37	0.0
4270	1.32	1.73	1.85	2.00	2.64	2.94
4300	1.44	1.75	1.84	1.97	2.46	3.01
4340	0.95	1.15	1.37	1.69	2.26	2.18
4360	0.87	1.07	1.28	1.60	2.23	2.46
4380	1.07	1.27	1.49	1.63	2.07	2.31
4400	0.98	1.15	1.34	1.49	2.14	2.43
4430	0.83	1.07	1.23	1.39	1.75	2.34
4500	0.53	0.73	0.83	1.05	1.34	1.57
4530	0.64	0.83	0.96	1.04	1.19	1.33
4620	0.37	0.49	0.56	0.78	0.95	1.06
4780	0.39	0.66	0.78	0.89	1.06	1.10
4860	0.35	0.46	0.55	0.75	0.87	0.69
4900	0.28	0.41	0.50	0.59	0.63	0.63

TABLE B2 (CONTINUED)

MEAN NORMALIZED MAGNITUDES

	K3-5 V	K7 V	M0 V	M1-4 V	M5-6 V	M7-8 V
LAMBDA	MAG	MAG	MAG	MAG	MAG	MAG
5050	0.37	0.56	0.63	0.61	0.65	0.50
5180	0.65	0.83	0.85	0.70	0.78	0.91
5250	0.16	0.23	0.27	0.29	0.26	0.17
5270	0.32	0.40	0.42	0.32	0.26	0.14
5300	0.11	0.17	0.19	0.18	0.12	-0.01
5330	0.17	0.23	0.24	0.18	0.10	-0.01
5400	0.14	0.14	0.13	0.04	-0.14	-0.29
5450	-0.00	0.02	0.03	0.03	0.01	-0.10
5820	-0.28	-0.34	-0.40	-0.36	-0.25	-0.45
5900	-0.16	-0.14	-0.03	-0.00	0.31	0.39
6100	-0.33	-0.44	-0.48	-0.55	-0.55	-0.45
6180	-0.34	-0.37	-0.42	-0.32	-0.07	0.07
6380	-0.42	-0.52	-0.56	-0.68	-0.77	-0.80
6560	-0.48	-0.66	-0.76	-1.00	-1.32	-1.67
6620	-0.52	-0.70	-0.78	-0.96	-1.17	-1.30
6800	-0.54	-0.65	-0.69	-0.70	-0.85	-1.01
7040	-0.61	-0.78	-0.90	-1.23	-1.66	-2.15
7100	-0.61	-0.78	-0.88	-1.09	-1.34	-1.56
7400	-0.64	-0.91	-1.04	-1.61	-2.27	-2.92
8060	-0.78	-1.10	-1.26	-1.96	-2.77	-3.52
8180	-0.77	-1.10	-1.23	-1.93	-2.71	-3.62
8400	-0.80	-1.14	-1.31	-2.03	-2.88	-3.77
8540	-0.77	-1.12	-1.27	-2.00	-2.84	-3.63
8800	-0.82	-1.18	-1.36	-2.12	-3.05	-4.00
8880	-0.89	-1.22	-1.39	-2.13	-3.01	-3.88
9200	-0.93	-1.30	-1.45	-2.27	-3.24	-4.28
9880	-0.96	-1.34	-1.53	-2.36	-3.36	-4.48
9920	-0.99	-1.34	-1.52	-2.33	-3.28	-4.23
9960	-1.00	-1.37	-1.55	-2.37	-3.35	-4.40
10400	-1.02	-1.45	-1.61	-2.45	-3.49	-4.65
10680	-1.05	-1.44	-1.63	-2.48	-3.61	-4.70
<SIGMA> =	0.04	0.04	0.02	0.05	0.06	0.04

TABLE B2 (CONTINUED)

MEAN NORMALIZED MAGNITUDES

	F5-8 IV	G0-4 IV	G5-8 IV	K0-2 IV	G5-K1 III	K2-5 III
LAMBDA	MAG	MAG	MAG	MAG	MAG	MAG
3300	1.32	1.76	2.26	2.79	2.48	4.12
3350	1.34	1.76	2.22	2.88	2.57	4.08
3400	1.28	1.75	2.25	2.72	2.46	3.88
3450	1.35	1.88	2.32	2.74	2.54	4.09
3570	1.25	1.75	2.22	2.72	2.42	4.09
3620	1.21	1.63	1.99	2.36	2.19	3.45
3780	0.83	1.23	1.58	2.00	1.74	3.08
3800	0.92	1.41	1.76	2.14	1.95	3.27
3820	0.88	1.58	2.01	2.48	2.16	3.72
3830	1.13	1.85	2.16	2.60	2.37	3.85
3840	1.08	1.78	2.10	2.48	2.29	3.55
3860	0.75	1.65	2.07	2.46	2.15	3.53
3870	0.76	1.63	2.04	2.42	2.16	3.46
3890	0.93	1.43	1.76	2.07	1.92	3.19
3910	0.69	1.15	1.56	1.90	1.63	2.99
3930	1.09	1.64	1.99	2.33	2.26	3.64
3970	1.06	1.53	1.77	2.03	2.02	3.27
4020	0.34	0.68	0.98	1.25	1.10	1.99
4100	0.53	0.72	0.93	1.18	1.04	1.88
4170	0.34	0.68	0.95	1.22	1.08	1.93
4200	0.32	0.67	0.95	1.18	1.06	1.87
4230	0.34	0.67	0.96	1.14	0.97	1.85
4270	0.31	0.67	0.89	1.10	0.94	1.64
4300	0.46	0.91	1.09	1.29	1.16	1.79
4340	0.46	0.56	0.72	0.93	0.74	1.25
4360	0.22	0.48	0.66	0.88	0.69	1.16
4380	0.26	0.59	0.76	0.98	0.81	1.40
4400	0.23	0.57	0.69	0.90	0.77	1.26
4430	0.18	0.43	0.59	0.77	0.67	1.14
4500	0.12	0.30	0.42	0.55	0.49	0.81
4530	0.18	0.33	0.48	0.60	0.55	0.90
4620	0.07	0.20	0.31	0.42	0.35	0.56
4780	0.01	0.09	0.19	0.30	0.22	0.51
4860	0.25	0.23	0.28	0.36	0.31	0.48
4900	0.02	0.09	0.18	0.25	0.21	0.37

TABLE B2 (CONTINUED)

MEAN NORMALIZED MAGNITUDES

	F5-8 IV	G0-4 IV	G5-8 IV	K0-2 IV	G5-K1 III	K2-5 III
LAMBDA	MAG	MAG	MAG	MAG	MAG	MAG
5050	0.05	0.15	0.19	0.23	0.20	0.36
5180	0.10	0.22	0.29	0.29	0.28	0.55
5250	0.02	0.04	0.11	0.17	0.13	0.23
5270	0.09	0.15	0.20	0.21	0.21	0.33
5300	0.01	0.02	0.07	0.10	0.06	0.13
5330	0.04	0.05	0.10	0.13	0.09	0.16
5400	0.03	0.04	0.07	0.10	0.07	0.15
5450	-0.03	-0.05	-0.02	-0.00	-0.02	0.01
5820	-0.02	-0.04	-0.13	-0.20	-0.14	-0.29
5900	-0.00	-0.06	-0.11	-0.17	-0.09	-0.21
6100	-0.07	-0.15	-0.21	-0.27	-0.23	-0.38
6180	-0.04	-0.11	-0.20	-0.29	-0.20	-0.39
6380	-0.06	-0.18	-0.26	-0.35	-0.28	-0.49
6560	0.06	-0.14	-0.27	-0.37	-0.29	-0.53
6620	-0.07	-0.22	-0.33	-0.41	-0.34	-0.60
6800	-0.08	-0.23	-0.37	-0.44	-0.42	-0.66
7040	-0.07	-0.24	-0.40	-0.49	-0.42	-0.72
7100	-0.08	-0.25	-0.40	-0.49	-0.43	-0.72
7400	-0.06	-0.26	-0.42	-0.53	-0.45	-0.80
8060	-0.08	-0.29	-0.48	-0.67	-0.49	-0.89
8180	-0.07	-0.30	-0.46	-0.66	-0.52	-0.91
8400	-0.11	-0.35	-0.51	-0.71	-0.56	-0.99
8540	-0.04	-0.30	-0.46	-0.66	-0.54	-0.97
8800	-0.08	-0.33	-0.55	-0.74	-0.64	-1.12
8880	-0.10	-0.34	-0.56	-0.75	-0.65	-1.14
9200	-0.09	-0.36	-0.60	-0.80	-0.69	-1.15
9880	-0.07	-0.40	-0.62	-0.86	-0.69	-1.26
9920	-0.11	-0.40	-0.62	-0.86	-0.71	-1.23
9960	-0.10	-0.42	-0.63	-0.86	-0.70	-1.26
10400	-0.11	-0.43	-0.67	-0.91	-0.71	-1.33
10680	-0.04	-0.40	-0.67	-0.91	-0.69	-1.35
<SIGMA> =	0.01	0.01	0.02	0.02	0.01	0.03

TABLE B2 (CONTINUED)

MEAN NORMALIZED MAGNITUDES

	K0-1 III SL	K2-3 III SL	K4-5 III SL	M0-1 III	M2-5 III	M6-8 III
LAMBDA	MAG	MAG	MAG	MAG	MAG	MAG
3300	2.93	3.77	4.71	4.95	5.58	3.98
3350	3.02	3.75	4.66	4.88	5.40	4.48
3400	2.91	3.76	4.48	4.73	5.02	4.10
3450	3.01	3.92	4.53	4.68	4.88	2.86
3570	3.15	3.86	4.53	4.58	4.37	2.76
3620	2.57	3.37	3.95	4.09	3.97	2.20
3780	2.19	2.84	3.48	3.59	3.27	1.38
3800	2.44	3.19	3.67	3.68	3.29	1.45
3820	2.82	3.62	4.10	4.02	3.46	1.85
3830	3.03	3.83	4.09	4.04	3.41	1.44
3840	2.86	3.53	3.89	3.85	3.30	1.29
3860	2.79	3.57	3.85	3.77	3.35	1.56
3870	2.84	3.53	3.88	3.78	3.25	1.55
3890	2.27	3.04	3.56	3.61	3.16	1.24
3910	2.10	2.72	3.37	3.51	3.18	1.30
3930	2.70	3.37	3.94	4.07	3.54	1.94
3970	2.32	3.06	3.53	3.67	3.21	1.68
4020	1.28	1.80	2.34	2.51	2.29	0.79
4100	1.26	1.77	2.20	2.30	1.95	0.25
4170	1.38	1.92	2.22	2.24	1.92	0.69
4200	1.33	1.82	2.14	2.16	1.87	0.74
4230	1.20	1.69	2.25	2.36	2.13	1.72
4270	1.14	1.53	1.89	1.94	1.82	1.25
4300	1.38	1.73	2.00	2.01	1.82	1.20
4340	0.87	1.13	1.41	1.51	1.48	0.87
4360	0.86	1.06	1.34	1.43	1.55	1.45
4380	0.99	1.28	1.56	1.58	1.52	1.13
4400	0.89	1.19	1.44	1.49	1.54	1.29
4430	0.77	1.07	1.25	1.37	1.56	1.84
4500	0.53	0.79	0.93	1.04	1.33	1.60
4530	0.59	0.86	1.06	1.15	1.28	1.49
4620	0.41	0.55	0.62	0.74	1.17	1.70
4780	0.28	0.46	0.65	0.82	1.24	2.13
4860	0.37	0.47	0.58	0.68	0.99	1.43
4900	0.26	0.36	0.44	0.49	0.58	0.78

TABLE B2 (CONTINUED)

MEAN NORMALIZED MAGNITUDES

	K0-1 III SL	K2-3 III SL	K4-5 III SL	M0-1 III	M2-5 III	M6-8 III
LAMBDA	MAG	MAG	MAG	MAG	MAG	MAG
5050	0.22	0.37	0.42	0.47	0.55	0.89
5180	0.33	0.51	0.69	0.80	0.97	1.80
5250	0.15	0.22	0.28	0.32	0.34	0.61
5270	0.25	0.32	0.36	0.33	0.27	0.45
5300	0.08	0.11	0.13	0.12	0.03	0.10
5330	0.13	0.16	0.18	0.14	0.05	0.17
5400	0.12	0.12	0.14	0.08	-0.11	-0.26
5450	-0.02	-0.01	0.01	0.04	0.03	-0.24
5820	-0.21	-0.27	-0.35	-0.37	-0.30	-0.45
5900	-0.16	-0.17	-0.14	-0.09	0.19	0.92
6100	-0.22	-0.35	-0.43	-0.53	-0.63	-0.79
6180	-0.29	-0.35	-0.39	-0.28	-0.12	0.13
6380	-0.34	-0.43	-0.56	-0.67	-0.89	-1.03
6560	-0.33	-0.49	-0.64	-0.80	-1.16	-1.94
6620	-0.40	-0.54	-0.71	-0.83	-1.05	-1.64
6800	-0.47	-0.62	-0.73	-0.77	-1.01	-1.49
7040	-0.49	-0.65	-0.89	-1.17	-1.91	-2.91
7100	-0.50	-0.65	-0.78	-0.89	-1.24	-1.73
7400	-0.51	-0.73	-1.01	-1.40	-2.50	-3.64
8060	-0.58	-0.86	-1.18	-1.58	-2.86	-4.35
8180	-0.59	-0.85	-1.14	-1.61	-3.05	-5.21
8400	-0.60	-0.94	-1.21	-1.67	-2.99	-4.73
8540	-0.58	-0.92	-1.14	-1.60	-2.82	-4.29
8800	-0.70	-1.04	-1.33	-1.83	-3.32	-5.37
8880	-0.71	-1.06	-1.37	-1.84	-3.16	-4.99
9200	-0.67	-1.03	-1.35	-1.91	-3.51	-5.92
9880	-0.79	-1.17	-1.51	-2.08	-3.69	-6.14
9920	-0.82	-1.18	-1.51	-2.08	-3.68	-6.12
9960	-0.79	-1.18	-1.53	-2.09	-3.72	-6.26
10400	-0.85	-1.26	-1.64	-2.20	-3.87	-6.51
10680	-0.85	-1.29	-1.66	-2.22	-3.89	-6.46
<SIGMA> =	0.02	0.02	0.02	0.06	0.08	0.16

TABLE B2 (CONTINUED)

MEAN NORMALIZED MAGNITUDES

	B0-1 I	B5-7 I	A2 I	M1-4 I
LAMBDA	MAG	MAG	MAG	MAG
3300	-0.67	0.02	1.08	4.98
3350	-0.69	0.00	1.11	4.91
3400	-0.69	0.00	1.03	4.84
3450	-0.65	0.01	0.99	4.87
3570	-0.63	0.03	0.90	4.51
3620	-0.57	0.03	0.90	4.10
3780	-0.62	-0.28	-0.07	3.60
3800	-0.56	-0.22	0.03	3.66
3820	-0.61	-0.29	-0.08	3.88
3830	-0.56	-0.25	0.05	3.89
3840	-0.56	-0.25	0.07	3.59
3860	-0.63	-0.33	-0.09	3.69
3870	-0.62	-0.32	-0.08	3.70
3890	-0.52	-0.21	0.02	3.38
3910	-0.62	-0.35	-0.11	3.54
3930	-0.58	-0.31	-0.08	4.11
3970	-0.46	-0.20	0.02	3.71
4020	-0.53	-0.29	-0.12	2.68
4100	-0.39	-0.18	0.04	2.44
4170	-0.49	-0.28	-0.12	2.41
4200	-0.47	-0.28	-0.12	2.33
4230	-0.46	-0.27	-0.11	2.45
4270	-0.44	-0.25	-0.09	2.03
4300	-0.44	-0.26	-0.06	2.15
4340	-0.30	-0.13	0.08	1.74
4360	-0.40	-0.22	-0.02	1.66
4380	-0.40	-0.24	-0.07	1.81
4400	-0.39	-0.24	-0.08	1.71
4430	-0.34	-0.17	-0.08	1.72
4500	-0.36	-0.23	-0.09	1.32
4530	-0.36	-0.23	-0.10	1.38
4620	-0.31	-0.20	-0.11	0.98
4780	-0.23	-0.15	-0.09	0.98
4860	-0.10	-0.01	0.11	0.81
4900	-0.19	-0.13	-0.09	0.52

TABLE B2 (CONTINUED)

MEAN NORMALIZED MAGNITUDES

	B0-1 I	B5-7 I	A2 I	M1-4 I
LAMBDA	MAG	MAG	MAG	MAG
5050	-0.14	-0.08	-0.06	0.47
5180	-0.12	-0.05	-0.03	0.78
5250	-0.10	-0.06	-0.04	0.30
5270	-0.08	-0.04	-0.01	0.32
5300	-0.07	-0.05	-0.02	0.12
5330	-0.06	-0.02	-0.00	0.14
5400	-0.04	-0.02	-0.02	0.09
5450	-0.01	-0.01	-0.02	0.05
5820	0.11	0.04	0.03	-0.35
5900	0.18	0.11	0.09	-0.00
6100	0.20	0.11	0.08	-0.60
6180	0.22	0.15	0.12	-0.19
6380	0.31	0.19	0.16	-0.74
6560	0.40	0.29	0.26	-0.89
6620	0.43	0.27	0.19	-0.92
6800	0.48	0.31	0.21	-1.00
7040	0.54	0.36	0.25	-1.31
7100	0.53	0.32	0.24	-0.93
7400	0.66	0.38	0.28	-1.60
8060	0.70	0.44	0.37	-1.86
8180	0.71	0.47	0.36	-1.90
8400	0.71	0.46	0.30	-1.98
8540	0.72	0.44	0.31	-1.89
8800	0.77	0.43	0.24	-2.22
8880	0.84	0.50	0.28	-2.20
9200	0.90	0.54	0.32	-2.23
9880	0.90	0.56	0.38	-2.46
9920	0.87	0.53	0.33	-2.46
9960	0.91	0.51	0.35	-2.47
10400	1.06	0.63	0.37	-2.63
10680	1.07	0.69	0.45	-2.65
<SIGMA> =	0.01	0.05	0.0	0.06

APPENDIX C

SYNTHESIS-STAR SPECTRAL INDICES

For each of the synthesis-group energy distributions (see Appendix B), we have computed absorption-strength indices and continuum indices as in O'Connell (1973), where explicit numerical definitions of these indices will be found. (An absorption-strength index is the magnitude equivalent of the ratio of the flux in a feature bandpass to the flux interpolated from the nearby continuum. Apart from sideband-blanketing effects, an absorption-strength index of zero indicates the absence of the particular feature in question; a positive index value indicates the presence of absorption in the feature bandpass. A continuum index is the magnitude equivalent to the ratio of the mean flux in two spectral regions.) Table C1 lists the absorption features measured by the present program along with the sideband wavelengths used to define the local "continuum" at each feature wavelength. Also listed are the wavelengths used to define the continuum indices. (See O'Connell 1973 for details).

In Figures C1 through C41 the behavior of the various absorption and continuum indices for all 34 synthesis groups is summarized. The absorption indices are plotted against the continuum index V/R which is shown by O'Connell (1973) to be a decreasing function of stellar temperature and a close narrow-band analog of the broad-band V-R color.

The index "(CaII + H) - (CaII K)" is the simple difference of the absorption indices indicated and illustrates the behavior of the relative strength of the absorptions at λ3933 and λ3968.

In Figures C1 through C41, the synthesis groups are differentiated according to luminosity class with the following legend:

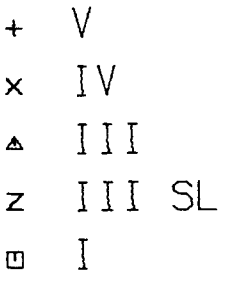

TABLE C1

INDEX WAVELENGTHS

INDEX	λ CENTRAL	λλ SIDEBANDS	
H 3798	3800	3780	3820
He I 3819	3820	3780	3860
H 3835A	3830	3820	3860
H 3835B	3840	3820	3860
BL 3830	3830	3780	3910
BL 3840	3840	3780	3910
CN 3860	3860	3780	3910
CN 3870	3870	3780	3910
H 3889	3890	3860	3910
Ca II 3933	3930	3910	4020
CaII+H 3970	3970	3910	4020
H 4101	4100	4020	4270
CN 4170	4170	4020	4270
CN 4200	4200	4020	4270
Ca I 4227	4230	4020	4270
CH 4305	4300	4270	4400
H 4340	4340	4270	4400
Fe I 4383	4380	4360	4400
Fe I 4529	4530	4500	4620
MgH 4780	4780	4620	4900
H 4861	4860	4780	5050
Mg I 5175	5180	5050	5300
Fe I 5269	5270	5250	5300
Fe I 5328	5330	5300	5450
Fe I 5400	5400	5300	5450
Na I 5892	5900	5820	6100
TiO 6180	6180	6100	6380
H 6563	6560	6380	6620
CaH 6800	6800	6620	7400
TiO 7100	7100	7040	7400
Na I 8190	8180	8060	8400
Ca II 8542	8540	8400	8800
TiO 8880	8880	8800	9200
CN 9190	9200	8800	9960
WF 9920	9920	9880	9960

CONTINUUM INDEX WAVELENGTHS

U	3450	3620
B	4270	4500
V	5300	5820
R	7040	7400
I	8400	8800
J	10400	10680

FIGURE C 1

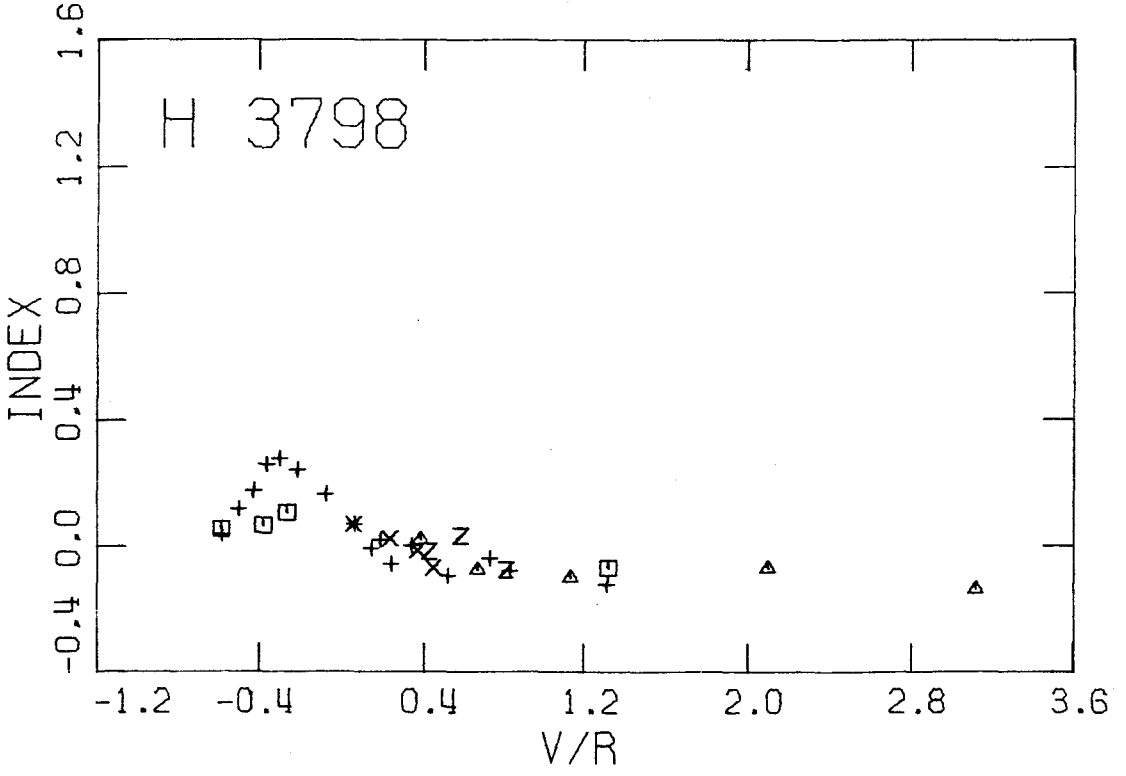

FIGURE C 2

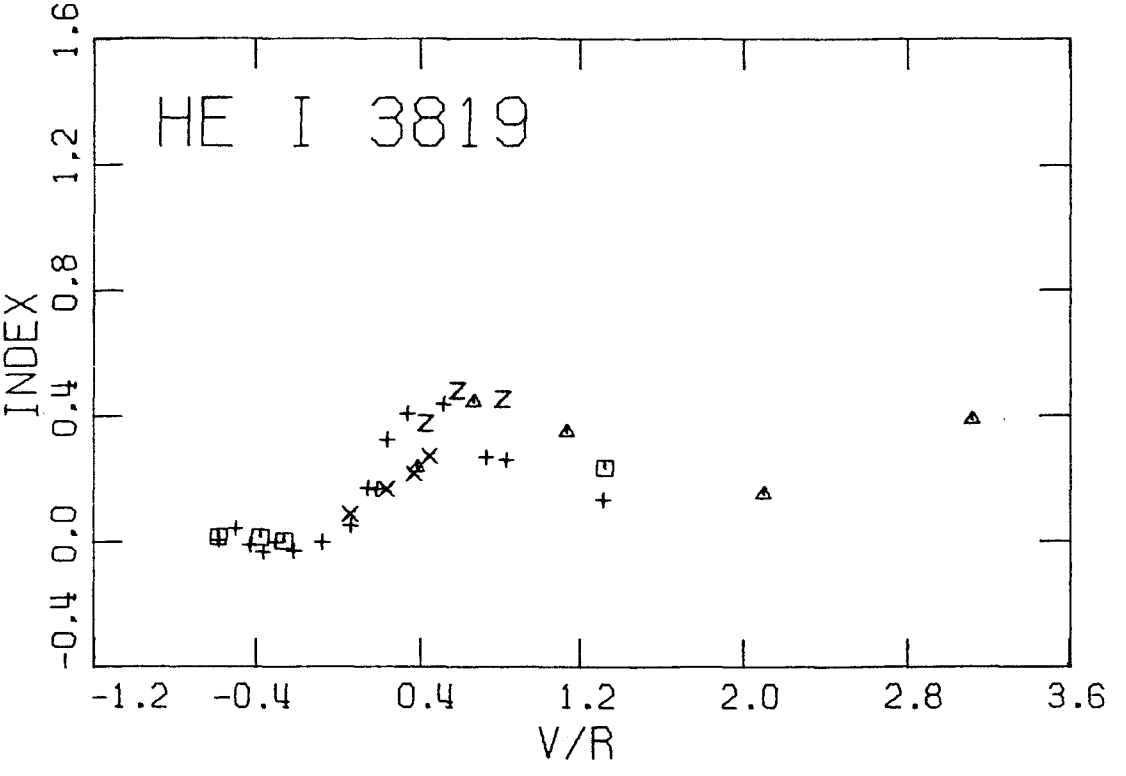

FIGURE C 3

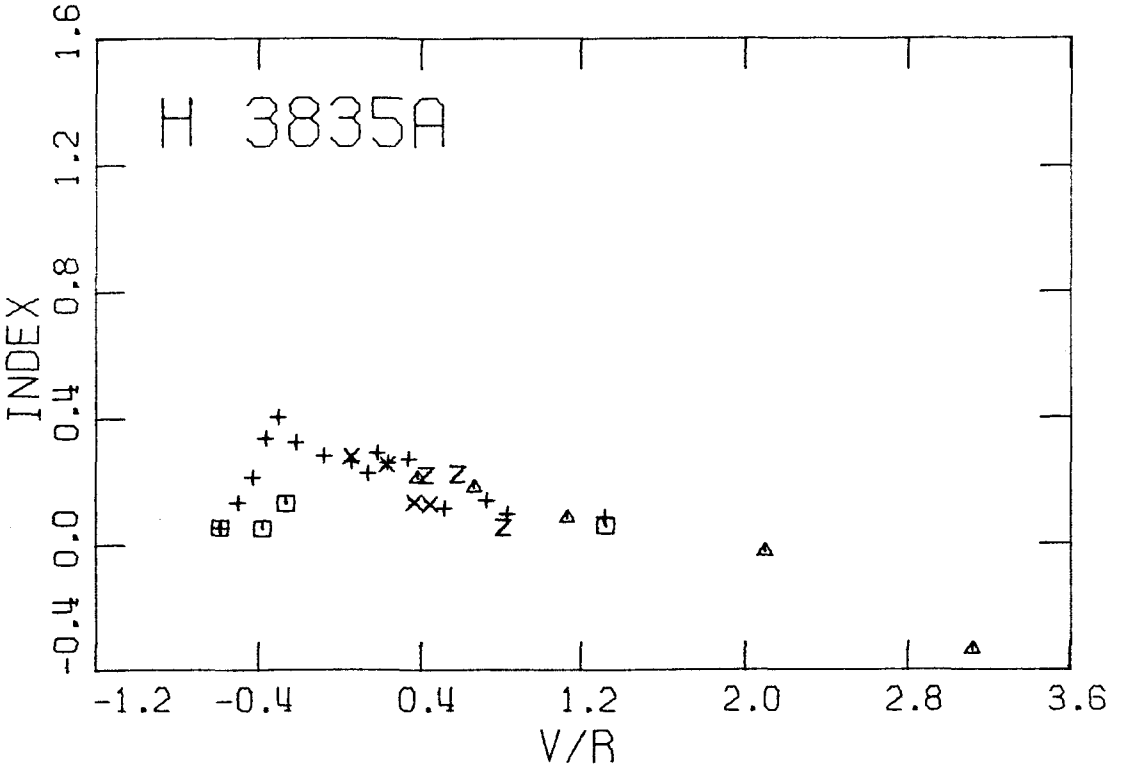

FIGURE C 4

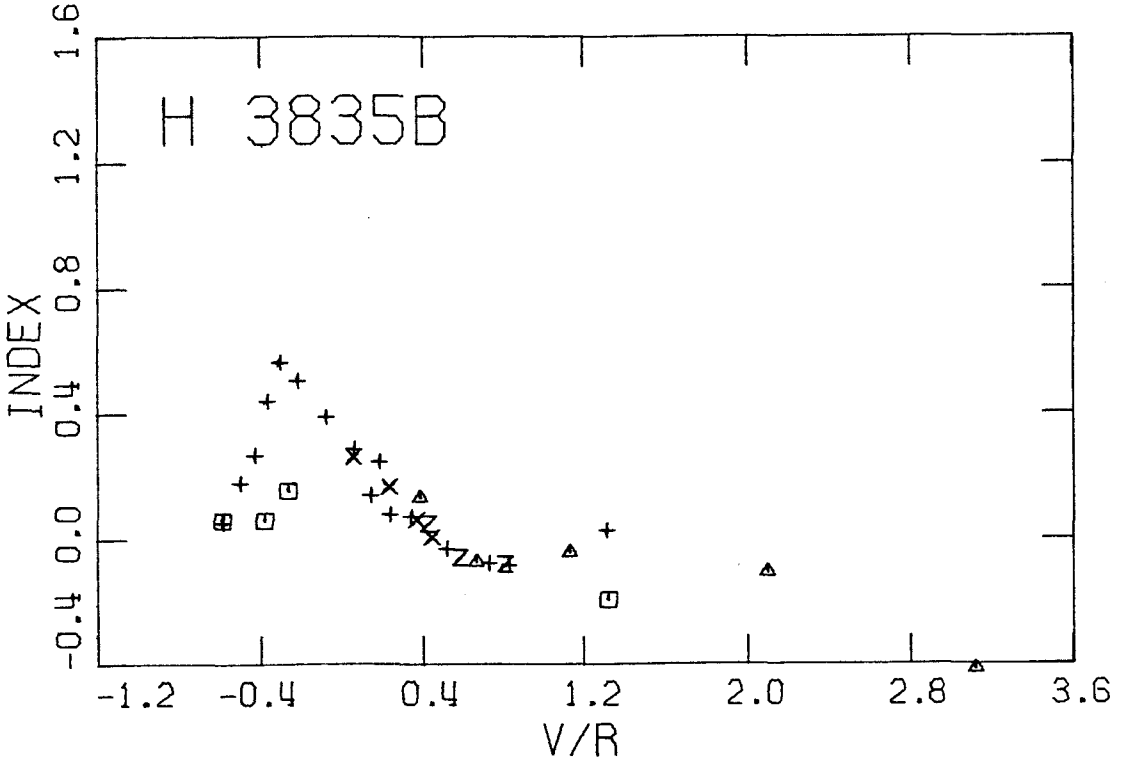

FIGURE C 5

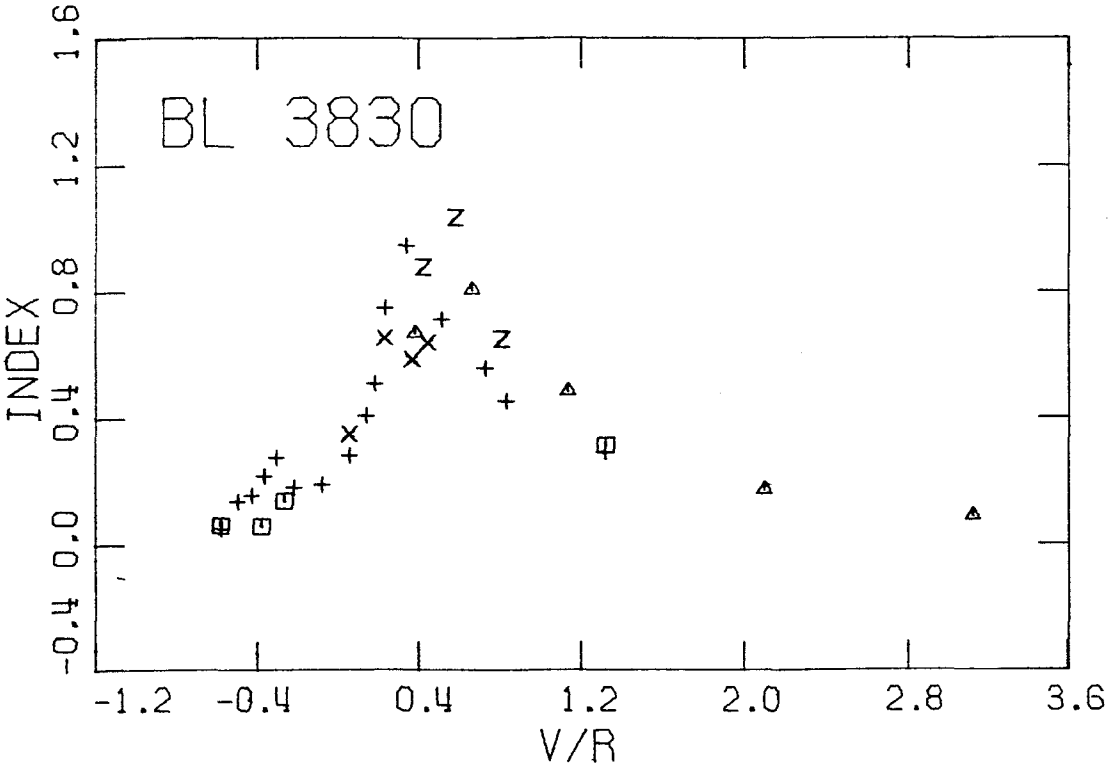

FIGURE C 6

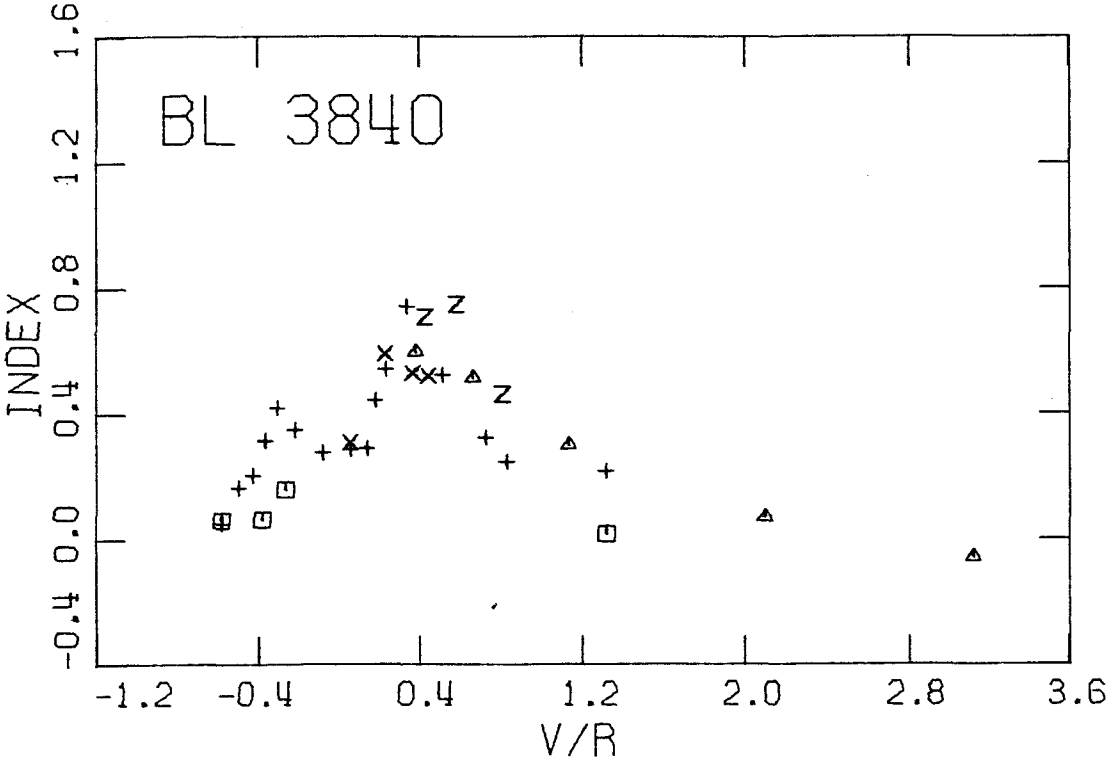

FIGURE C 7

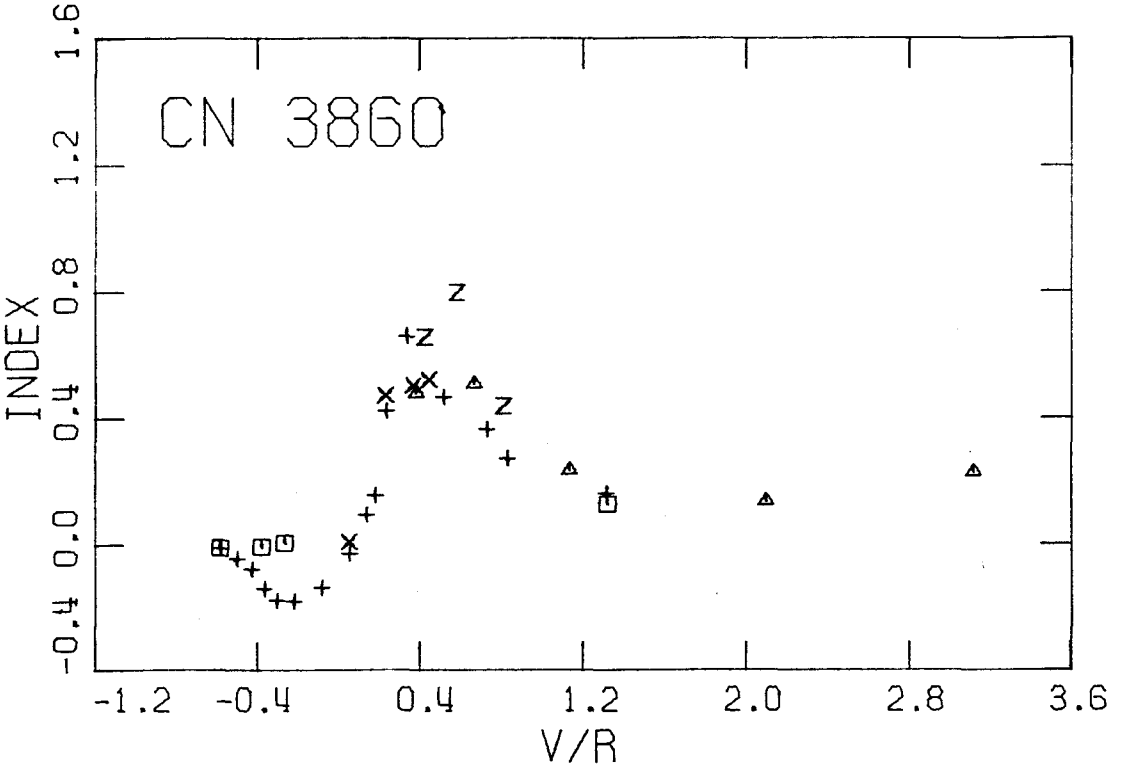

FIGURE C 8

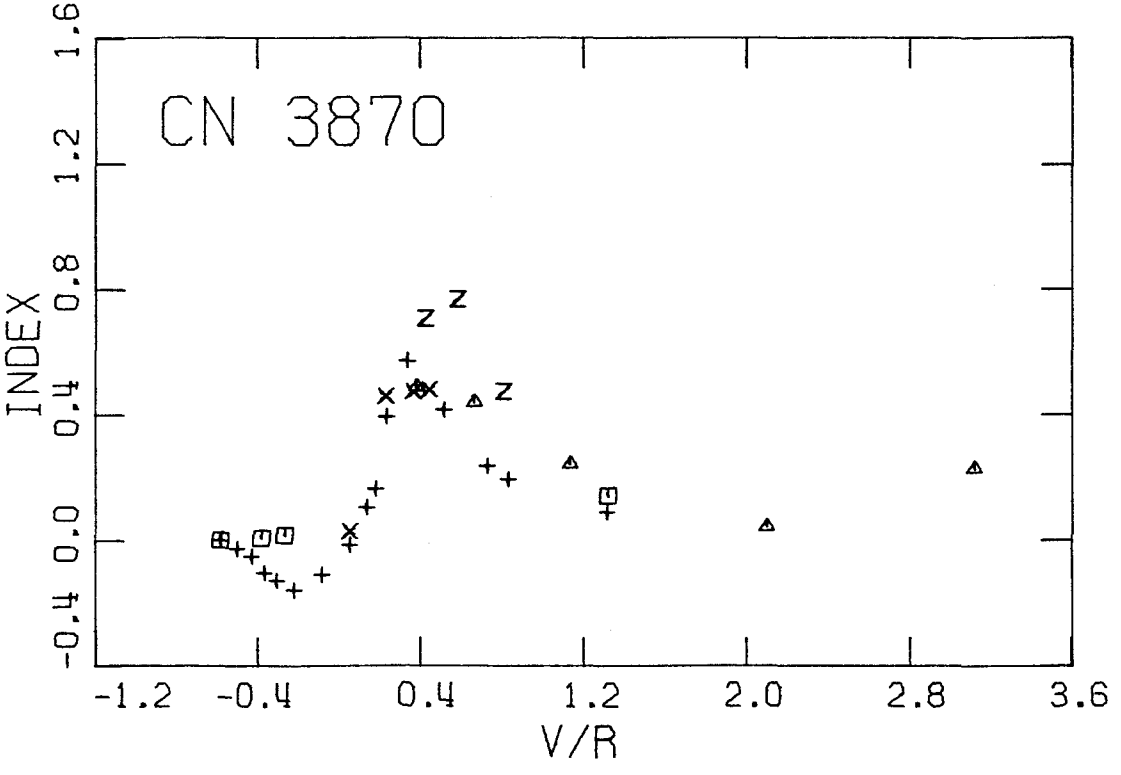

FIGURE C 9

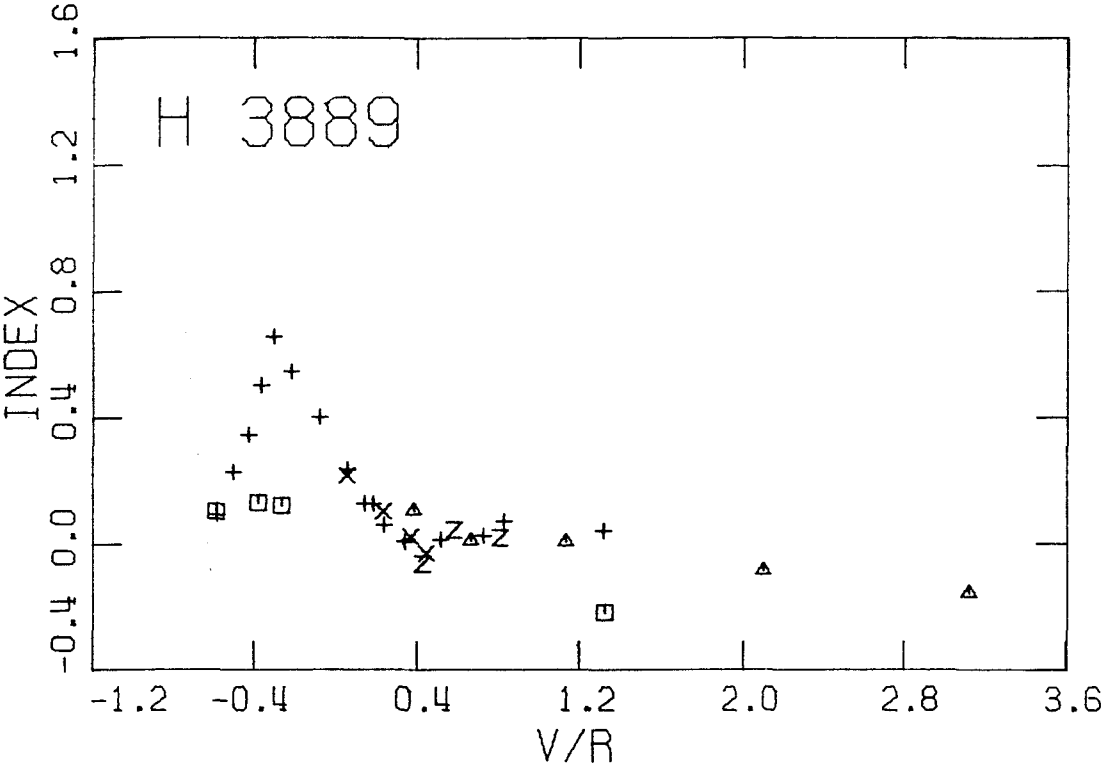

FIGURE C 10

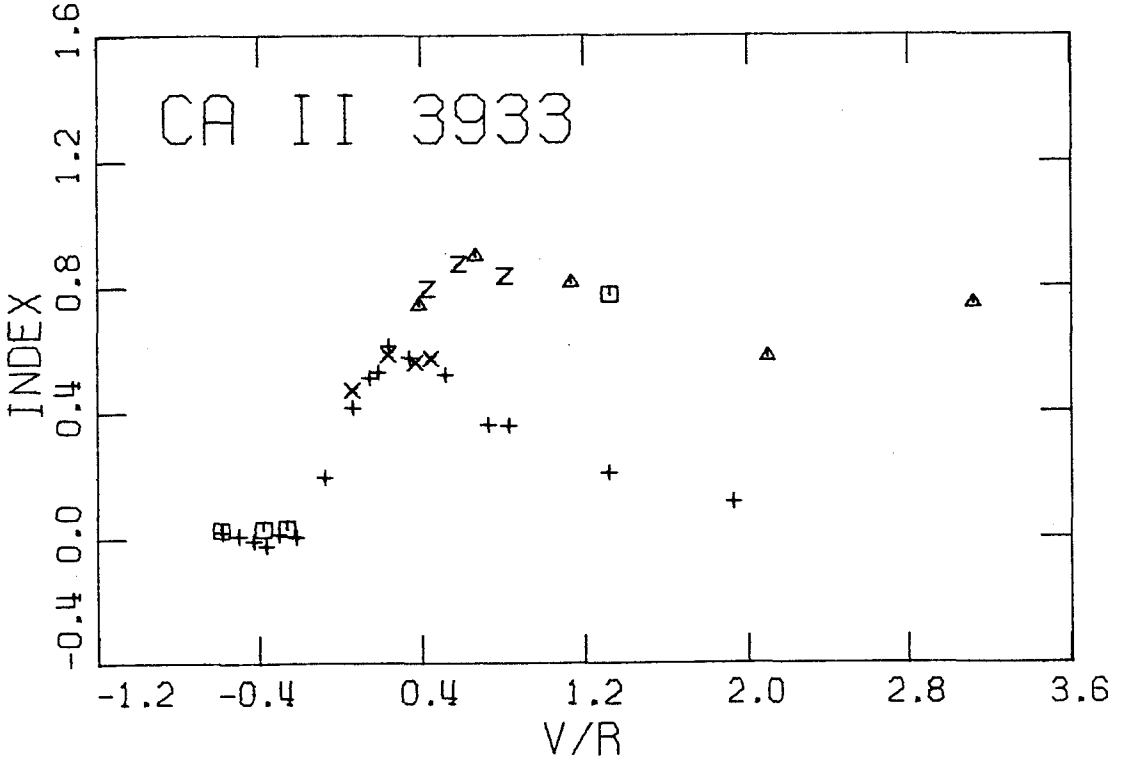

FIGURE C 11

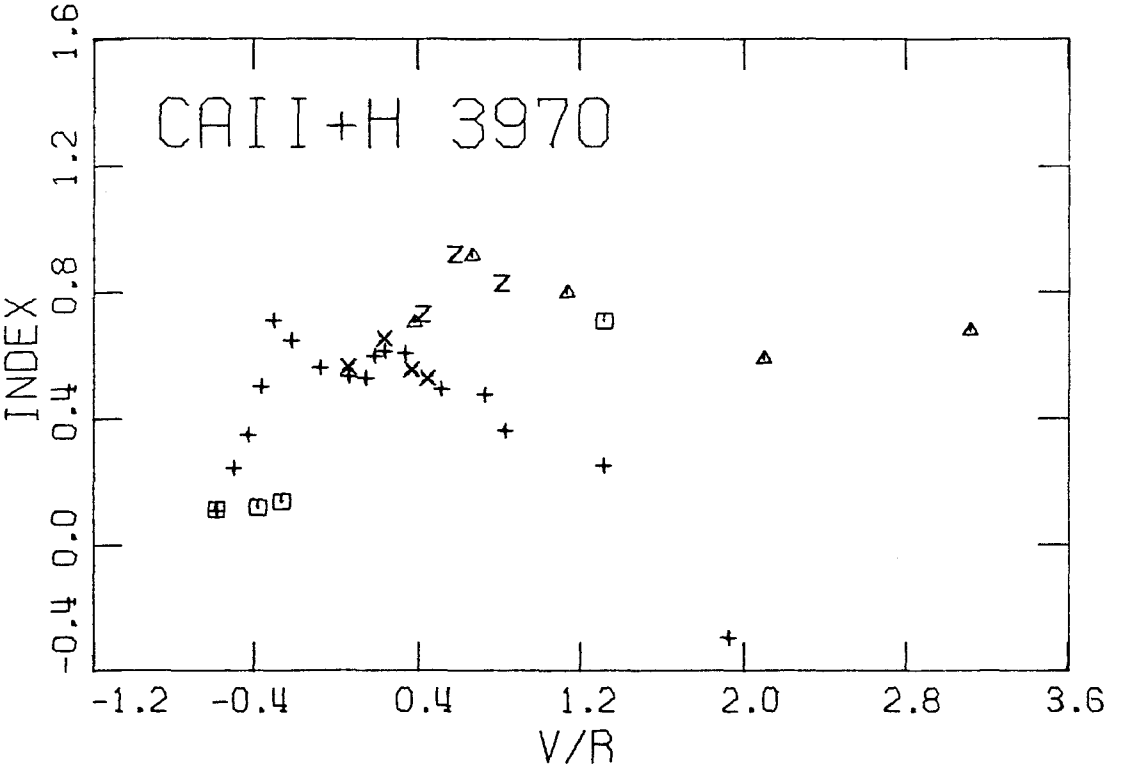

FIGURE C 12

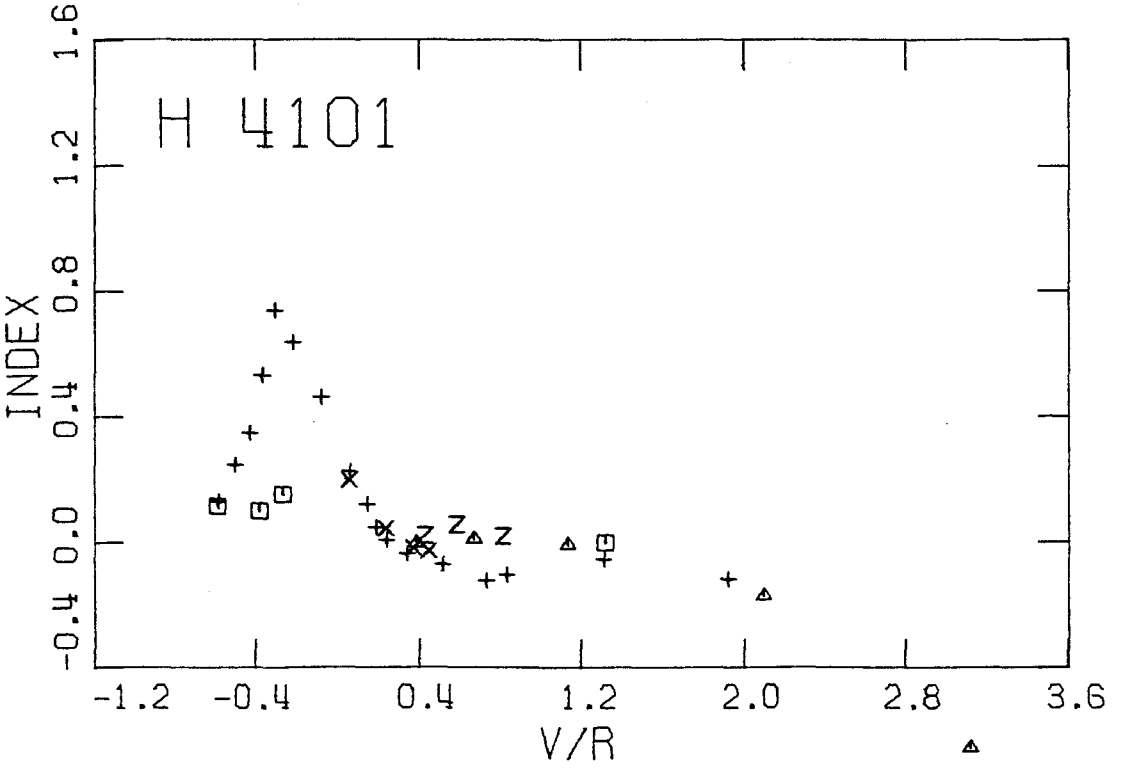

FIGURE C 13

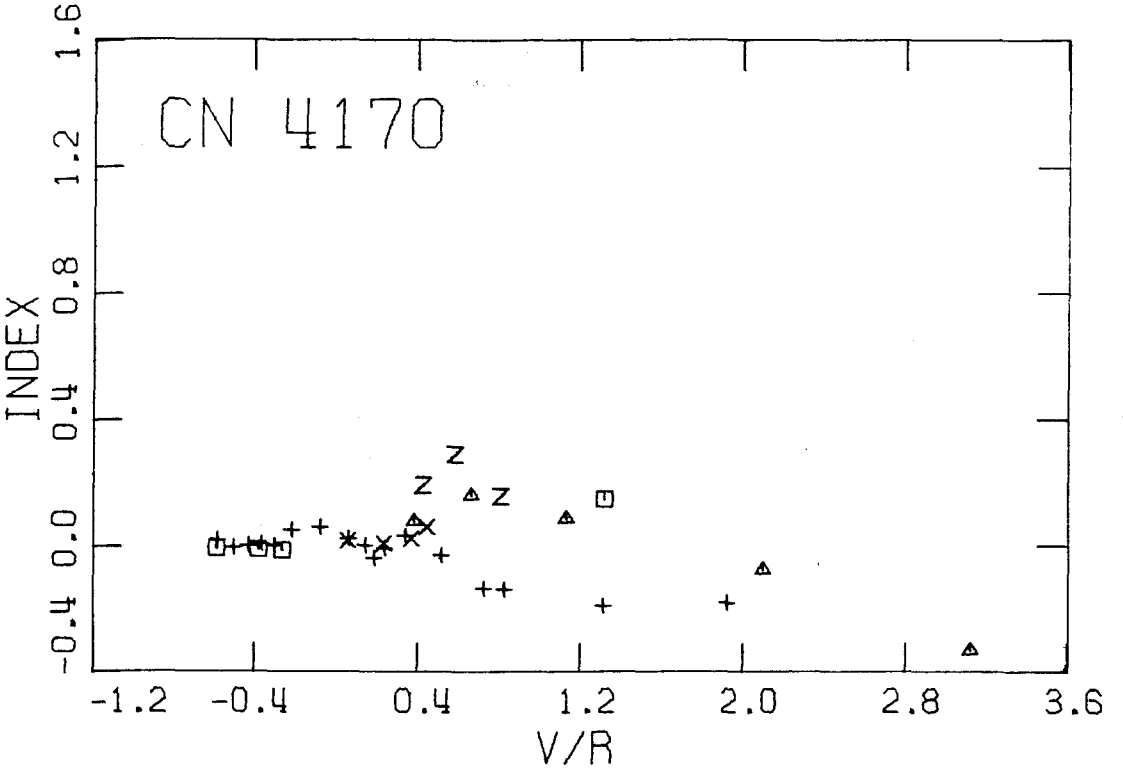

FIGURE C 14

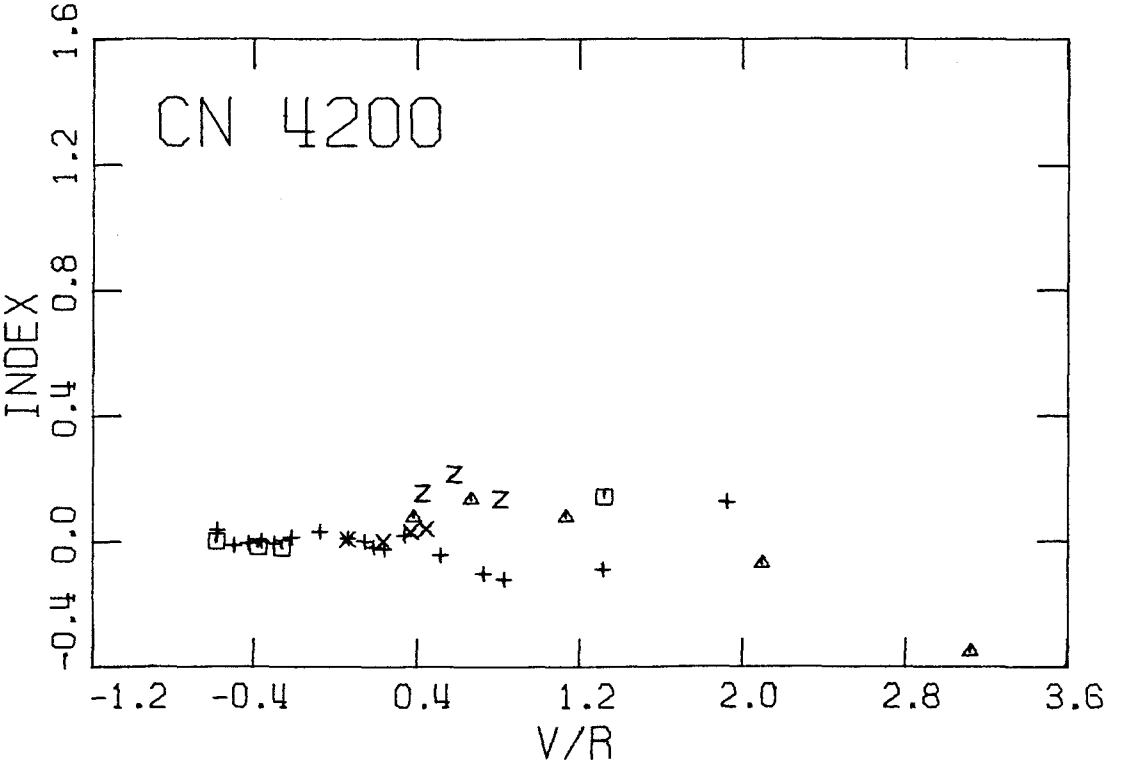

FIGURE C 15

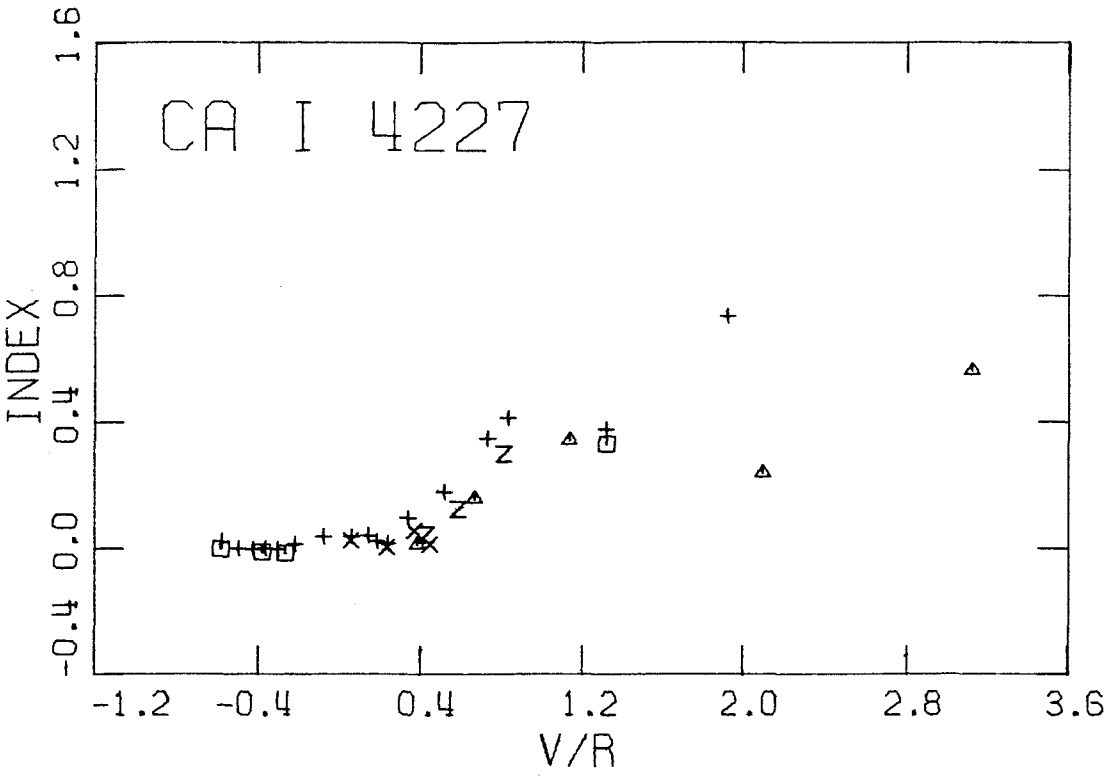

FIGURE C 16

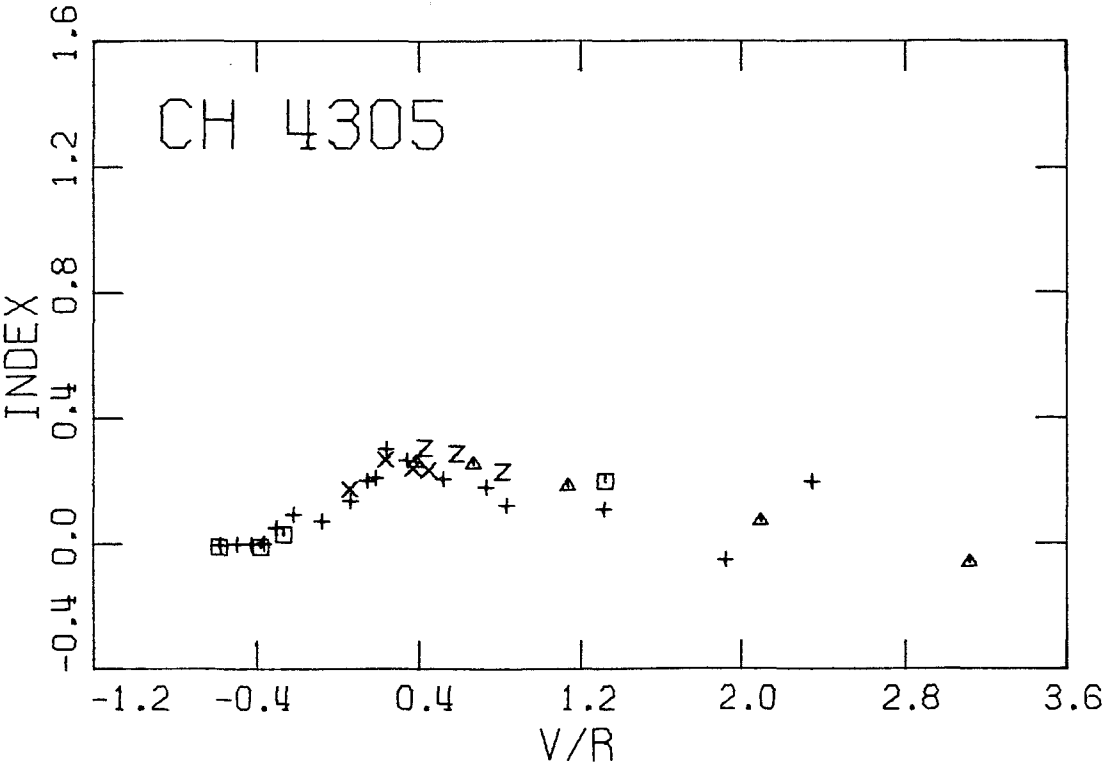

FIGURE C 17

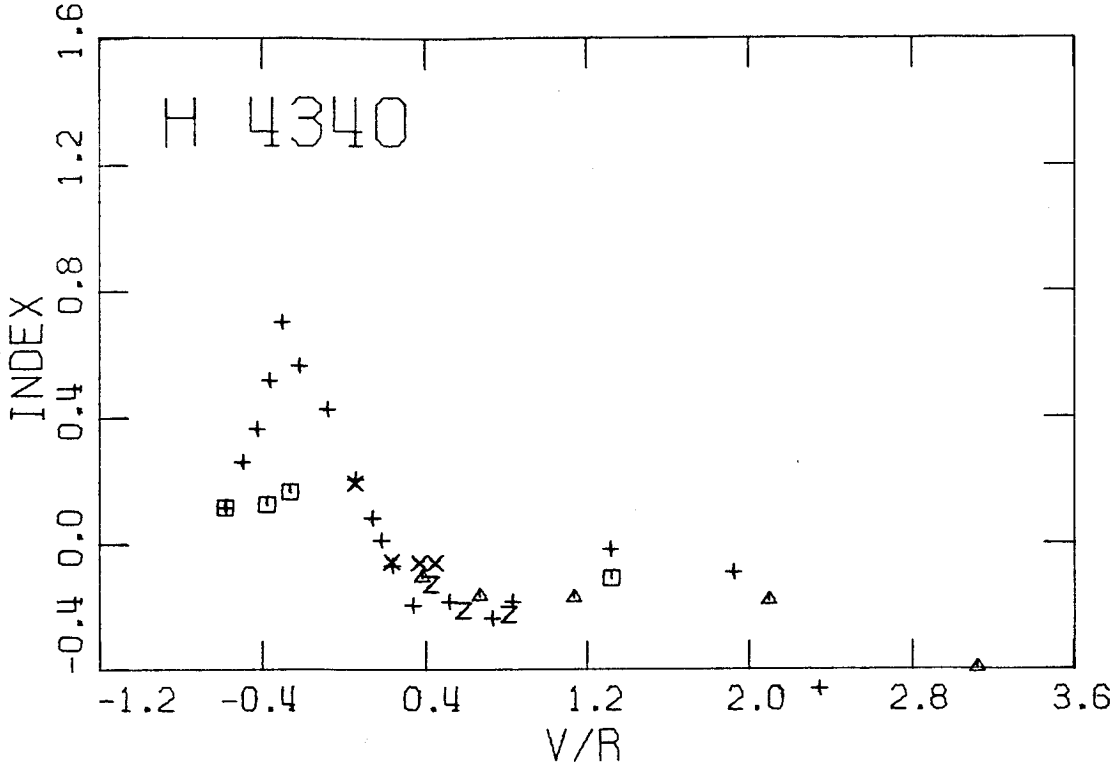

FIGURE C 18

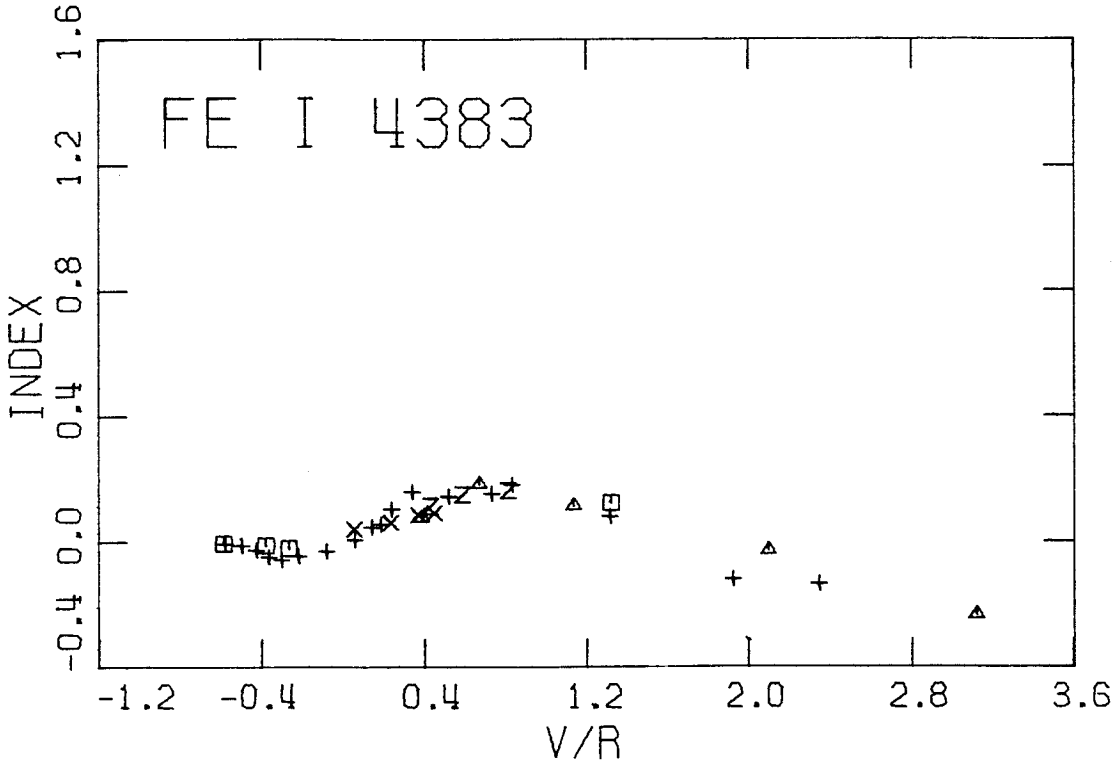

FIGURE C 19

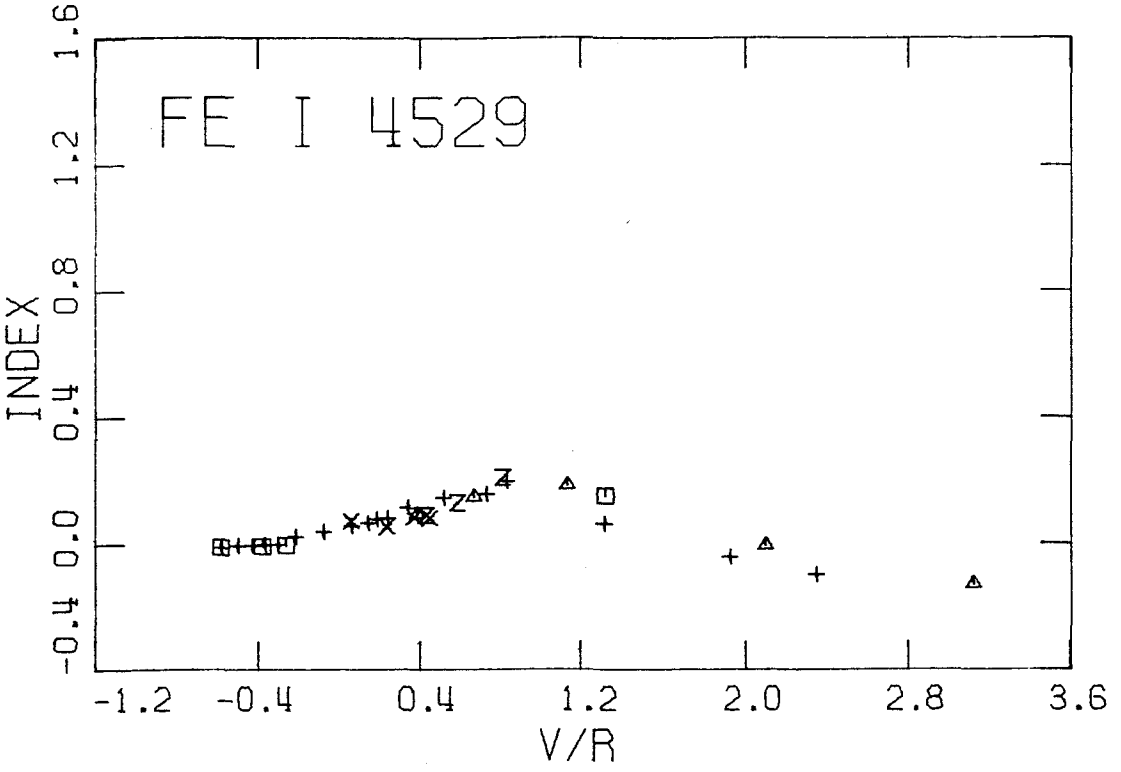

FIGURE C 20

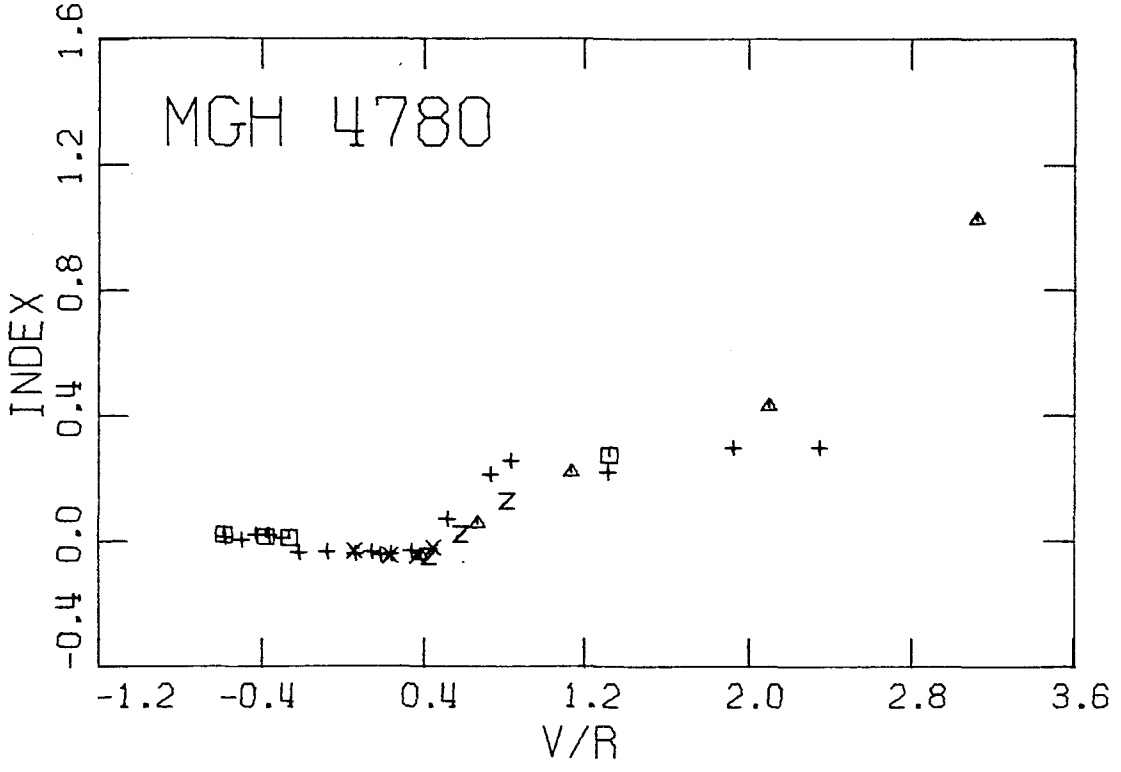

FIGURE C 21

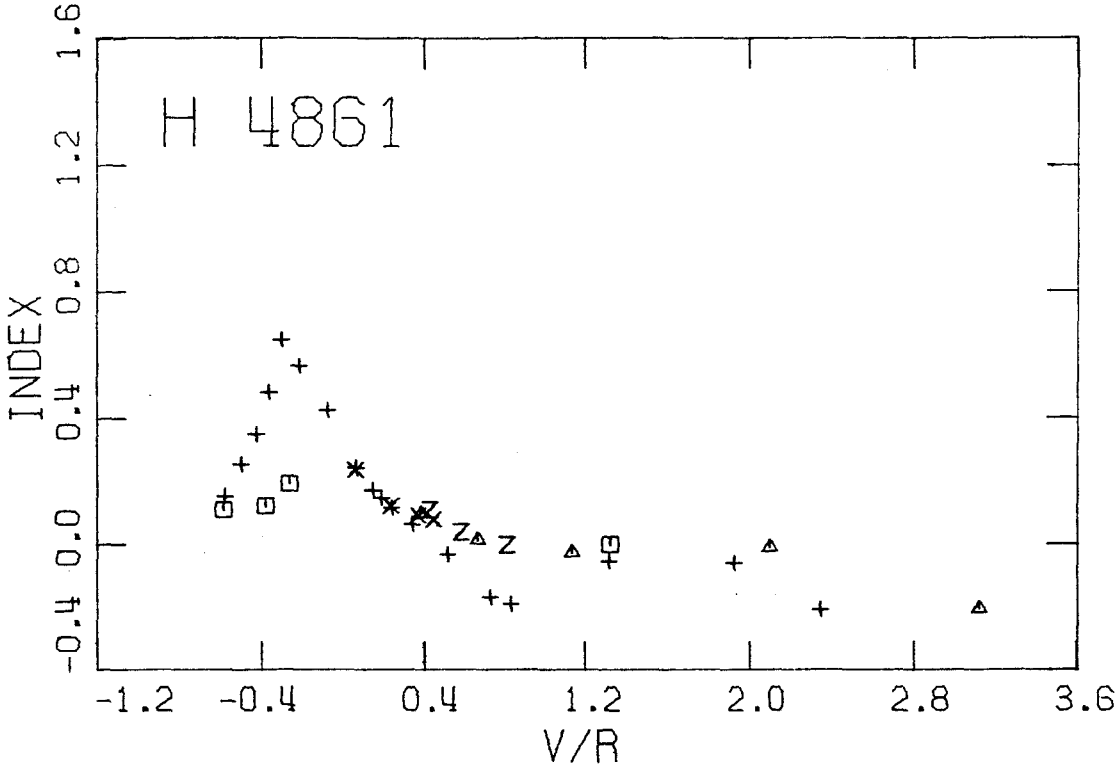

FIGURE C 22

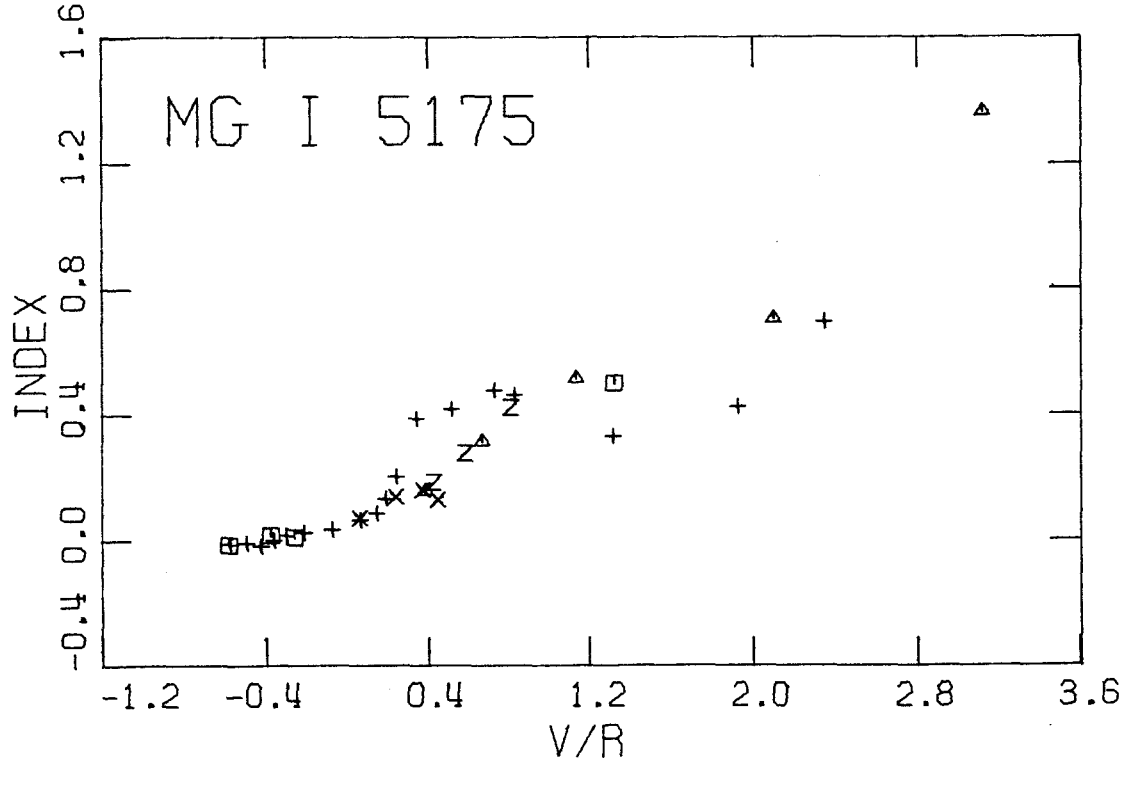

FIGURE C 23

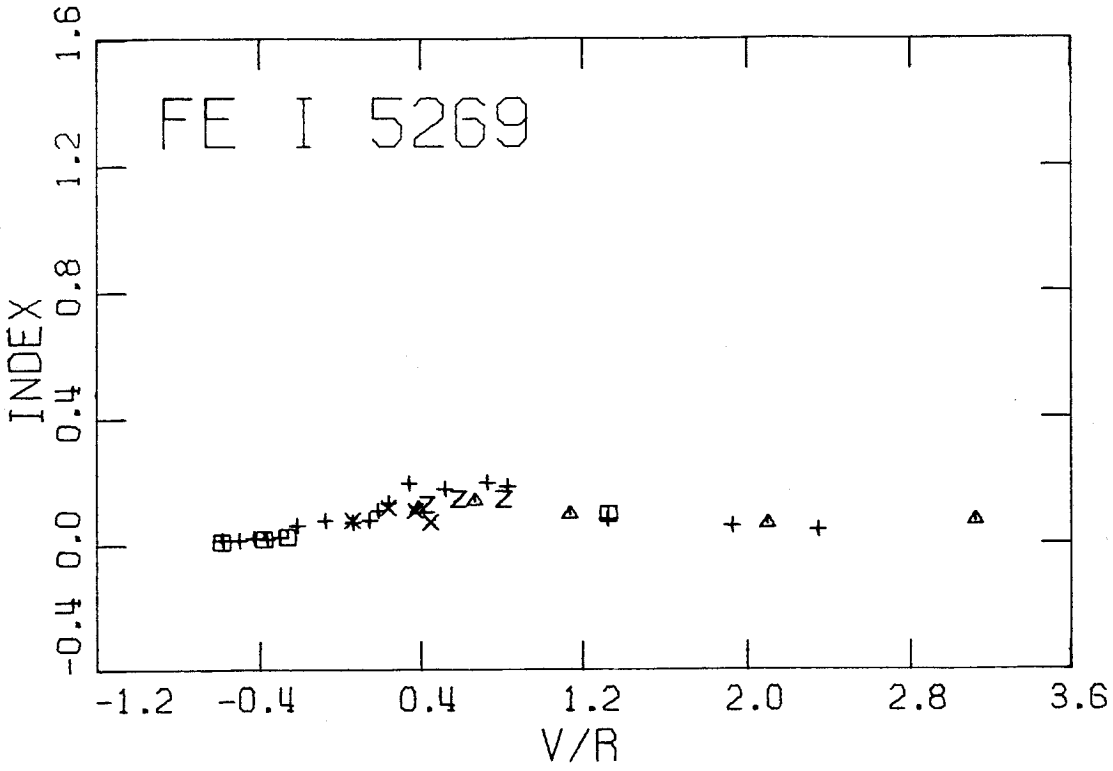

FIGURE C 24

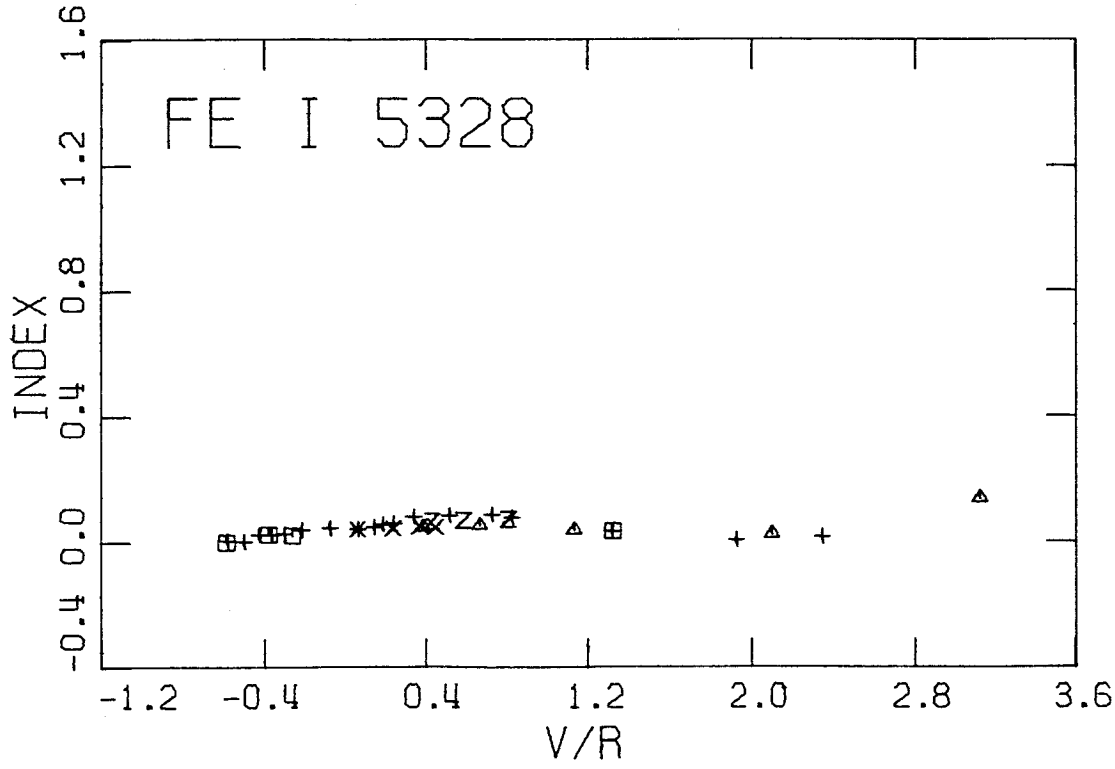

FIGURE C 25

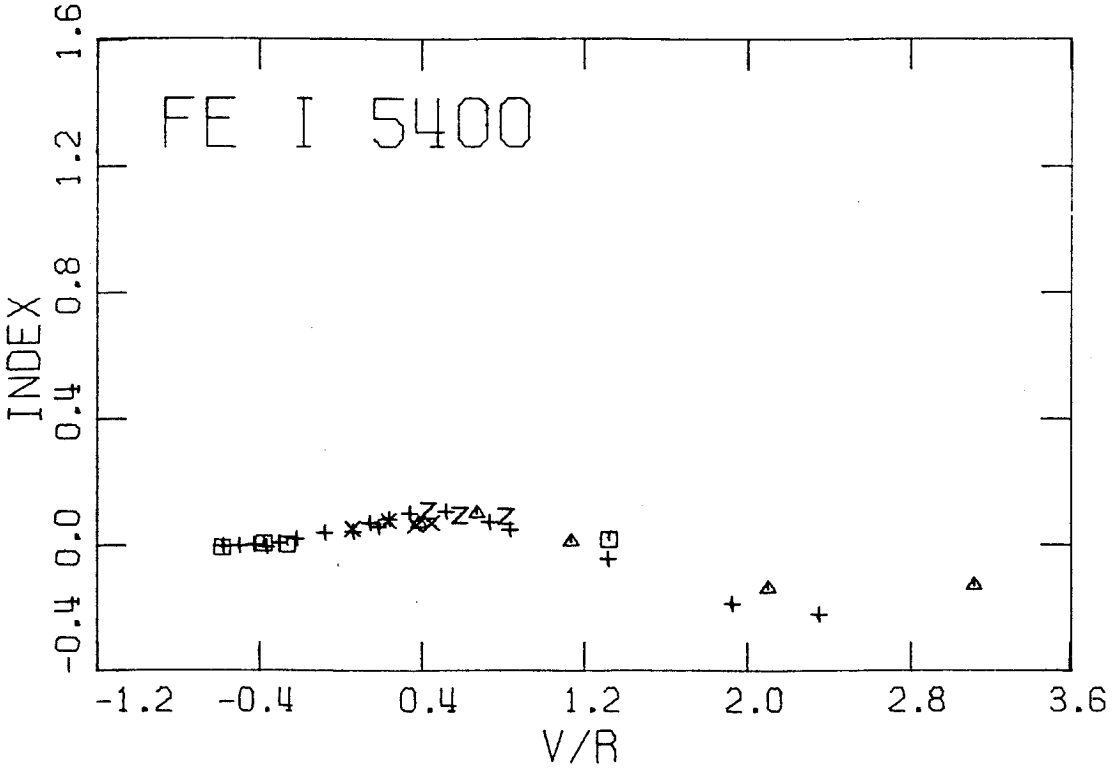

FIGURE C 26

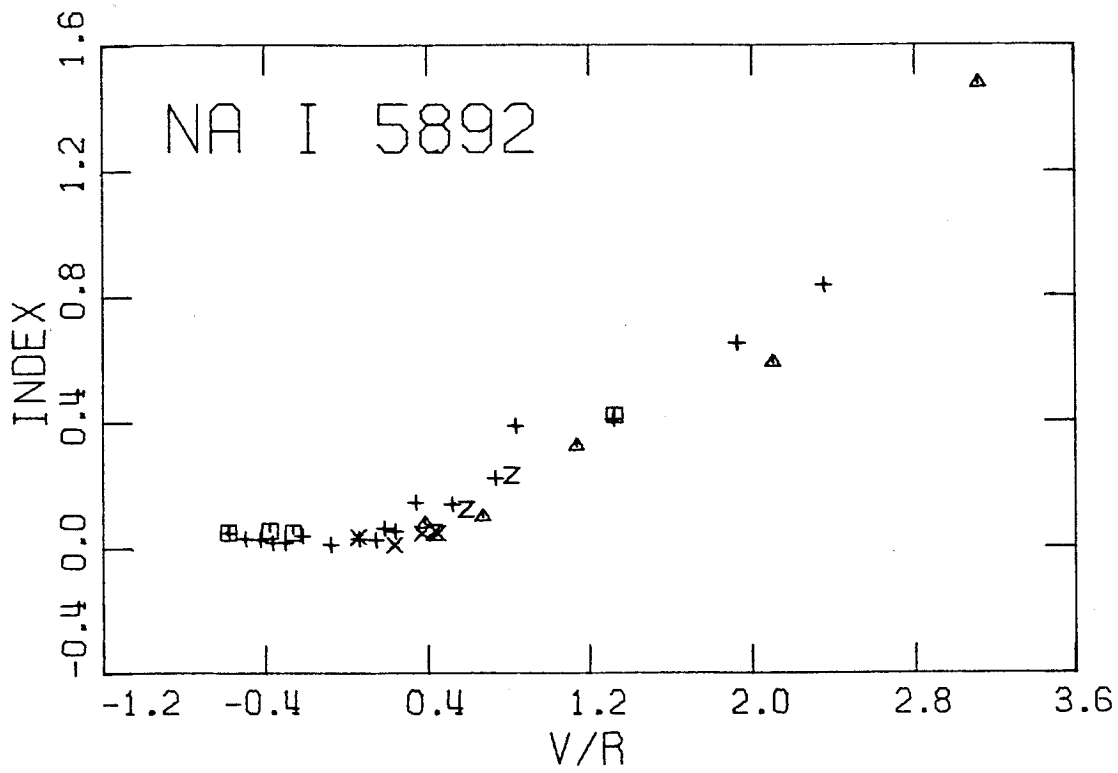

FIGURE C 27

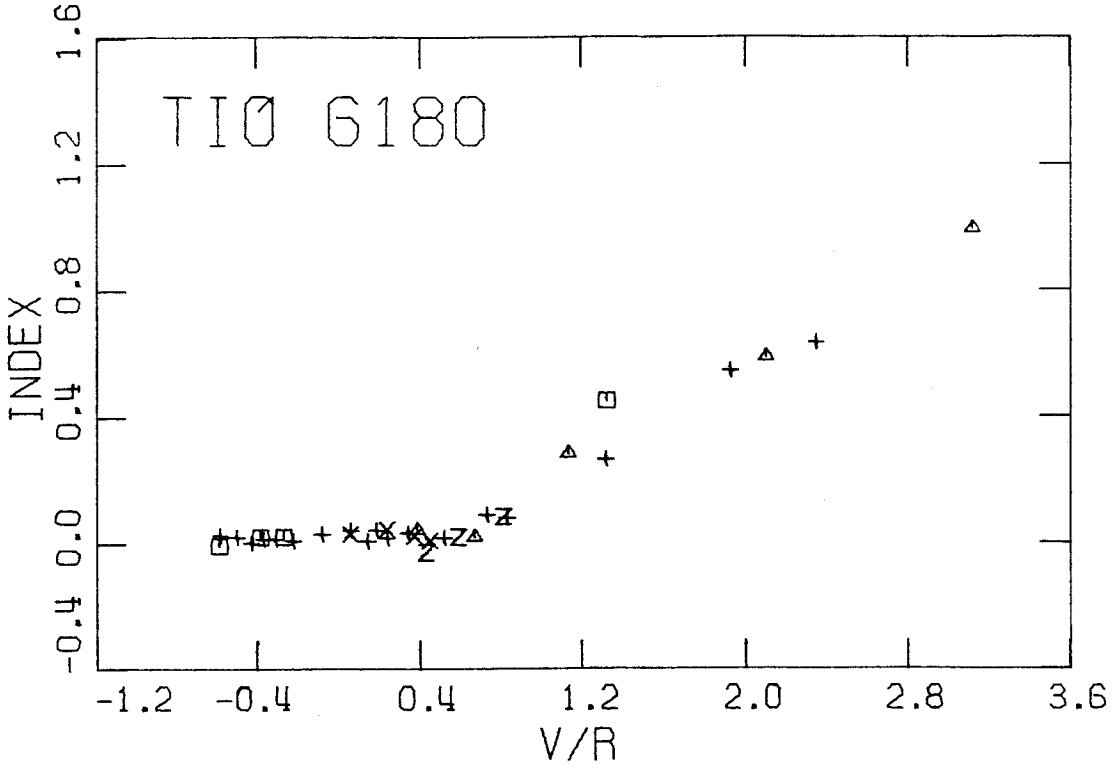

FIGURE C 28

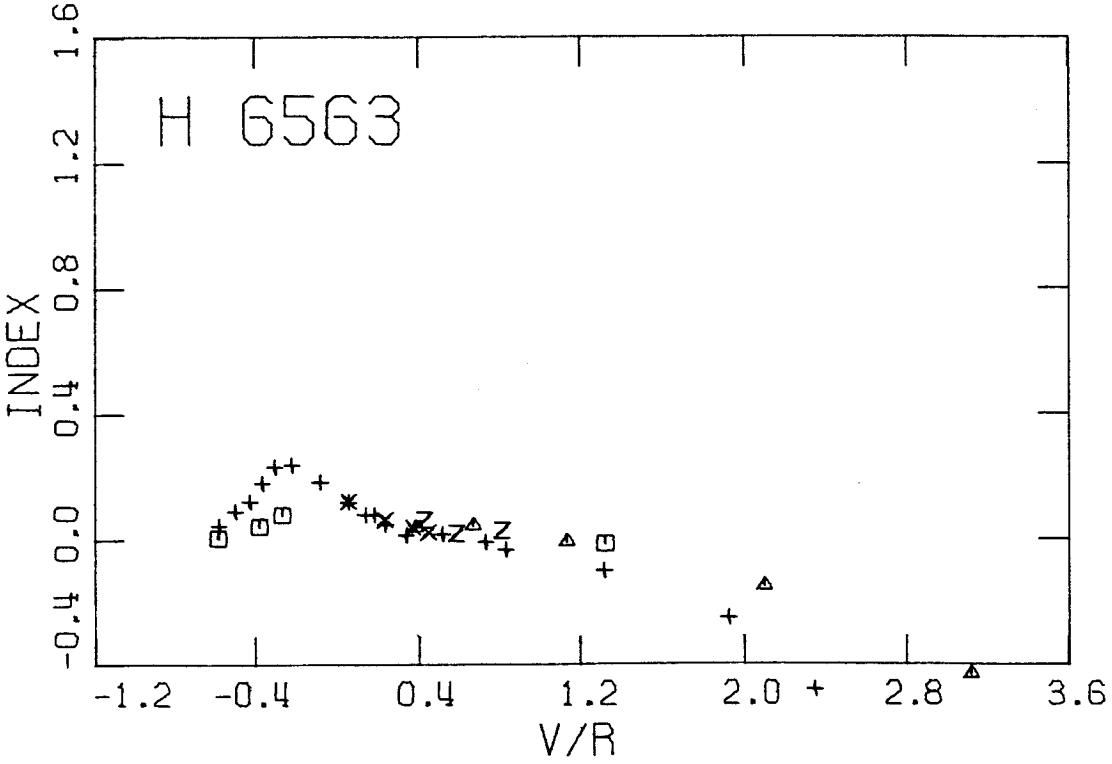

FIGURE C 29

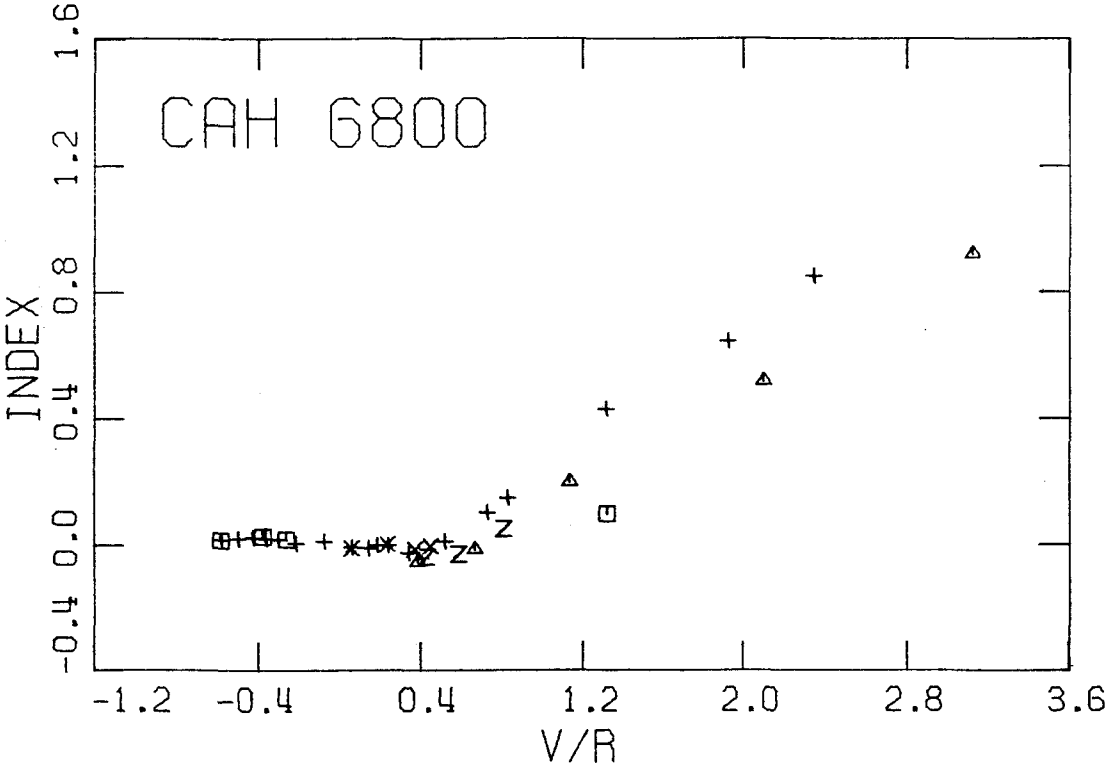

FIGURE C 30

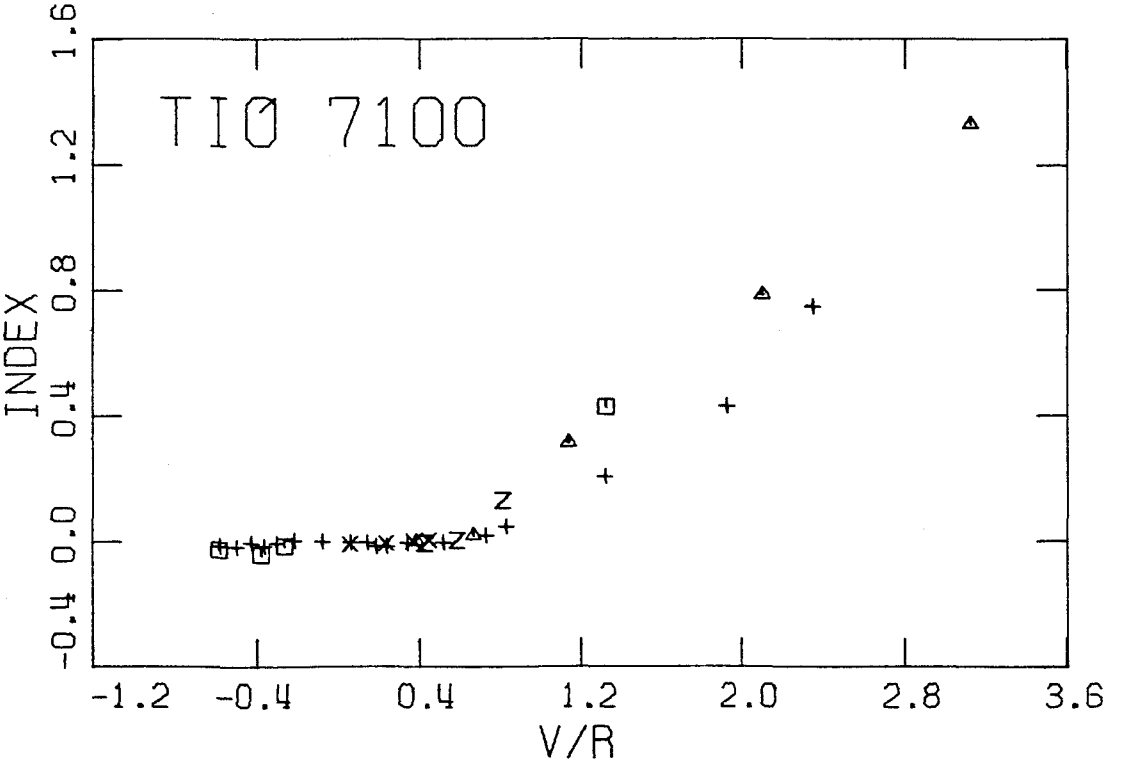

FIGURE C 31

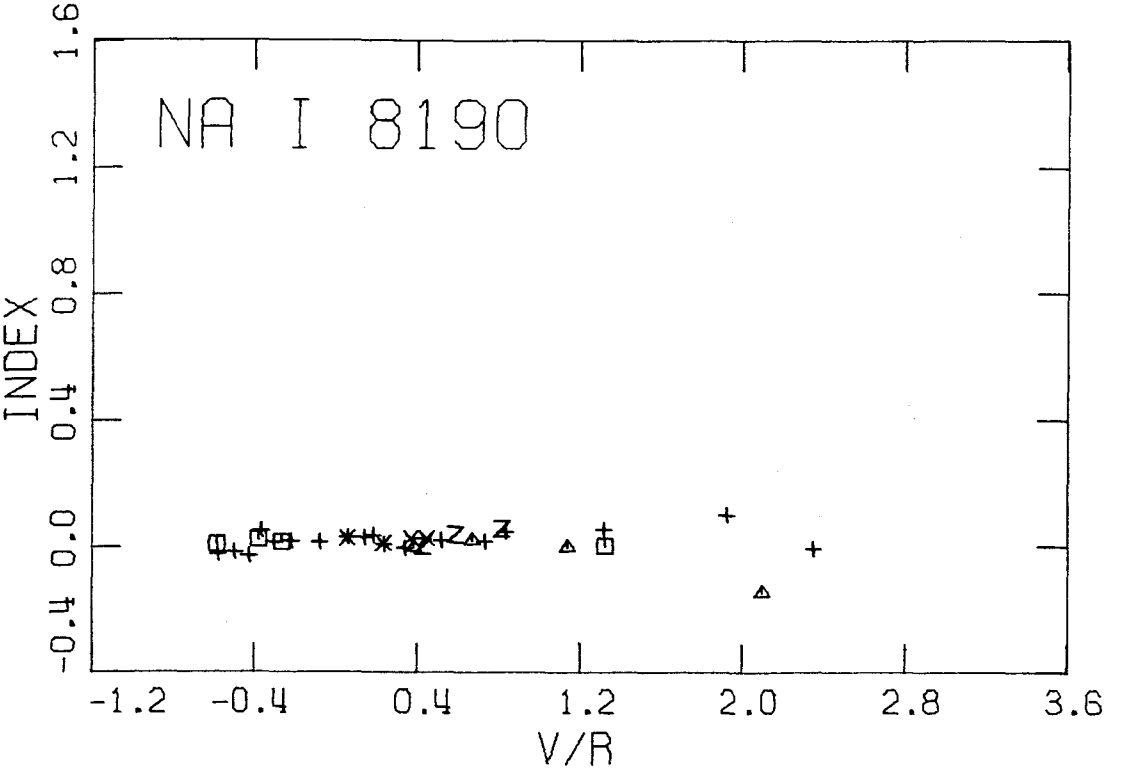

FIGURE C 32

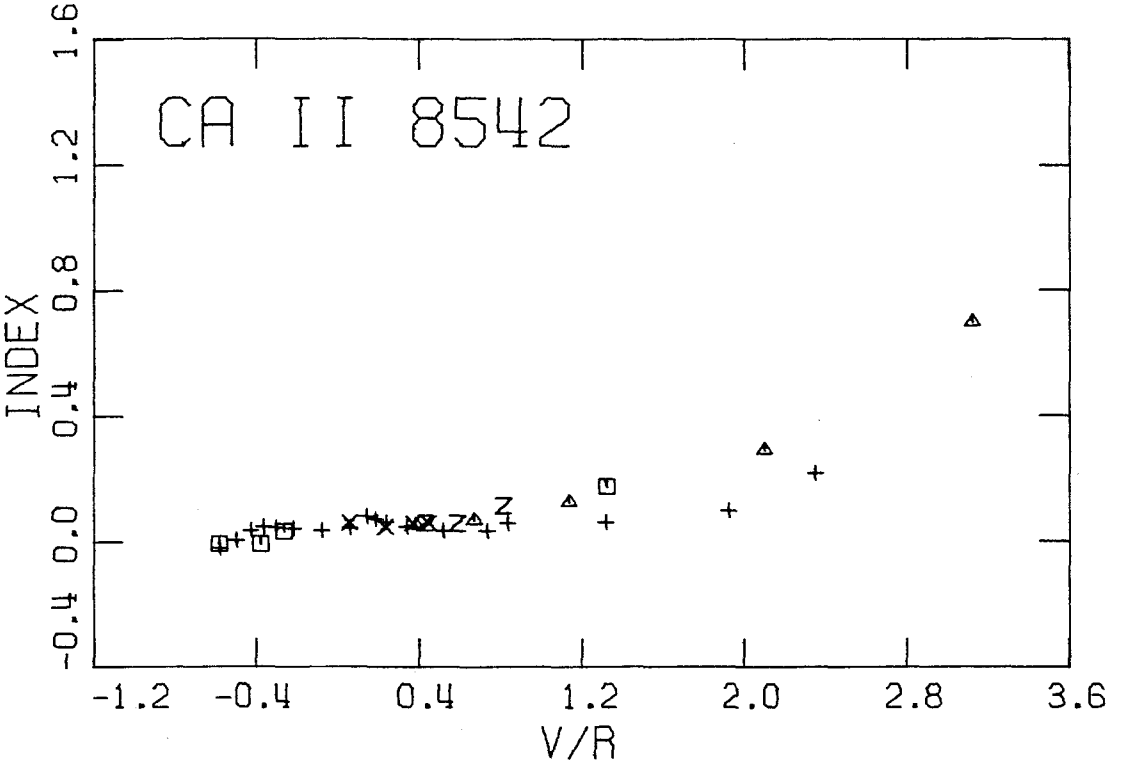

FIGURE C 33

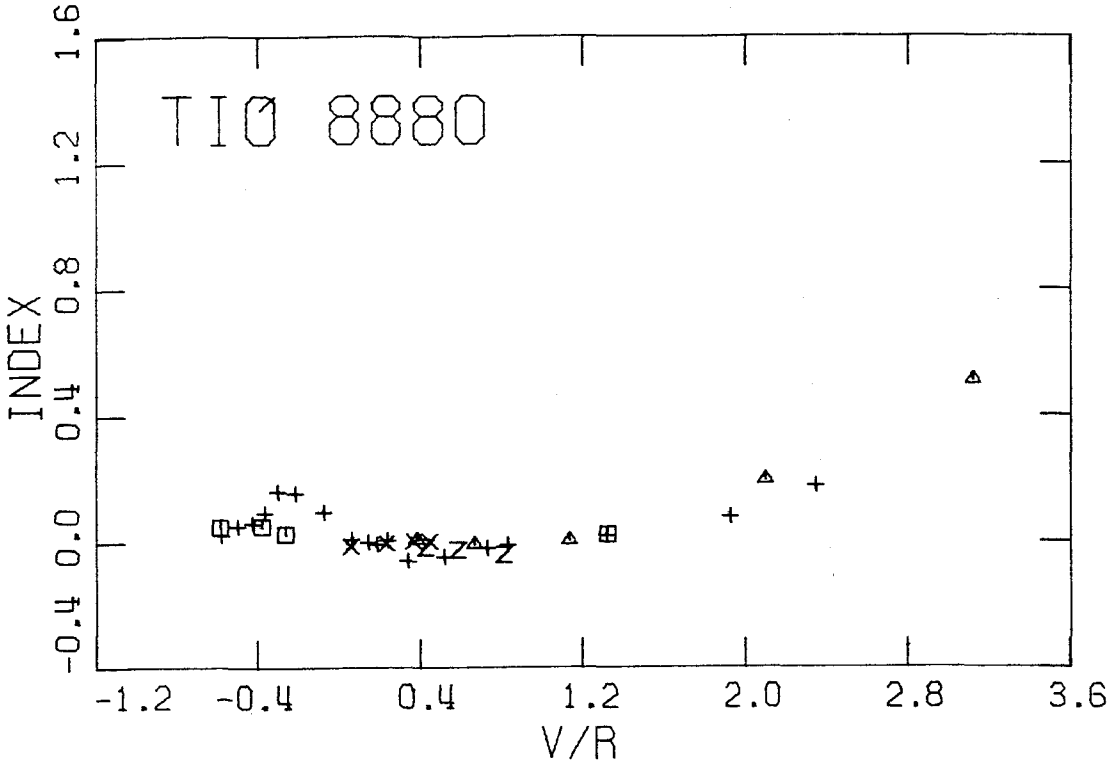

FIGURE C 34

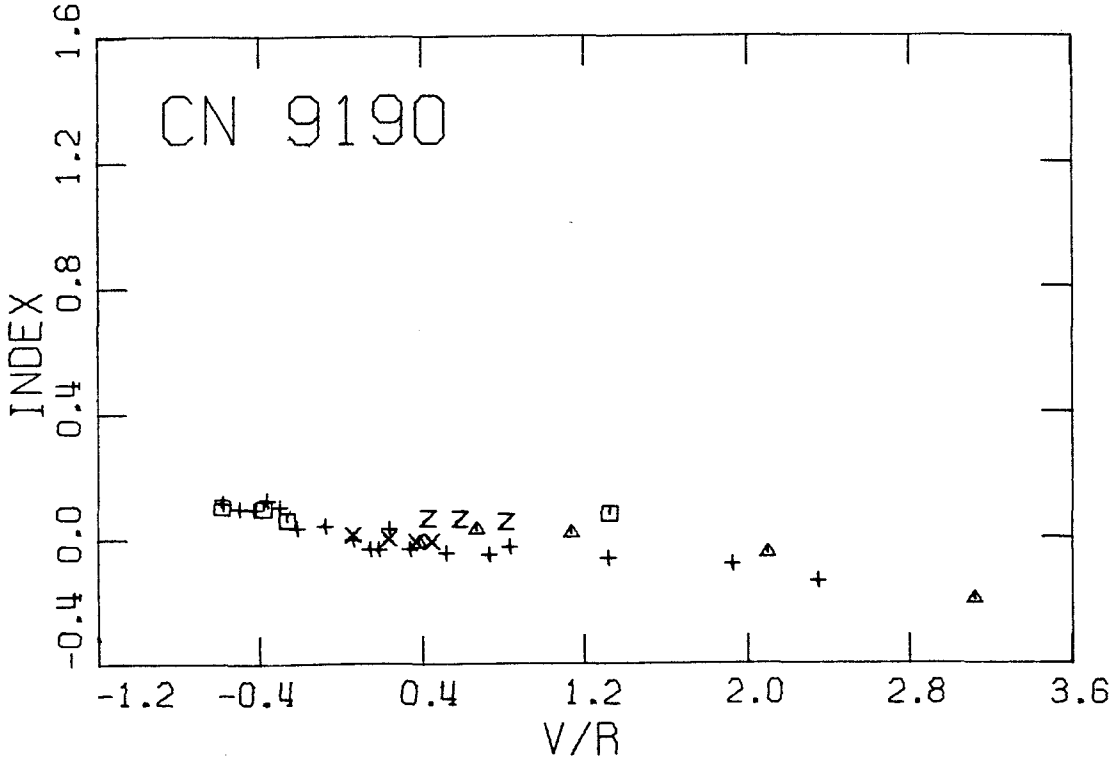

FIGURE C 35

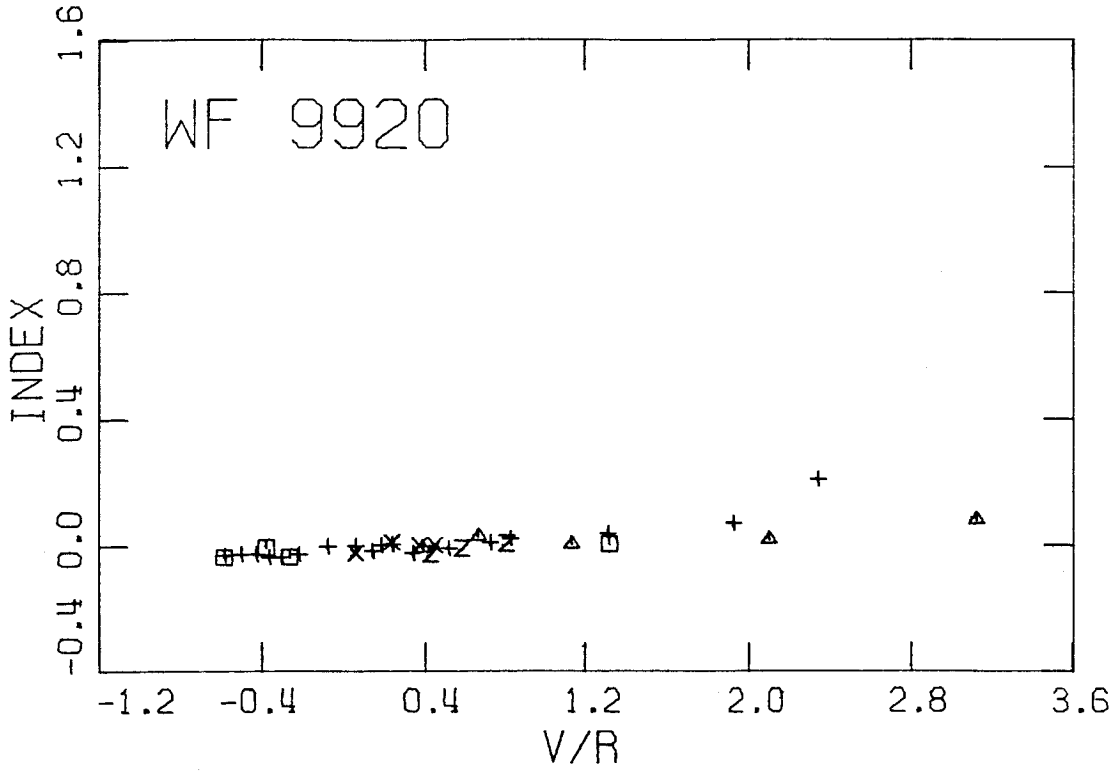

FIGURE C 36

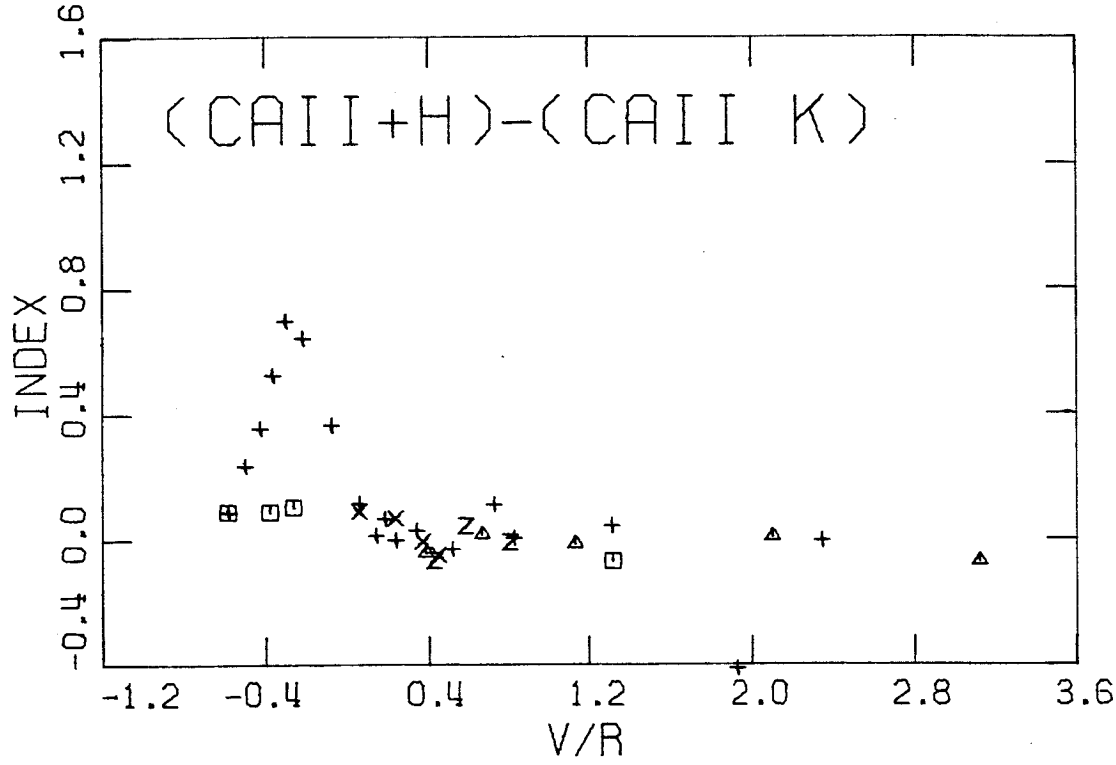

FIGURE C 37

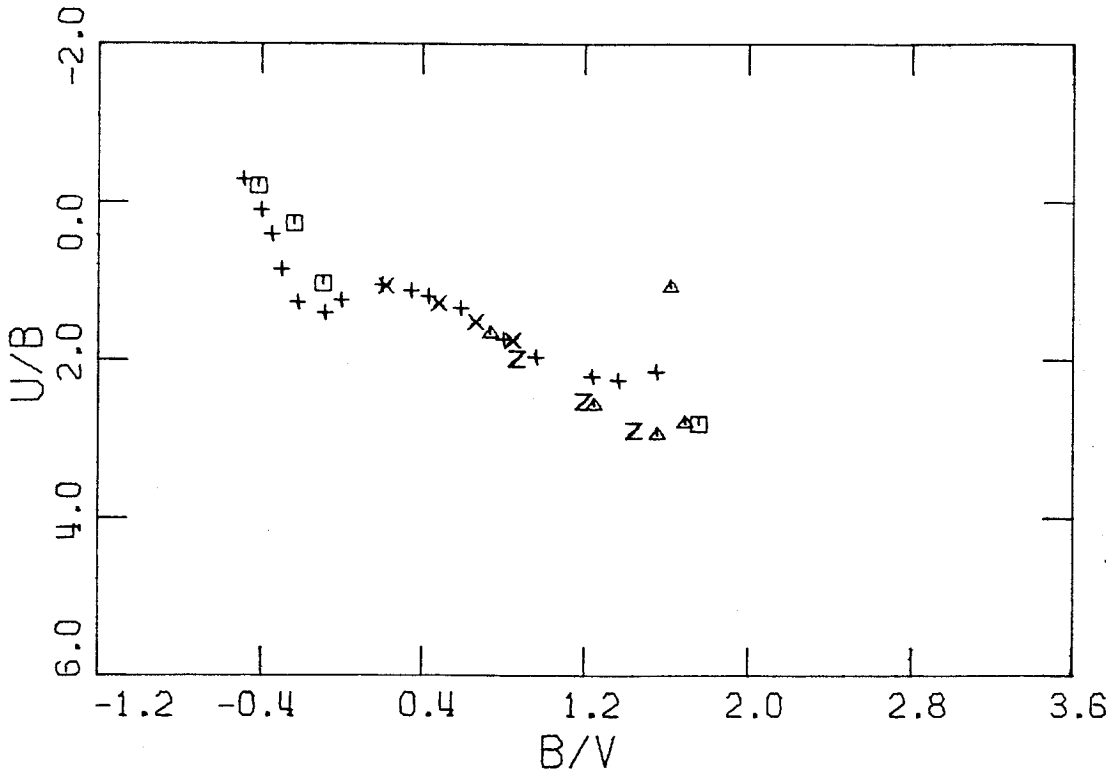

FIGURE C 38

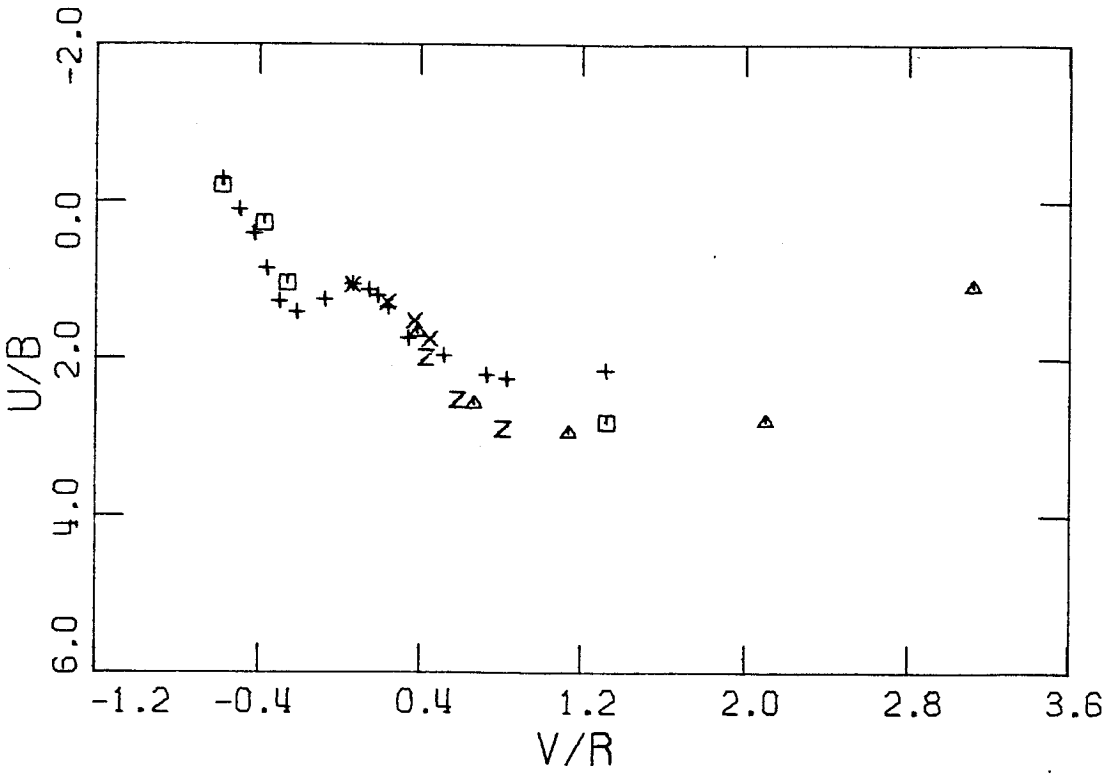

FIGURE C 39

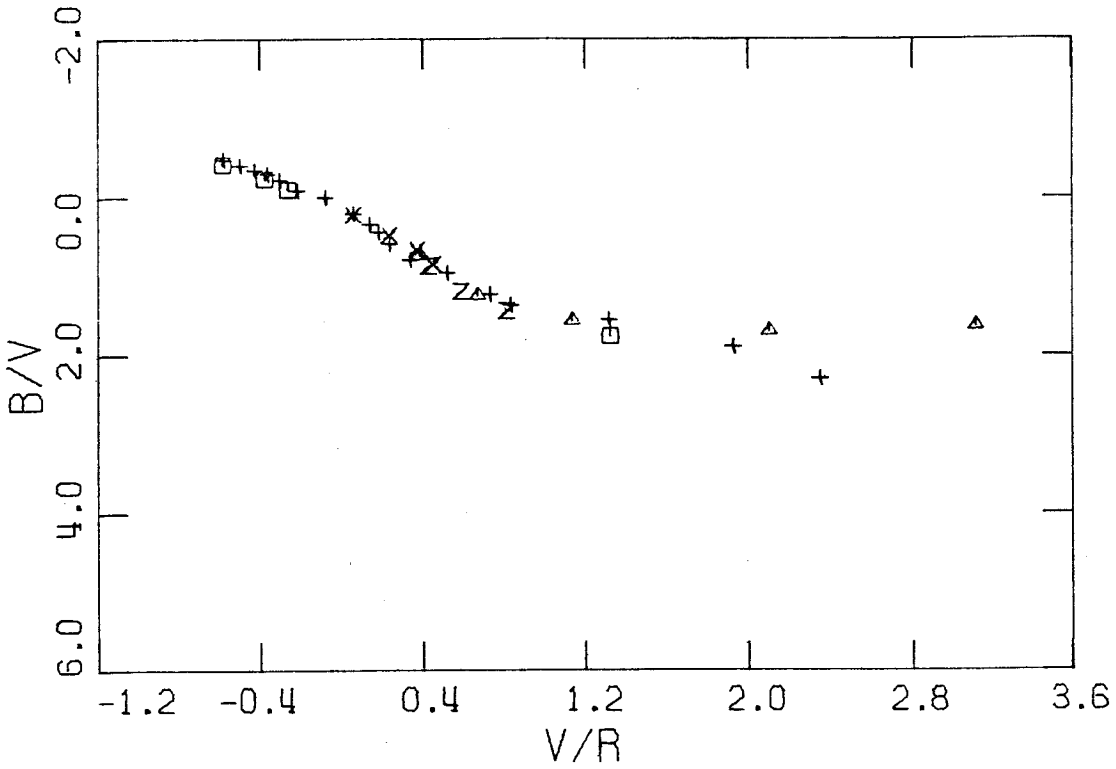

FIGURE C 40

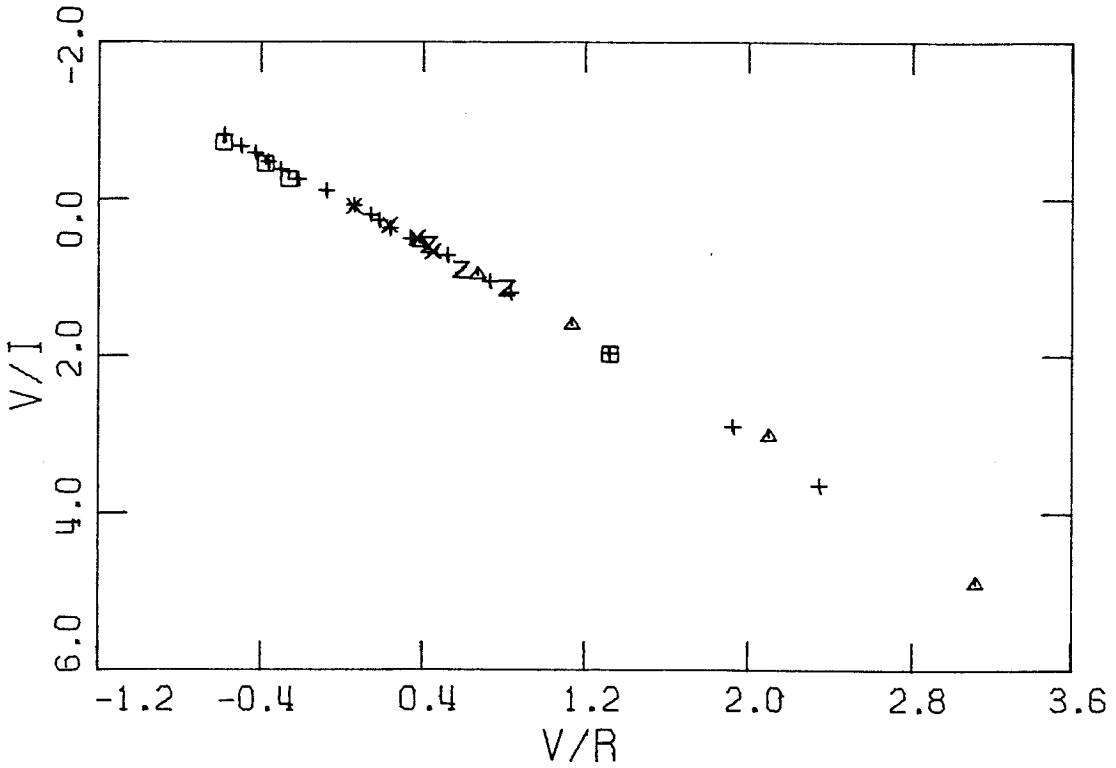

FIGURE C 41

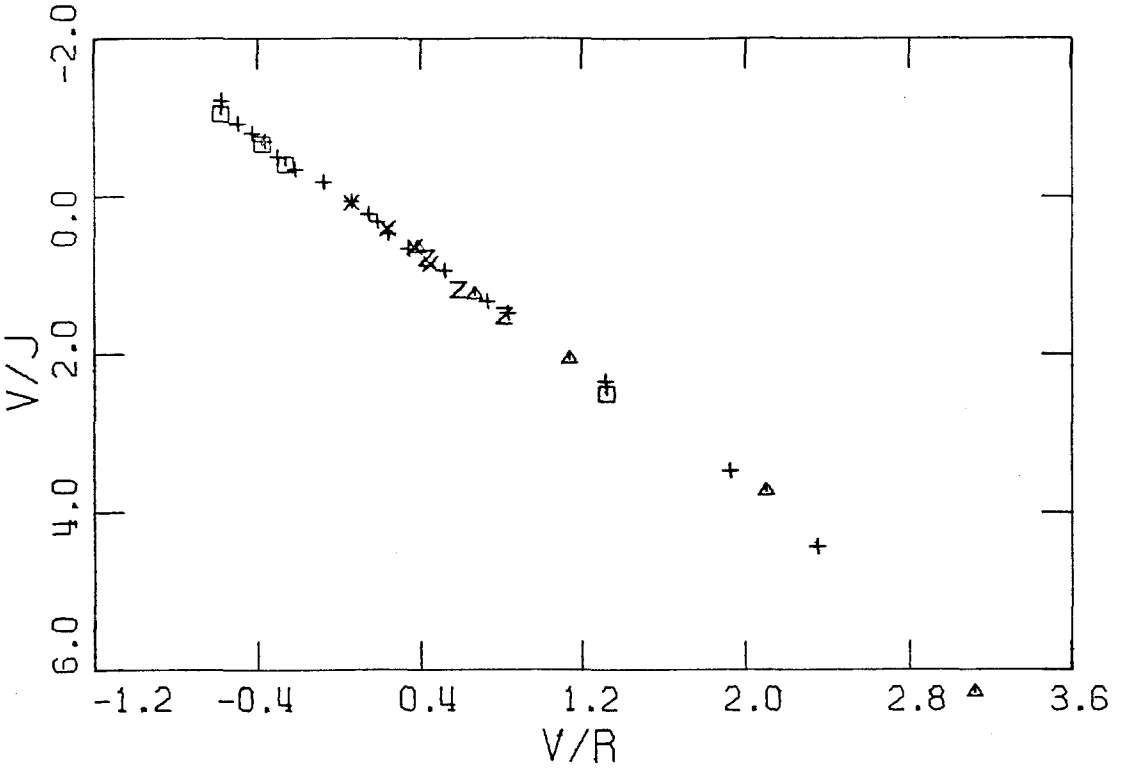

APPENDIX D

MODEL EVOLUTIONARY HISTORIES

Given the stellar birthrate function described by equation (3) of the text (Section IVc), the following procedures are used to derive the synthesis-group populations relevant to specific values of α and τ at an age of $T = 12 \times 10^9$ years. Since the properties of the continuum of stellar masses are represented in the present considerations by the properties of a succession of discrete masses, an appropriate discrete birthrate function is defined by integrating equation (3) over mass bins whose boundaries are chosen as in Tinsley (1968). Namely, if $m_1, m_2, \cdots$ etc. are the discrete masses used (in order of decreasing mass), then we define a function

$$\Phi(m_i) \equiv \int_{(m_i m_{i+1})^{1/2}}^{(m_i m_{i-1})^{1/2}} C m^{-\alpha}\, dm \qquad \text{(D1)}$$

where C and α are as in equation (3) so that the birthrate function of all stars in the mass bin centered at m_i (number of stars formed per unit time) is

$$B(m_i, t) \equiv \Phi(m_i)\, e^{-t/\tau} \qquad \text{(D2)}$$

For the main-sequence synthesis groups the bin-center masses are those adopted in Table 2 of the text (Section IIb). The lifetimes $\tau_{ms}(i)$ for stars in the i^{th} group

(evolutionary times to remain within about 1 magnitude of the initial main sequence) are listed in Table D1. These lifetimes are adopted from the literature as described in the text (Section IVc). For main-sequence groups for which $\tau_{ms}(i) > T = 12 \times 10^9$ years (groups 11-18), the present-day number of stars $N_T(i)$ in the i^{th} group is

$$N_T(i) = \int_0^T B(m_i,t)\, dt = \Phi(m_i)\tau(1 - e^{-T/\tau}) \qquad (D3)$$

For the remaining main-sequence groups,

$$N_T(i) = \int_{T-\tau_{ms}(i)}^{T} B(m_i,t)\, dt = \Phi(m_i)\, \tau(e^{-[T-\tau_{ms}(i)]/\tau} - e^{-T/\tau}) \qquad (D4)$$

In the case of the evolved-star synthesis groups of classes IV and III, the population is considered to arise chiefly from stars with masses of 1 $m_\odot$ to 3 $m_\odot$. This mass range is divided into 11 small, discrete bins as in Tinsley (1972b), using interpolated evolutionary tracks where necessary. The length of time spent in the i^{th} group domain by a star of the k^{th} small mass bin is estimated from the evolutionary tracks and will be denoted by $\tau_g(i,k)$. In a similar way, the total lifetime of a star of the k^{th} small mass bin <u>prior</u> to its entering the i^{th} group domain, $\tau_p(i,k)$, is estimated. The present population of the i^{th} evolved group may in general include stars from any of the

eleven small mass bins; thus,

$$N_T(i) = \sum_{k=1}^{11} \int_{T-\tau_p(i,k)-\tau_g(i,k)}^{T-\tau_p(i,k)} B(m_k,t)\,dt$$

$$= \tau \sum_{k=1}^{11} \Phi(m_k)\left(e^{-[T-\tau_p(i,k)-\tau_g(i,k)]/\tau} - e^{-[T-\tau_p(i,k)]/\tau}\right) \qquad \text{(D5)}$$

Equation (D5) reflects the fact that for the i^{th} group, the present contribution to the population from the k^{th} small mass bin is composed of stars formed in the interval of time between $t = T - \tau_p(i,k) - \tau_g(i,k)$ and $t = T - \tau_p(i,k)$. Note that the function $\Phi(m_k)$ in equation (D5) refers to integrals over the small mass bins between 1 $m_\odot$ and 3 $m_\odot$; the $\Phi(m_i)$ in equations (D3) and (D4) refers to integrals over the rather larger mass bins for the main-sequence synthesis groups.

Equations (D1) through (D5) specify the present populations of synthesis groups of class V, IV or III for any given α and τ. For the case of a birthrate constant in time, the exponential factor in equation (D2) is replaced by a constant, and equations (D3) through (D5) are thus modified in an obvious fashion. Class I groups are discussed in the text (Section IVc). The adopted timescales $\tau_g(i,k)$ and $\tau_p(i,k)$ for class IV and class III synthesis groups are listed in Table D2. The K III SL synthesis groups are not represented in Table D2. Their total populations and relative distribution

over spectral subtype are derived from the normal-giant-star data.

TABLE D1

MAIN-SEQUENCE LIFETIMES

GROUP NO.	MASS ($m/m_\odot$)	τ_{ms} *
1	20.00	0.0063
2	8.20	0.0240
3	4.80	0.0680
4	3.20	0.1800
5	2.30	0.4600
6	1.90	0.8100
7	1.70	1.2000
8	1.40	2.4000
9	1.10	5.6000
10	1.00	8.1000
11	0.85	>14.0000
12	0.80	>14.0000
13	0.70	>14.0000
14	0.60	>14.0000
15	0.55	>14.0000
16	0.35	>14.0000
17	0.20	>14.0000
18	0.10	>14.0000

* Measured in units of 10^9 years.

TABLE D2

EVOLVED-STAR TIMESCALES*

F5-8 IV (i = 19)

k^{th} mass bin ($m/m_\odot$)	$\tau_g(i,k)$	$\tau_p(i,k)$
1.000	0.0	0.0
1.023	0.0	0.0
1.057	1.22000	6.53000
1.091	0.54000	5.96000
1.132	0.62000	5.19000
1.186	0.43000	4.47000
1.250	0.51000	3.55000
1.370	0.26000	2.57000
1.500	0.16000	1.88000
2.250	0.0	0.0
3.000	0.0	0.0

G0-4 IV (i = 20)

k^{th} mass bin ($m/m_\odot$)	$\tau_g(i,k)$	$\tau_p(i,k)$
1.000	2.21000	8.10000
1.023	1.90000	7.41000
1.057	0.36900	7.75000
1.091	0.60700	6.50000
1.132	0.32300	5.81000
1.186	0.19700	4.90000
1.250	0.10000	4.06000
1.370	0.07800	2.83000
1.500	0.03700	2.04000
2.250	0.0	0.0
3.000	0.0	0.0

G5-8 IV (i = 21)

k^{th} mass bin ($m/m_\odot$)	$\tau_g(i,k)$	$\tau_p(i,k)$
1.000	0.41600	10.31000
1.023	0.35100	9.31000
1.057	0.29500	8.12000
1.091	0.27500	7.11000
1.132	0.22800	6.13000
1.186	0.20600	5.10000
1.250	0.18300	4.16000
1.370	0.02100	2.91000
1.500	0.01900	2.08000
2.250	0.0	0.0
3.000	0.0	0.0

K0-2 IV (i = 22)

k^{th} mass bin ($m/m_\odot$)	$\tau_g(i,k)$	$\tau_p(i,k)$
1.000	0.15000	10.73000
1.023	0.27000	9.66000
1.057	0.29000	8.42000
1.091	0.29000	7.39000
1.132	0.26000	6.36000
1.186	0.18000	5.31000
1.250	0.11000	4.43000
1.370	0.16000	2.93000
1.500	0.05000	2.21000
2.250	0.0	0.0
3.000	0.0	0.0

* All times measured in units of 10^9 years.

TABLE D2 (continued)

G5-K1 III (i = 23)

FIRST GIANT BRANCH			SUBSEQUENT STAGES		
k^{th} mass bin $(m/m_\odot)$	$\tau_g(i,k)$	$\tau_p(i,k)$	k^{th} mass bin $(m/m_\odot)$	$\tau_g(i,k)$	$\tau_p(i,k)$
1.000	0.26200	10.88000	1.000	0.04860	11.30000
1.023	0.23900	9.93000	1.023	0.04860	10.32000
1.057	0.20900	8.71000	1.057	0.04860	9.05000
1.091	0.18500	7.68000	1.091	0.04860	7.99000
1.132	0.15900	6.62000	1.132	0.04860	6.88000
1.186	0.13200	5.49000	1.186	0.04860	5.70000
1.250	0.10700	4.45000	1.250	0.04860	4.62000
1.370	0.19100	3.09000	1.370	0.0	0.0
1.500	0.34000	2.15000	1.500	0.0	0.0
2.250	0.00460	0.55000	2.250	0.06600	0.59000
3.000	0.0	0.0	3.000	0.02870	0.27800

K2-5 III (i = 24)

FIRST GIANT BRANCH			SUBSEQUENT STAGES		
k^{th} mass bin $(m/m_\odot)$	$\tau_g(i,k)$	$\tau_p(i,k)$	k^{th} mass bin $(m/m_\odot)$	$\tau_g(i,k)$	$\tau_p(i,k)$
1.000	0.15400	11.14000	1.000	0.0	0.0
1.023	0.14100	10.17000	1.023	0.0	0.0
1.057	0.12300	8.92000	1.057	0.0	0.0
1.091	0.10900	7.87000	1.091	0.0	0.0
1.132	0.09400	6.78000	1.132	0.0	0.0
1.186	0.07800	5.62000	1.186	0.0	0.0
1.250	0.06300	4.56000	1.250	0.0	0.0
1.370	0.09000	3.28000	1.370	0.0	0.0
1.500	0.12800	2.49000	1.500	0.0	0.0
2.250	0.03080	0.55500	2.250	0.0	0.0
3.000	0.02890	0.24900	3.000	0.03100	0.32500

TABLE D2 (continued)

M0-1 III (i = 28)

FIRST GIANT BRANCH			SUBSEQUENT STAGES		
k^{th} mass bin $(m/m_\odot)$	$\tau_g(i,k)$	$\tau_p(i,k)$	k^{th} mass bin $(m/m_\odot)$	$\tau_g(i,k)$	$\tau_p(i,k)$
1.000	0.01000	11.29000	1.000	0.0	0.0
1.023	0.00900	10.31000	1.023	0.0	0.0
1.057	0.00800	9.04000	1.057	0.0	0.0
1.091	0.00700	7.98000	1.091	0.0	0.0
1.132	0.00600	6.87000	1.132	0.0	0.0
1.186	0.00500	5.70000	1.186	0.0	0.0
1.250	0.00400	4.62000	1.250	0.0	0.0
1.370	0.01250	3.37000	1.370	0.0	0.0
1.500	0.03880	2.62000	1.500	0.0	0.0
2.250	0.00470	0.58600	2.250	0.0	0.0
3.000	0.0	0.0	3.000	0.00100	0.35600

M2-5 III (i = 29)

FIRST GIANT BRANCH			SUBSEQUENT STAGES		
k^{th} mass bin $(m/m_\odot)$	$\tau_g(i,k)$	$\tau_p(i,k)$	k^{th} mass bin $(m/m_\odot)$	$\tau_g(i,k)$	$\tau_p(i,k)$
1.000	0.00200	11.30000	1.000	0.00460	11.35000
1.023	0.00200	10.32000	1.023	0.00460	10.37000
1.057	0.00200	9.05000	1.057	0.00460	9.10000
1.091	0.00200	7.99000	1.091	0.00460	8.04000
1.132	0.00100	6.88000	1.132	0.00460	6.93000
1.186	0.00100	5.70000	1.186	0.00460	5.75000
1.250	0.00100	4.62000	1.250	0.00460	4.67000
1.370	0.00324	3.38000	1.370	0.0	0.0
1.500	0.01050	2.66000	1.500	0.0	0.0
2.250	0.0	0.0	2.250	0.0	0.0
3.000	0.0	0.0	3.000	0.00700	0.35700

TABLE D2 (continued)

M6-8 III (i = 30)

FIRST GIANT BRANCH			SUBSEQUENT STAGES		
k^{th} mass bin $(m/m_\odot)$	$\tau_g(i,k)$	$\tau_p(i,k)$	k^{th} mass bin $(m/m_\odot)$	$\tau_g(i,k)$	$\tau_p(i,k)$
1.000	0.0	0.0	1.000	0.00071	11.35000
1.023	0.0	0.0	1.023	0.00071	10.37000
1.057	0.0	0.0	1.057	0.00071	9.10000
1.091	0.0	0.0	1.091	0.00071	8.04000
1.132	0.0	0.0	1.132	0.00071	6.93000
1.186	0.0	0.0	1.186	0.00071	5.75000
1.250	0.0	0.0	1.250	0.00071	4.67000
1.370	0.0	0.0	1.370	0.0	0.0
1.500	0.0	0.0	1.500	0.0	0.0
2.250	0.0	0.0	2.250	0.0	0.0
3.000	0.0	0.0	3.000	0.0	0.0

APPENDIX E

LINEAR PROGRAMMING

1. Introduction

Linear programming is a field of mathematical analysis concerned with the solution of a restricted class of extreme-value problems. Specifically, linear programming provides efficient numerical methods for optimizing linear expressions with nonnegative variables which are in turn subject to linear constraints. In this Appendix, a short review of the mathematical framework of linear programming is given for the reader's convenience. Such a recapitulation of well-known theory seems in order in view of the heretofore scant applications of linear programming to the physical sciences. Further details of a theoretical or computational nature may be found in any of a large number of textbooks, such as Gale (1960) and Garvin (1960).

Following the discussion of linear-programming techniques, a description of their present application to the problem of galaxy stellar-population synthesis is given.

2. Theory and Definitions

Let A be a matrix of m rows and n columns, and let y, b, and c be column vectors with n, n, and m components respectively. Denote the transpose of b by b^T, a row vector. Consider the problem of solving the following linear system for the vector y :

$$b^T y = \text{minimum}$$

subject to $Ay \geq c$

and $y \geq 0 \quad (y_i \geq 0 \text{ for } i=1,n) \qquad (E1)$

The constrained minimization problem (E1) is a classical linear-programming situation. If conventional nomenclature is employed and (E1) is referred to as the "primal" problem, then the related maximization problem of finding x such that

$$x^T c = \text{maximum}$$

$$x^T A \leq b^T$$

$$x \geq 0 \qquad (E2)$$

is referred to as the "dual" of (E1), where we have introduced a new column vector x and its transpose x^T, each with m components, and A, b^T and c are the same as in (E1). The uses of the dual problem will be described later.

It is convenient here to introduce the following definitions: y is called a "feasible" solution of the primal problem (E1) if the constraints $Ay \geq c$ and $y \geq 0$ are satisfied; similarly, x is a "feasible" solution of the dual problem (E2) if $x^T A \leq b^T$ and $x \geq 0$ are satisfied. The scalar quantities $b^T y$ and $x^T c$ are called the "values" of their respective problems, and "optimal" solutions are those feasible solutions which yield the desired

extreme values for their problems.

It is easily shown that if y and x are feasible solutions, then $x^T c \leq b^T y$. Furthermore, the special case of equal finite values, $x^T c = b^T y$, for feasible y and x is a sufficient condition for y and x to be optimal solutions. It should be noted that it is possible for either the primal or dual problem not to possess a finite optimal value. (See, for example, a text regarding the "duality theorem" of linear programming). In most instances relating to physical situations, however, the primal and dual problems both have optimal solutions with equal finite values. This equality provides a convenient check on the consistency of any actual calculations of the optimal vectors y_o and x_o. It will be shown later that knowledge of the optimal dual solution is also useful in assessing the changes induced in the optimal primal solution by small perturbations in the constraints. For these reasons, it is often advantageous to seek solutions to <u>both</u> the dual and primal problems simultaneously.

We may, without loss of generality, consider the constraints of the primal problem to be of the form $Ay = c$, inasmuch as any strict inequalities can be recast as equations by the introduction of additional nonnegative components of y (conventionally called "slack variables") and corresponding additional unit-vector columns of A. (See Garvin 1960, p. 4). The primal expressed with pure equality

constraints is said to be in "canonical" form. This is of importance since the principal computational technique in linear programming, the "simplex method" to be discussed in a subsequent section, assumes the problem to be expressed in canonical form.

It can be shown (Gale 1960) that if a canonical primal has a feasible solution, it has at least one "basic" feasible solution, where a solution is said to be basic if it involves only linearly-independent columns of the matrix A: i.e., the only components of a basic solution y which are not zero are those multiplying linearly-independent columns of A (usually m in number) in the product Ay. The nonzero components of a basic solution are called the "basic variables", and the set of linearly-independent columns of A corresponding to the basic variables is called the "basis" of the solution. In a similar manner it can be shown (Gale 1960) that if a canonical primal has an optimal solution, it has at least one basic optimal solution. This implies that in searching for an optimal solution it is sufficient to consider only basic feasible solutions.

The actual calculation of an optimal solution is of course the central concern in any practical application of linear programming, and one method for solving (E1) is discussed in Section 3. For the present, however, let us suppose that a basic optimal solution y_o of the primal problem has been somehow found, involving m linearly-

independent columns of A. The product Ay may clearly be rewritten as $A_o y_o$ where A_o is the $m \times m$ matrix of linearly-independent columns of A comprising the optimal basis. Hence

$$A_o y_o = c \tag{E3}$$

Since A_o is a square matrix of linearly-independent columns, its inverse A_o^{-1} exists. We may therefore write

$$y_o = A_o^{-1} c \tag{E4}$$

Equation (E4) is significant because it expresses the optimal basic solution y_o in terms of the inverse of the optimal basis and the right-hand side of the primal constraint equation. The elements of A_o^{-1} may therefore be identified with the partial derivatives of the optimal basic variables with respect to the components of the vector c:

$$\frac{\partial y_{oi}}{\partial c_j} = A^{-1}_{oij} \qquad i=1,m;\ j=1,m \tag{E5}$$

If we consider the small yet finite perturbation δc to the vector c, such that $c' \equiv c + \delta c$, and if

$$\delta y_o \equiv A_o^{-1} \delta c \tag{E6}$$

then the vector

$$y_o' \equiv y_o + \delta y_o \tag{E7}$$

correctly gives the optimal solution to the primal problem with perturbed constraints $Ay = c'$ provided that the perturbation δc is small enough that y'_o is still feasible; i.e., provided $y'_o \geq 0$ (see Garvin 1960).

Through equations (E6) and (E7) we may thus evaluate exactly how the optimal primal solution will change as the right-hand side of the constraint equation (the vector c) is perturbed by small amounts. One may also demonstrate that under the perturbation δc the optimal value of the primal solution changes by an amount

$$\delta(b^T y) = x_o^T \delta c \qquad \text{(E8)}$$

where x_o is the original optimal dual solution and where the above restriction on the smallness of the perturbation applies. The optimal dual variables x_{oj} may thus be identified with the partial derivatives of the optimal primal value:

$$\frac{\partial(b^T y_o)}{\partial c_j} = x_{oj} \qquad j=1,m \qquad \text{(E9)}$$

The ability to identify and evaluate the partial derivatives defined by equations (E5) and (E9) in general provides a means of assessing the stability of the optimal solution against small changes in the vector c. Techniques also exist for calculating the effects on the optimal solution of changes in A or b, but they are not considered

here inasmuch as such perturbations are not extremely relevant to the present application of linear programming discussed in Section 4.

3. Computational Techniques

a. Simplex method

From the theory in Section 2, it is known that to find an optimal solution of the linear-programming problem (E1) it is sufficient to consider only basic feasible solutions. The "simplex method" of linear programming is an efficient computational technique utilizing this fact. Starting with any basic feasible solution, it proceeds iteratively to the optimal solution, if it exists, or to a suitable termination in the event no optimum exists. (Section 3b of this Appendix considers the question of finding an initial basic feasible solution for the simplex method.) Detailed explanations of the method may be found in Gale (1960) and Garvin (1960). Briefly stated, however, the simplex method examines in an orderly fashion the set of all basic feasible solutions to the system of equations expressed by $Ay = c$ for the solution yielding the smallest value of $b^T y$. The minimum so found is global within the bounds set by the constraints $Ay = c$ and the condition of feasibility ($y \geq 0$). In most instances, this minimum is mathematically unique. In the context of the present application (see Section 4), however, this fact is by itself of little value, as slightly "worse"

solutions may be equally acceptable considering observational uncertainties. The reliability of the optimal solutions obtained in the application to be described is judged chiefly by the effect of perturbations in the input data consistent with the observational errors.

Each successive basis in the iteration process differs from the preceding basis in only one vector; i.e., only one of the m basic variables is different. The key to the efficiency of the simplex method lies in the algorithm by which the choices are made as to which currently nonbasic vector should be introduced into the next basis and which currently basic vector should in turn leave the basis. Except for infrequently-occurring instances of "degeneracy" (see, e.g., Gale 1960), these choices are well defined and such as to insure that the value of the primal problem is reduced at each step.

The actual transition from each basic feasible solution to the next, given the decision on which vectors are to enter and to leave the basis, is numerically performed by a convenient row-replacement operation on an array of coefficients for the system $Ay = c$. This array is conventionally called the "simplex tableau" and consists of the coefficients of the expansion of the vector c and the columns of the matrix A in terms of the current basis vectors. If we denote the m current basis vectors by v^i, $i=1,m$ (each v^i is a column of A with m components)

and the columns of A by a^j, $j=1,n$, then the tableau elements t_{ij} for $i=1,m$ and $j=1,n$ are defined by the vector equations

$$a^j = \sum_{i=1}^{m} t_{ij} v^i \qquad j=1,n \tag{E10}$$

The tableau elements for c are denoted by t_{io} $i=1,m$ and thus

$$c = \sum_{i=1}^{m} t_{io} v^i \tag{E11}$$

Since the basis vectors v^i are linearly-independent columns of A, it is apparent that at any stage of the simplex process the elements t_{io} give the components of the current basic feasible solution. In particular, at successful termination of the process, the t_{io} are the required optimal basic variables.

The reader is referred to Gale (1960) for complete information on the transformations performed on the t_{ij} and t_{io} to proceed to successive basic solutions as well as details of the algorithm which chooses the entering and exiting vectors at each step and signals the termination of the iteration process. In that reference will also be found a description of a modified approach called the "dual simplex method" by which the dual optimal solution may be simultaneously obtained through the use of appended unit-vector columns in the simplex tableau. The dual simplex

method is the computational technique actually used in the present application and has the advantage of providing the inverse matrix elements A^{-1}_{oij} (see equation (E4)) automatically. Termination of the dual simplex method at optimum thus provides directly all the quantities required for the perturbation analysis discussed in Section 2 (equations (E5)-(E9)) as well as the optimal primal solution y_o itself.

b. Artificial variables

The simplex (or dual simplex) method requires an initial basic feasible solution with which to start the search for an optimum. It is sometimes possible to find this initial solution by inspection. Depending on the nature of the original constraints, however, this is often impossible or very difficult to do, as is the case in the present application. In such instances, the simplex algorithm may itself be used to find an initial basic feasible solution (see Garvin 1960). This is done by using the simplex method to solve a related problem having an obvious initial solution which utilizes so-called "artificial variables" and whose final optimal solution serves as the initial solution to the original problem.

The artificial variables are additional nonnegative components appended to the vector y (with corresponding unit-vector columns appended to A). As many may be used

as are needed (up to the total number of basic variables, m) to provide the initial solution. For example, if all m initial basic feasible variables are taken to be artificial variables, their values are simply the m components of the vector c , and all other (non-artificial) variables are assigned the value zero. It is clear that such a vector of artificial variables is a solution of the appended system of equations (which reduces to the identity c = c), is basic (the corresponding columns of A are m unit vectors), and is feasible. (It is presumed that any originally negative components of c are made positive by multiplying such components and their corresponding rows of A through by -1. Furthermore, since cases of degeneracy often arise from initial components of c being zero, it is also presumed that such zeros may be replaced by infinitesimally small positive numbers. See Geary and McCarthy 1964).

The simplex method is applied to the appended system of equations so as to minimize the sum of the artificial variables. As long as the original problem has a feasible solution, then the optimal solution of the appended system will have all artificial variables equal to zero and thus will serve as the required initial basic feasible solution to the original problem. The process of solving the appended problem and driving the artificial components out of the basis is commonly referred to as "Phase I" of the simplex

method; the subsequent process of solving the original optimization problem is called "Phase II". It will be noted that the use of a Phase I computation requires a redefinition of the vector b which, through the product $b^T y$, determines the function being optimized. The original definition of b must be restored as Phase II is entered.

4. Application to Galaxy Stellar-Population Synthesis

The theory of linear programming reviewed in the preceding sections is here applied to the problem of optimizing the fit of synthetic model-galaxy energy distributions to actual observations, thereby providing a measure of the relative stellar distribution over spectral type and luminosity class within the galaxy. The fitting parameter chosen for optimization is the weighted sum of the absolute values of the percentage residuals between model and observation.

Let g_i be the observed absolute flux density from a galaxy at wavelength i $(i=1,m)$. Let a_{ij} similarly be the absolute flux density from a "mean star" of type j $(j=1,n)$ at wavelength i $(i=1,m)$. If x_j is the (nonnegative) number of mean stars of type j present in the synthetic galaxy, then the synthetic-model absolute flux density at wavelength i is $\sum_{j=1}^{n} a_{ij}x_j$. Finally, if ρ_i is a nonnegative weight factor $(i=1,m)$, the minimization sought is

$$\sum_{i=1}^{m} \rho_i \left| \frac{\sum_{j=1}^{n} a_{ij}x_j - g_i}{g_i} \right| = \text{minimum} \qquad \text{(E12)}$$

The problem (E12) may be made strictly linear through the introduction of two new nonnegative vectors u and v of m components each such that

$$\rho_i \left(\frac{\sum_{j=1}^{n} a_{ij}x_j - g_i}{g_i} \right) \equiv u_i - v_i \quad i=1,m \qquad \text{(E13)}$$

(Note that the vector v here is <u>not</u> related to the vectors v^i introduced in Section 3.) Given this definition of u and v, the problem (E12) reduces to

$$\sum_{i=1}^{m} |u_i - v_i| = \text{minimum} \qquad \text{(E14)}$$

which may be shown to be equivalent to

$$\sum_{i=1}^{m} (u_i + v_i) = \text{minimum} \qquad \text{(E15)}$$

(I am indebted to Dr. J. N. Franklin for suggesting the above linearization approach. The required equivalence of (E14) and (E15) is most readily seen by noting that for a given $u_i - v_i$, $\sum_{i=1}^{m} (u_i + v_i)$ is a minimum if $u \cdot v = 0$.)

Additional "astrophysical constraints" of the type discussed by Faber (1972) are also imposed on the synthetic model. These constraints may all be expressed by the matrix

relation $Cx \leq 0$ where C is a matrix of p rows and n columns. Three types of constraints are explicitly considered:

1) group-ratio constraints of the form

$$d_1 \leq \frac{x_k}{x_{k'}} \leq d_2 \qquad \text{and/or} \qquad d_3 \leq \frac{\sum x_j}{\sum x'_j} \leq d_4$$

where in the latter form up to 10 groups may be summed in both numerator and denominator.

2) fractional-light-contribution constraints of the form

$$d_5 \leq \frac{x_k a_{jk}}{\sum_{\ell=1}^{n} x_\ell a_{j\ell}} \leq d_6$$

3) mass-luminosity-ratio constraint of the form

$$r_1 \leq \frac{\sum_{k=1}^{n} x_k m_k}{\sum_{k=1}^{n} x_k \frac{a_{jk}}{a_{j\odot}}} \leq r_2$$

where d_1, d_2, d_3, d_4, d_5, d_6, r_1, and r_2 are nonnegative constants, $a_{j\odot}$ represents the absolute flux density at wavelength j for a mean star of solar type, and m_k is the mass of a mean star of type k in solar units. For each constraint applied, two rows of the matrix C are generated (one for each of the inequalities). A vector z of p nonnegative slack variables is introduced to recast

the astrophysical constraints in equation form:

$$Cx + z = 0 \tag{E16}$$

Equation (E13) may be rewritten as

$$\rho_i \sum_{j=1}^{n} (a_{ij}x_j) + g_i v_i - g_i u_i = \rho_i g_i \quad i=1,m \tag{E17}$$

and thus (E15)-(E17) together define a canonical linear-programming problem to which the dual simplex method is applied. To suppress degeneracy, the zeros on the right-hand-side of (E16) are replaced by positive numbers of order 10^{-3}. This replacement makes no practical difference in the applied constraints.

A Phase I calculation is employed to provide the required initial basic feasible solution. The initial Phase I basic feasible solution consists of the p slack variables from the vector z and m additional nonnegative artificial variables comprising a vector denoted by w. The Phase I problem is thus

$$b^T y = \text{minimum}$$

$$Ay = c$$

$$y \geq 0$$

where

$$y \equiv \begin{bmatrix} x \\ v \\ u \\ z \\ w \end{bmatrix} \Bigg\} 3m+n+p \text{ components} \tag{E18}$$

$$b^T = (\underbrace{0,\ldots,0}_{2m+p+n},\underbrace{1,\ldots,1}_{m}) \qquad \text{(E19)}$$

$$c = \begin{bmatrix} \rho_1 g_1 \\ \vdots \\ \rho_m g_m \\ \\ \varepsilon_1 \\ \vdots \\ \varepsilon_p \end{bmatrix} \quad \text{with } \varepsilon_k = 10^{-3}(1.01)^k \quad k=1,p \qquad \text{(E20)}$$

$$A = \begin{bmatrix} \overbrace{\rho_1 a_{11} \cdots \rho_1 a_{1n}}^{n} & \overbrace{g_1 \; 0 \cdots 0}^{m} & \overbrace{-g_1 \; 0 \cdots 0}^{m} & \overbrace{0 \cdots 0}^{p} & \overbrace{1 \; 0 \cdots 0}^{m} \\ \vdots \quad\quad \vdots & 0 \quad \ddots \quad \vdots & 0 \quad \ddots \quad \vdots & \vdots \quad\quad \vdots & 0 \quad \ddots \quad \vdots \\ \rho_m a_{m1} \cdots \rho_m a_{mn} & 0 \cdots 0 \; g_m & 0 \cdots 0 \; -g_m & 0 \cdots 0 & 0 \cdots 0 \; 1 \\ & & & & \end{bmatrix} \begin{matrix} \\ \\ \} m \\ \\ \end{matrix}$$

$$\begin{bmatrix} c_{11} \cdots\cdots c_{1n} & 0 \cdots\cdots 0 & 0 \cdots\cdots 0 & 1 \; 0 \; 0 & 0 \cdots\cdots 0 \\ \vdots \quad\quad \vdots & \vdots \quad\quad \vdots & \vdots \quad\quad \vdots & 0 \quad \ddots \quad \vdots & \vdots \quad\quad \vdots \\ c_{p1} \cdots\cdots c_{pn} & 0 \cdots\cdots 0 & 0 \cdots\cdots 0 & 0 \; 0 \; 1 & 0 \cdots\cdots 0 \end{bmatrix} \begin{matrix} \\ \} p \end{matrix} \qquad \text{(E21)}$$

where the c_{ij} (i=1,p; j=i,n) are the elements of the matrix C. For clarity, it should be noted that the m and n defined in this Section (m = number of wavelengths, n = number of mean stellar types) do <u>not</u> play the same role as the m and n defined in Sections 2 and 3 (where m and n specified the size of the matrix A).

The Phase I solution is calculated by the simplex algorithm coded in Fortran on the Caltech IBM 370/158 computer. One iteration per artificial variable is required.

Upon completion of Phase I, a Phase II calculation is automatically initiated with

$$b^T = (\overbrace{0,\ldots,0}^{n},\overbrace{1,\ldots,1}^{2m},\overbrace{0,\ldots,0}^{p+m}) \quad . \qquad \text{(E22)}$$

The last m columns of A (corresponding to the artificial-variable vector w) which were driven out of the basis in Phase I are retained in Phase II as "inactive" columns. That is, they are not allowed to re-enter the basis but are used along with the p active columns corresponding to the slack vector z to calculate the dual solution and the inverse matrix A_o^{-1}. For $n \sim 34$, $m \sim 50$, and $p \sim 60$, the optimal Phase II solution is typically obtained after ~ 200 iterations.

A perturbation analysis of the type described in Section 2 may be performed using the optimal dual solution and the elements of A_o^{-1} to determine the stability of the solution against small changes in the galaxy data. In practice, the usefulness of this analysis is limited, due to the possible interchange of basic variables among the u_i and the v_i under the effect of perturbations. (Recall that the perturbation analysis remains valid only if the perturbed basis is the same as the unperturbed optimal basis; i.e., only if the y_o' in equation (E7) remains feasible.) In the present case, the effects of perturbations are investigated by means

of direct computation of perturbed solutions.

REFERENCES

Alloin, D. 1973, Astr. and Ap., 27, 433.

Alloin, D., Andrillat, Y., and Souffrin, S. 1971, Astr. and Ap., 10, 401.

Andrillat, Y., Souffrin, S., and Alloin, D. 1972, Astr. and Ap., 19, 405.

Baldwin, J.R., Danziger, I.J., Frogel, J.A., and Persson, S.E. 1973, Ap. Letters, 14, 1.

Bergh, S. van den 1960a, Ap. J., 131, 215.

_____1960b, Ap. J. 131, 558.

Blaauw, A. 1963, in Basic Astronomical Data, Ed. K. Aa. Strand (Chicago: University of Chicago Press), p. 383.

Blanco, V.M., Demers, S., Douglass, G.G., and Fitzgerald, M.P. 1968, Pub. U.S. Naval Obs., Ser II, 13.

Brown, R.L., and Mathews, W.G., 1970, Ap. J., 160, 939.

Burbidge, E.M., and Burbidge, G.R. 1964, Ap. J., 140, 1445.

Burbidge, E.M., Burbidge, G.R., and Prendergast, K.H. 1960, Ap. J., 132, 640.

_____1963, Ap. J., 137, 376.

Christensen, C.G. 1972, Ph.D. Thesis, California Institute of Technology.

de Vaucouleurs, G., and de Vaucouleurs, A. 1964, Reference Catalogue of Bright Galaxies (Austin: University of Texas Press).

Epstein, E.E. 1964, A.J., 69, 490.

Faber, S.M. 1972, Astr. and Ap., 20, 361.

Fagerholm, E. 1906, Inaugural Dissertation, Uppsala.

Fäy, T.D., Stein, W.L., and Warren, W.H. 1974, Pub. A.S.P., 86, 772.

Gale, D. 1960, The Theory of Linear Economic Models (New York: McGraw-Hill).

Garvin, W.W. 1960, Introduction to Linear Programming (New York: McGraw-Hill).

Geary, R.C., and McCarthy, M.D. 1964, Elements of Linear Programming (New York: Hafner Publishing Co.).

Gliese, W. 1957, Mitt. Astr. Rechen-Inst., Ser. A., No. 8.

_____ 1969, Veroff-Astr. Rechen-Inst., No. 22.

Greenstein, J.L. 1975, private communication.

Griffin, R. 1975, M.N.R.A.S., 171, 181

Gunn, J.E. 1974 private communication.

Harris, D.L. III, Strand, K.As., and Worley, C.E. 1963 in Basic Astronomical Data, ed. K.Aa. Strand (Chicago: University of Chicago Press) p. 273.

Hickok, F.R. and Morton, D.C. 1968, Ap. J., 152, 203.

Hjellming, R.M. 1968, Ap. J., 154, 533.

Hoffleit, D. 1964, Catalogue of Bright Stars (New Haven: Yale University Press).

Holmberg, E. 1958, Medd. Lunds. Obs., Ser. 2, No. 128.

_____ 1969, Arkiv For Astronomi, Band 5 nr 20.

Humason, M.L., Mayall, N.U., and Sandage, A.R. 1956, A. J., 61, 97

Iben, I. 1965, Ap. J., 142, 1447

Iben, I. 1966a, Ap. J., 143, 483.

_____ 1966b Ap. J., 143, 505.

_____ 1966c Ap. J., 143, 516.

_____ 1967a Ap. J., 147, 624.

_____ 1967b Ap. J., 147, 650.

Iskudaryan, S.G. 1968, Astrofiz., 4, 385.

Johnson, H.L. 1952, Ap. J., 116, 640.

_____1963, in Basic Astronomical Data, ed. K.Aa. Strand (Chicago: University of Chicago Press), p. 214.

_____ 1966, A. R. A. A., 4, 193.

Johnson, H.L., and Knuckles, C.F. 1955, Ap. J., 122, 209.

Joly, M. 1973, Astr. and Ap., 33, 177.

_____1974, Astr. and Ap., 37, 57.

Joly, M., and Andrillat, Y. 1973, Astr. and Ap., 26, 95.

Keenan, P.C. 1963, in Basic Astronomical Data, ed. K.Aa. Strand (Chicago: University of Chicago Press), p. 78.

Krueger, T.K., Aller, L.H., and Czyzak, S.J. 1970, Ap. J., 160, 921.

Kruit, P.C. van der 1973, Ap. J., 186, 807.

Larson, R.B., and Tinsley, B.M. 1974, Ap. J., 192, 293.

Lasker, B.M. 1970, A.J., 75, 21.

Lee, T.A. 1970, Ap. J., 162, 217.

Liebowitz E.M. 1973, Ap. J., 186, 899.

Lin, C.C. 1971, Highlights of Astr., 2, 81.

Limber, D.W. 1960, Ap. J., 131, 168.

Mathewson, D.S., and Clarke, J.N. 1973, Ap. J., 179, 89.

Mathis, J. S. 1970, Ap. J., 159, 263.

Matthews, T.A., and Sandage, A.R. 1963, Ap. J., 138, 30.

McClure, R.D., and Bergh, S . van den 1968, A.J., 73, 313.

Mihalas, D. 1965, Ap. J. Suppl., 9 , 321.

Miller, J.S., and Mathews, W.G. 1972, Ap. J., 172, 606.

Morgan, W.W. 1958, Pub. A.S.P., 70, 364.

_____ 1959, Pub. A.S.P., 71, 394 .

_____ 1962, Ap. J., 135, 1.

Morgan, W.W., and Mayall, N.U. 1957, Pub. A.S.P., 69, 291.

Morgan, W.W., and Osterbrock, D.E. 1969, A.J., 74, 515.

Morton, D.C. 1969, Ap. J., 158, 629.

Morton, D.C. and Adams, T.F. 1968, Ap. J., 151, 611.

O'Connell, R.F. 1970, Ph.D. Thesis, California Institute of Technology.

_____ 1973, A.J., 78, 1074.

_____ 1974, Ap. J. Lett., 193, L 49.

Oke, J.B. 1969, Pub. A.S.P., 81, 11.

Oke, J.B., and Schild, R.E. 1970, Ap. J., 161, 1015.

Osmer, P.S., Smith, M.G., and Weedman, D.W. 1974, Ap. J., 192, 279.

Osterbrock, D.E. 1971, in Nuclei of Galaxies, D.J. O'Connell, ed. (New York: American Elsevier).

Osterbrock, D.E., and Dufour, R.J. 1973, Ap. J., 185, 441.

Ostriker, J.P., and Thuan, T.X. 1975, preprint.

Pengelly, R.M. 1964, M.N.R.A.S., 127, 145.

Peterson, D.M., and Scholz, M. 1971, Ap. J., 163, 51.

Peimbert, M. 1968, Ap. J., 154, 33.

_____ 1971, Bol. Obs. Tonantzintla y Tacubaya, 6, 97.

Peimbert, M. and Costero, R. 1969, Bol. Obs. Tonantzintla y Tacubaya, 5, 3.

Pronik, I.I. 1973, Soviet A.J., 16 628.

Roberts, M.S. 1969, A.J., 74, 859.

Roberts, W.W., Roberts, M.S., and Shu, F.H. 1975, Ap. J., 196, 381.

Rogstad, D.H., Rougoor, G.W., and Whiteoak, J.B. 1967 Ap. J., 150, 9.

Salpeter, E.E. 1955, Ap. J., 121, 161.

Sandage, A. 1961, The Hubble Atlas of Galaxies (Washington, D.C.: The Carnegie Institution of Washington).

_____1962, Ap. J., 135, 333.

_____ 1973, Ap. J., 183, 711.

Sandage, A., and Tammann, G.A. 1974, Ap. J., 194, 559.

_____ 1975, Ap. J., 196, 313.

Saslaw, W.C. 1971, Ap. J., 163, 249.

Schild, R.E. 1970, Ap. J., 161, 855.

Schmidt-Kaler, T. 1965, in Numerical Data and Functional Relationships in Science and Technology Group VI, 1, ed. H.H. Voigt (Berlin: Springer-Verlag), p. 284.

Searle, L. 1971, Ap. J., 168, 327.

_____ 1974, private communication.

Searle, L., Sargent, W.L.W., and Bagnuolo, W.G. 1973, Ap. J., 179, 427.

Seaton, M.J. 1960, Rept. Progr. Phys., 23, 313.

Shu, F.H. Stachnik, R.V., and Yost, J.C. 1971, Ap. J., 166, 465.

Simkin, S.M. 1975, Ap. J., 195, 293.

Spinrad, H., and Taylor, B.J. 1969, Ap. J., 157, 1279.

_____ 1971, Ap. J. Suppl., 22, 445.

Spinrad, H., Smith, H.E., and Taylor, D.J. 1972, Ap. J., 175 649.

Stebbins, J., and Kron, G.E. 1957, Ap. J., 126, 266.

Stothers, R. 1969, Ap. J., 155, 935.

_____ 1972a Pub. A.S.P., 84, 373.

_____ 1972b Ap. J., 175, 717.

Thuan, T.X., Hart, M.H., and Ostriker, J.P. 1975, preprint.

Tifft, W.G. 1963, A.J., 68, 302.

Tinsley, B.M. 1968, Ap. J., 151, 547.

_____1972a, Ap. J., 178, 319.

_____1972b, Astr. and Ap., 20, 383.

Tully, R.B. 1974 Ap. J. Suppl., 27, 449.

Turnrose, B.E. 1974, Pub. A.S.P., 86, 545.

Veeder, G.J. 1974, Ap. J. Lett., 191, L 57.

Warner, J.W. 1973, Ap. J., 186, 21.

Whitford, A.E. 1972, Bull. Amer. Astron. Soc., 4, 230.

Wildey, R.L. 1962, Ph.D. Thesis, California Institute of Technology

Williams, T.B. 1975, private communication.

Wing, R.F., and Ford, W.K. 1969, Pub. A.S.P., 81, 527.

Wood, D.B. 1966, Ap. J., 145, 36.